A trait-based model to describe plant community dynamics in managed grasslands (GrasslandTraitSim.jl v1.0.0)

Felix Nößler[1], Thibault Moulin[1], Oksana Buzhdygan[1], Britta Tietjen[1,2], and Felix May[1]

[1]Institute of Biology, Freie Universität Berlin, Theoretical Ecology, Berlin, Germany
[2]Berlin-Brandenburg Institute of Advanced Biodiversity Research, Berlin, Germany

Correspondence: Felix Nößler (felix.noessler@fu-berlin.de)

Abstract. Temperate semi-natural grassland plant communities are expected to shift under global change, mainly due to land use and climate change. However, the interaction of different drivers on diversity and the influence of diversity on the provision of ecosystem services are not fully understood. To synthesise the knowledge on grassland dynamics and to be able to predict community shifts under different land use and climate change scenarios, we developed the GrasslandTraitSim.jl model. In contrast to previously published grassland models, we link morphological plant traits to species-specific processes via transfer functions, thus avoiding a large number of species-specific parameters that are difficult to measure and calibrate. This allows any number of species to be simulated based on a list of commonly measured traits: specific leaf area, maximum height, leaf nitrogen per leaf mass, leaf biomass per plant biomass, above-ground biomass per plant biomass, root surface area per below-ground biomass, and arbuscular mycorrhizal colonisation rate. For each species, the dynamics of the above- and below-ground biomass and its height are simulated with a daily time step. While the soil water content is simulated dynamically, the nutrient dynamics are kept simple, assuming that the nutrient availability depends on total soil nitrogen, yearly fertilization with nitrogen and the total plant biomass. We present a model description, which is complemented by online documentation with tutorials, flowcharts, and interactive graphics, and calibrate and validate the model with two different datasets. We show that the model replicates seasonal dynamics of productivity for experimental sites of the grass species *Lolium perenne* across Europe satisfactory well. Furthermore, we demonstrate that the model can be used to simulate the productivity and functional composition of grassland sites with different number of mowing events and grazing intensity in three regions in Germany. Therefore, GrasslandTraitSim.jl model is presented as a useful tool for predicting plant biomass production and plant functional composition of temperate grasslands in response to management under climate change.

1 Introduction

Permanent semi-natural grasslands cover 30.5% of the agricultural area of the European Union (Eurostat, 2020) and many of them are known to support high levels of biodiversity (Petermann and Buzhdygan, 2021). At small spatial scales (< 100 m^2), extensively managed grasslands have the highest recorded plant species richness per area in the world (Wilson et al., 2012). These plant species-rich habitats can in turn support many other taxonomic groups, such as insects (European Environment Agency et al., 2013; Fartmann, 2024), which are adapted to open habitats. Moreover, 29% of the European bird species are associated with grassland habitats (Nagy, 2009). In conclusion, temperate grasslands play an important role in supporting biodiversity in agricultural landscapes.

The key factor in maintaining the semi-natural grasslands in the temperate zone is management, as well as regular natural disturbances, such as low-intensity fires or avalanches, without which grasslands would become woodlands. This is because the abiotic conditions on most grassland sites favour tree growth, by having the sufficient temperature, precipitation, soil moisture and nutrients (Petermann and Buzhdygan, 2021). Mowing and/or grazing influence the plant species composition of grasslands and prevent the encroachment of woody species (Tälle et al., 2016). Therefore, grasslands and agriculture have been coevolving in Europe since the last glacial period (Hejcman et al., 2013; Pärtel et al., 2005). The intensity and type of land use influence the level of grassland biodiversity. Both intensification and abandonment can lead to a decline in grassland biodiversity (Gossner et al., 2016; Schils et al., 2020; Piseddu et al., 2021). Intensification, more specifically higher fertilization, more mowing events per year, and/or a higher livestock density lead to a dominance of a few fast-growing plant species that are adapted to the high disturbance frequency by mowing and/or grazing. Abandonment, on the other hand, leads to the growth of woody species and a loss of specialists of open habitats (Hilpold et al., 2018). Management is therefore a key driver of plant community composition in the large majority of temperate grasslands.

Furthermore, climate change is expected to alter the plant community composition of grasslands, particularly during periods of heat waves and droughts, for example by suppressing dominant species (Luo et al., 2025) and/or favouring plants with drought avoidance strategies (Griffin-Nolan et al., 2019; Schils et al., 2020). In addition, diversity and composition of the plant community in grasslands affect the provision of ecosystem services, such as biomass production, resistance to climatic events, and pollination (Van Oijen et al., 2020; Buzhdygan et al., 2020). However, how different drivers and their interactions impact the community composition and how the composition relates to ecosystem service provision is poorly understood. In particular, the conditions under which a diverse plant community leads to higher biomass production remain a topic of debate (Adler et al., 2011; Chen et al., 2018; Dee et al., 2023). This highlights the need for a more comprehensive mechanistic understanding of the underlying processes. Simulation models can complement experimental and observational studies to predict the effects of management and climate change on grassland community dynamics and ecosystem service provision, and can help provide a better mechanistic understanding of processes. Current scientific knowledge is integrated into the models, and the models can be used to test hypotheses and to generate new knowledge (Clark et al., 2001; Jeltsch et al., 2008). Dynamic simulation models are therefore a useful tool

for disentangling the effects of land use and climate on the plant community composition and the provision of ecosystem
55   services by grasslands.

Historically, different research questions on grasslands, ranging from ecology to biogeochemistry, have led to the development of different grassland models by focusing on some parts of the grassland system while simplifying others (for an overview of representative models, see Table 1 and for more details in Tables A1 and A2). In ecology, for example, questions about plant coexistence in grasslands have led to models with a strong focus on species interactions. In the
60   biogeochemical community, questions were asked about the emission of greenhouse gases from grasslands, leading to the development of models with a focus on biogeochemical cycles in grasslands (Van Oijen et al., 2018). Ecological models are often simpler models and can be divided into difference or differential equation models and individual-based models. While individual-based models are characterised by a bottom-up approach by modelling the interactions of individuals, difference/differential equation models are characterised by a top-down approach by modelling the interactions
65   of species, leading in both cases to the emergence of grassland community patterns. Examples of individual-based models are IBC-grass (May et al., 2009), originally developed to analyse the effects of grazing on plant communities, and GRASSMIND (Taubert et al., 2012), which can simulate the effects of climate change, mowing, fertilization and irrigation on plant community dynamics. Examples of ecological differential equation models are DynaGraM (Moulin et al., 2021) and GraS (Siehoff et al., 2011), both of which can simulate the effect of mowing and grazing on the plant community.
70   There are also more theoretical models that adopt the Lotka-Volterra differential equations for species competition to simulate grassland dynamics (Geijzendorffer et al., 2011; Fort, 2018; Pulungan et al., 2019; Chalmandrier et al., 2021). Competition between plant species is included in these models with interaction coefficients. The way species or plant functional types are represented in all these models differ. The species in IBC-grass and GRASSMIND are described by morphological and physiological traits. GraS represents species mostly by species indicator values and in DynaGraM
75   species are represented by a combination of morphological and physiological traits and parameters derived from species indicator values. While IBC-grass, GraS and the models using Lotka-Volterra type equations focus strongly on ecological issues and are weak in representing biogeochemical cycles, GRASSMIND is coupled with a soil model and DynaGram has a basic representation of nutrient and water cycles included.

In contrast, models developed by the biogeochemical scientific community have a thorough representation of the nutri-
80   ent, water and carbon cycles in grasslands (Van Oijen et al., 2020). Examples include PaSim (Riedo et al., 1998), LPJmL (Rolinski et al., 2018) and CENTURY/DayCent (Parton, 1996; Parton et al., 1998). However, the representation of plant functional diversity in these models is limited. For example, in LPJmL only two plant functional types (C3 and C4 grasses) are simulated in natural and managed grasslands (Rolinski et al., 2018). Recently, progress has been made to improve the representation of plant functional diversity by simulating C-, S-, and R-plant functional types in correspondence with
85   the CSR-model of plant strategies (Grime, 1977) in LPJmL (Wirth et al., 2024). Another approach to include a representation of plant functional diversity in a single species grassland model is described by the CoSMo-approach (Confalonieri, 2014). Before each time step, the relative abundance of several species is updated based on suitability functions of species to drivers. The relative abundance is used to calculate new community weighted mean traits which are used

Table 1. Overview of representative grassland models simulating several plant species or plant functional types. A more comprehensive overview, including models that simulate only one species, can be found in the appendix (Tables A1 and A2).

Model name with reference	State variables of vegetation	Climate factors[1]	Water (W) & nitrogen (N) cycle[2]	Resource competition	Management factors	No. species / PFTs[3]	IBM?[4]	TFA?[5]
GrasslandTraitSim.jl, presented here	above- and below-ground biomass, height	T, PAR, P, PET	W	water, nitrogen, light	mowing, grazing, fertilization	25-70		✓
Lotka-Volterra competition model, Chalmandrier et al. 2021	above-ground biomass	T	-	-	-	118		✓
DynaGraM, Moulin et al. 2021	above-ground biomass	T, PAR, P, PET	W, N	water, nitrogen, light	mowing, grazing, fertilization	15		
GraS, Siehoff et al. 2011	cover	-	-	space	mowing, grazing, trampling	10		
LPJmL-CSR, Wirth et al. 2024	above- and below-ground biomass, number of individuals	T, PAR, P, PET	W, N	water, nitrogen, light, space	mowing, grazing, fertilization, irrigation	3		
ModVege-CoSMo, Confalonieri 2014, Piseddu et al. 2022	reproductive and vegetative above-ground biomass with age	T, PAR, P, PET	W	water, nitrogen, light (by suitability functions)	mowing, grazing, fertilization	8		
GRASSMIND, Taubert et al. 2012, Taubert et al. 2020	reproductive and vegetative above-ground and below-ground biomass, height	T, PAR, P, PET	W, N	water, nitrogen, light	mowing, fertilization, irrigation	3-5	✓	
IBC-grass, May et al. 2009	reproductive and vegetative above-ground and below-ground biomass	-	-	generic above- and below-ground resources	grazing	81	✓	

[1]We have reviewed whether air temperature (T), photosynthetically active radiation (PAR), precipitation (P), and potential evapotranspiration (PET) are used in a model. Other external climate drivers, even if used in the specific model, are not shown in the table. [2]We evaluated whether the soil water and the soil nitrogen cycle are explicitly simulated in the models. [3]We reviewed the number of simulated species or plant functional types (PFTs), regardless of whether the species parameters were calibrated to data or whether the species were generated more theoretically. [4]We distinguish between individual-based models (IBM), which directly simulate plant individuals, and population-based models, which simulate plant populations. [5]We distinguish between models in which parameters of transfer functions mapping morphological functional traits to species demographic rates are calibrated (TFA: "transfer function approach"), and models in which species demographic parameters are calibrated directly (Chalmandrier et al., 2021).

as an input for the single species grassland model for one time step. Thereby, the plant competition and the community growth dynamics are decoupled. An example is the coupling of the ModVege model with the CoSMo approach (Jouven et al., 2006; Piseddu et al., 2022). In summary, existing grassland models vary in their complexity in representing plant diversity and biogeochemical cycles, and in how species are represented: by species indicator values, morphological traits and/or physiological traits.

Modelling multi-species assemblages in grasslands has been identified as one of the key challenges in grassland modelling (Kipling et al., 2016). This is due to the fact that process-based grassland models require data on the physiological and demographic processes of species, such as measurements of growth rates of species under different radiation intensities. However, as demographic and physiological data are not readily available for many species, the number of

species that can be modelled is limited (Jeltsch et al., 2008; Chalmandrier et al., 2021). To overcome the problem of missing demographic and physiological data, measurable morphological trait data can be used instead. Morphological trait data can be measured more easily and are available for many plant species, for example from the plant trait database TRY (Kattge et al., 2020). For many morphological traits, it is known from experimental and observational studies how they affect species-specific processes (Funk et al., 2017). For example, a high specific leaf area is associated with high photosynthetic activity per leaf mass and a high senescence rate (Wright et al., 2004). So-called transfer functions can be built to map morphological parameters to physiological and demographic processes of species ("transfer function approach (TFA)", see Table 1 and Chalmandrier et al. 2021). Parameters in the transfer function can control the strength of the link between morphological traits and physiological processes, for example how strongly does the specific leaf area correlate to the senescence rate of leaves. This has the technical advantage that the number of parameters for the model calibration does not increase with the species number. While this morphological trait-based approach enables broader species coverage and generality, it also comes with limitations. Morphological traits do not fully capture intra-specific genetic variation or phenotypic plasticity, both of which can be important for species' responses to environmental change. Additionally, environmental heterogeneity—such as soil texture, nutrient availability, and microclimate—may modulate the functional effects of traits in context-dependent ways.

Here, we use this transfer function approach of linking morphological traits to species-specific processes to develop the process-based model GrasslandTraitSim.jl. We extend the approach from Chalmandrier et al. (2021), which used a theoretical model with little or no representation of climate, management and resource competition (see Table 1), to a model that can analyse the influence of management and climate on the productivity and plant functional composition of a grassland. The model is partly based on the DynaGraM model (Moulin et al., 2021), which in turn is based on LINGRA (Schapendonk et al., 1998) and ModVege (Jouven et al., 2006). Both ModVege and LINGRA only simulate one species or plant functional type (see Table A1). With DynaGraM it is possible to study the influence of climate and management on the productivity and plant functional composition and DynaGraM can simulate several species. However, DynaGraM does not rely solely on morphological species-specific parameters but uses instead a combination of morphological, demographic and indicator values (see Table A2). This hinders the use of the transfer function approach of linking morphological traits to species' demographic rates and has the disadvantage that the species-specific demographic parameters are not available for many plant species. We decided to design a population-based model to not have the computational cost of calibrating an individual-based model. Moreover, we decided to keep the plant competition directly in the growth dynamics as in the DynaGraM model and not update the relative abundance of the species based on suitability functions as with the CoSMo-approach (Confalonieri, 2014). Our model is of intermediate complexity compared to the above-mentioned models in terms of the number of equations, which is reflected in the number of simulated state variables and the number of parameters (species-specific and global, non-species-specific, parameters, see Tables 1, A1 and A2). Consequently, our GrasslandTraitSim.jl model addresses a gap in existing grassland simulation models by simulating multi-species assemblages and predicting the functional composition of plant communities in response to management practices and climate change. As plant functional composition influences biomass supply in the model,

cascading effects from management and climate through plant functional composition to biomass supply can be analysed. We will present a comprehensive model description and a calibration and validation using two different datasets of managed grasslands in Europe.

135

2 Description of the GrasslandTraitSim.jl model

The GrasslandTraitSim.jl model is designed to simulate the dynamics of grassland communities under different management scenarios, soil and climatic conditions. The state variables of many plant species (denoted by the subscript s) are simulated with daily time steps (indicated by the t subscript): above-ground dry biomass $B_{A,ts}$ $[\text{kg} \cdot \text{ha}^{-1}]$, below-ground dry biomass $B_{B,ts}$ $[\text{kg} \cdot \text{ha}^{-1}]$, height H_{ts} [m]. The sum of the above-ground and below-ground dry biomass equals the total dry biomass B_{ts} $[\text{kg} \cdot \text{ha}^{-1}]$. Additionally, the state variable soil water content in the rooting zone W_t [mm] is simulated (Fig. 1). Changes in the state variables from one day to the next are described by a set of difference equations (for details see Table A5). The morphological functional traits of all plant species are fixed (time-invariant inputs, for example the maximum plant height) and linked by model parameters to the species' demographic processes (Fig. 2). As a result of the differences in the demographic rates of all species, the performance of individual plant species differs (biomass increase or decrease under particular conditions), leading to the emergence of plant community dynamics. While reading the model description, we encourage the reader to have a look at the online documentation, which contains many interactive graphics and flowcharts that make the model description more accessible (see data accessibility statement).

The required model inputs are the plant functional traits of each species, soil properties, daily climatic data and daily management data (e.g., timing and intensity of grazing, Table A3). The model has in total 54 global parameters (for details see Table A4) that are neither site, time nor species dependent. Outputs include the state variables, grazed and mown biomass, community-weighted mean and variance of each trait. Additionally, taxonomic diversity indices (e.g., Simpson diversity) and plant functional diversity indices (e.g., Functional dispersion and Functional evenness) are provided. Both state variables and diversity metrics can be calculated for each day. The model is not spatially explicit and does not account for spatial heterogeneity. As the assumption of spatial homogeneity is only met approximately for smaller spatial dimensions, we suggest using the model for areas between 1 m^2 and 1 ha.

The model procedure is divided into an initialisation and a simulation part. During the initialisation, the state variables (height, above-ground and below-ground biomass of species, and soil water content) are set to user supplied initial values. During the simulation, a loop is run over each day. For each day, very low or negative values ($< 10^{-30}$) of the height H_{ts} and biomass state variables (B_{ts}, $B_{A,ts}$, and $B_{B,ts}$) are set to zero to avoid numerical problems. We have deliberately kept the threshold at a low level because the plant species should be able to recover even from a very low biomass level. After that, the main part of the model is executed with the calculation of growth (Sections 2.1-2.1.7, Eqs. 5-33), senescence (Section 2.1.8, Eqs. 34-35), biomass removal by management (Section 2.1.9, Eqs. 36-42), height dynamics (Section 2.2, Eq. 43), and soil water dynamics (Section 2.3, Eqs. 44-52).

2.1 Biomass dynamics

The change in the total biomass B from day t to $t+1$ of species s $[\text{kg} \cdot \text{ha}^{-1}]$ is calculated based on the actual growth $G_{act,ts}$ $[\text{kg} \cdot \text{ha}^{-1}]$ (Eq. 5), and the losses by senescence S_{ts} $[\text{kg} \cdot \text{ha}^{-1}]$ (Eq. 34) and management M_{ts} $[\text{kg} \cdot \text{ha}^{-1}]$ (Eq.

36):

$$B_{t+1s} = B_{ts} + G_{act,ts} - S_{ts} - M_{ts} \tag{1}$$

170 The change in the total biomass B_{ts} is divided into the change in above-ground $B_{A,ts}$ [$\text{kg} \cdot \text{ha}^{-1}$] and below-ground biomass B_{ts} [$\text{kg} \cdot \text{ha}^{-1}$]. We assume that plants aim to achieve a similar level of above-ground biomass per total biomass similar to the time-invariant trait above-ground biomass per total biomass abp_s [$-$]. We therefore calculate A_{ts} [$-$] the ratio between the actual biomass ratio and the trait abp_s:

$$A_{ts} = \frac{\left(\frac{B_{A,ts}}{B_{ts}}\right)}{abp_s} \tag{2}$$

175 A_{ts} is less than one if the above-ground biomass per total biomass is less than expected by the trait abp_s, for example after a mowing event. This variable can be used to allocate biomass changes by growth and senescence to above-ground and below-ground biomass. Biomass loss by mowing and grazing affects only the above-ground biomass:

$$B_{A,t+1s} = B_{A,ts} + A_{ts} \cdot G_{act,ts} - (1 - A_{ts}) \cdot S_{ts} - M_{ts} \tag{3}$$

$$B_{B,t+1s} = B_{B,ts} + (1 - A_{ts}) \cdot G_{act,ts} - A_{ts} \cdot S_{ts} \tag{4}$$

180 This formulation allows for rapid regrowth of above-ground biomass after a grazing period or a mowing event, as little of the growth is allocated to below-ground biomass and most is allocated to above-ground biomass.

  The actual growth is derived from the community potential growth $G_{pot,t}$ [$\text{kg} \cdot \text{ha}^{-1}$] (Eq. 6) and the multiplicative effect of five growth adjustment factors:

$$G_{act,ts} = G_{pot,t} \cdot LIG_{ts} \cdot NUT_{ts} \cdot WAT_{ts} \cdot ROOT_{ts} \cdot ENV_t \tag{5}$$

185 where LIG_{ts} [$-$] is the species-specific competition for light (Eq. 12), NUT_{ts} [$-$] is the species-specific competition for nutrients (Eq. 15), WAT_{ts} [$-$] is the species-specific competition for soil water (Section 2.1.5), $ROOT_{ts}$ [$-$] is the species-specific cost for maintaining roots and mycorrhiza (Eq. 26), and ENV_t [$-$] is the non-species-specific adjustment based on environmental and seasonal factors (Eq. 29).

2.1.1 Community potential growth

190 The model follows the concept of the light use efficiency (Monteith, 1972) that describes how much dry matter the plants can build based on the solar radiation. This concept was widely adopted in grassland modelling studies (Schapendonk et al. 1998; Jouven et al. 2006; Moulin et al. 2021; for a review see Pei et al. 2022). The community potential growth $G_{pot,t}$ is described by:

$$G_{pot,t} = PAR_t \cdot \gamma_{RUEmax} \cdot FPAR_t \tag{6}$$

195 with the photosynthetic active radiation PAR_t [$\text{MJ} \cdot \text{ha}^{-1}$], maximal radiation use efficiency γ_{RUEmax} [$\text{kg} \cdot \text{MJ}^{-1}$], and the fraction of PAR_t that is intercepted by the plants $FPAR_t$ [$-$].
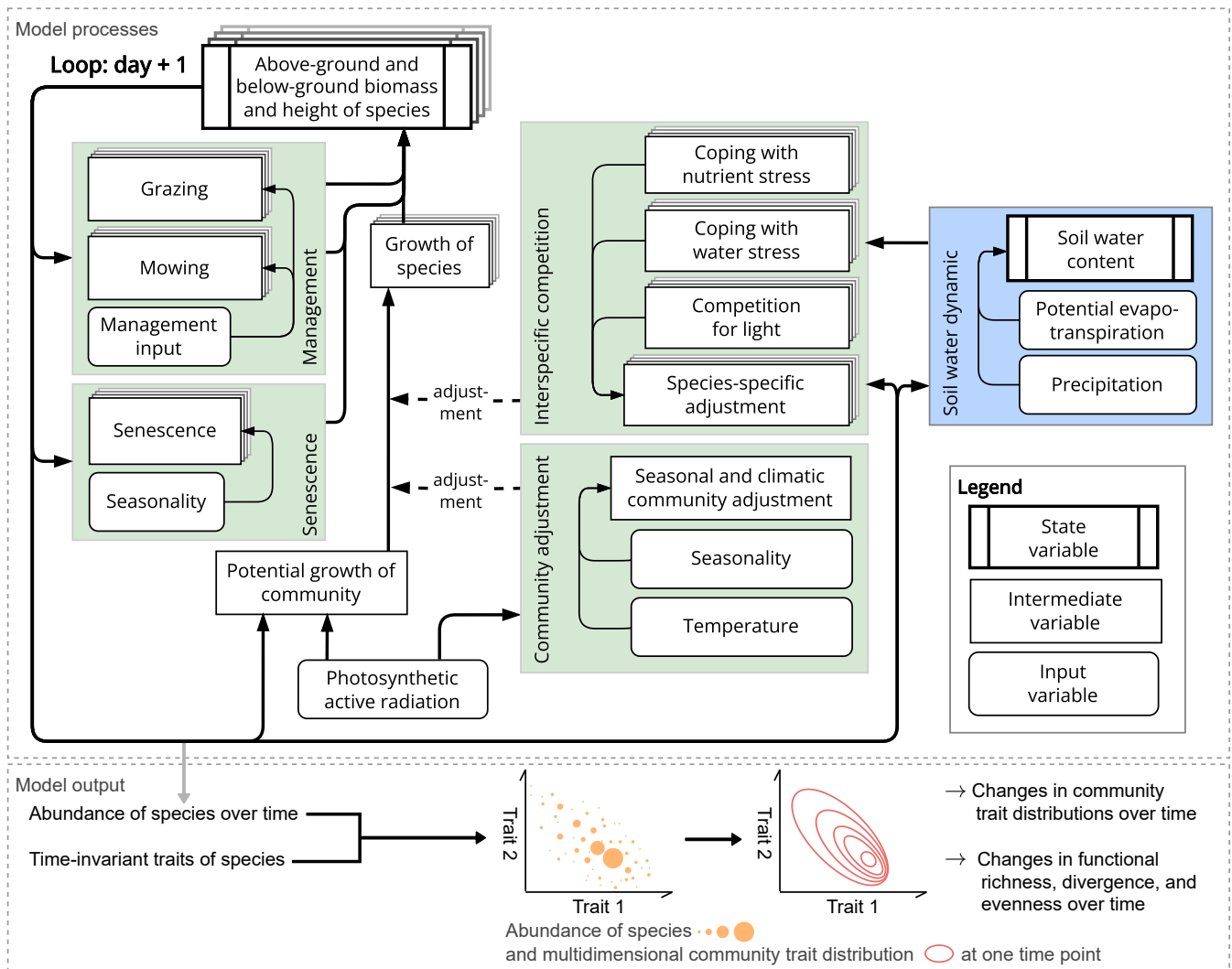
Figure 1. Structure of the GrasslandTraitSim.jl model. Boxes represent state, intermediate, and input variables (forcing functions), and arrows indicate the influence of one variable on another. We use the term intermediate variables to describe variables that are neither inputs nor state variables, but are important intermediate results in the calculation of the change in state variables. While the green areas show calculations that influence the change in above- and below-ground biomass and height, the blue area shows the calculation of the change in soil water content in the rooting zone. The arrows originating from the biomass and height of the species indicate that both the biomass and height play a role in the processes outlined in the green and blue areas. However, for simplicity, they do not indicate the exact position within the areas. Species-specific variables are represented by a series of offset boxes positioned behind one another, indicating the presence of multiple species within the model. We show how the distribution of community traits can be calculated from the model output; other model outputs include the state variables and the grazed and mown biomass, which can be summarised at the community level.
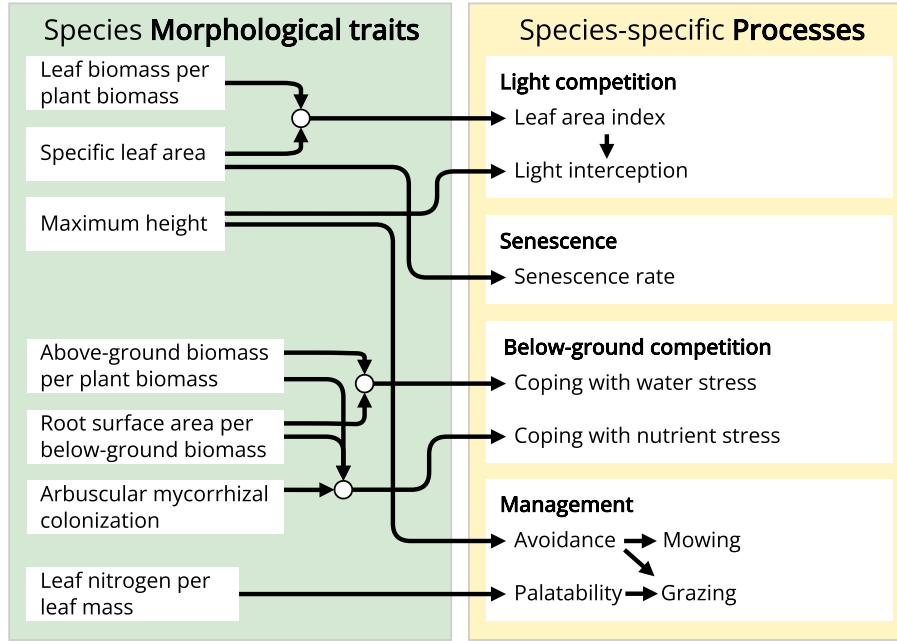
Figure 2. The GrasslandTraitSim.jl model links morphological plant functional traits to processes. Arrows indicate which process or variable is influenced by each plant functional trait. Each plant functional trait can have species-specific values, allowing for species-specific responses in many of the model's processes.

The modelled fraction of radiation intercepted by the plants is determined by the number of leaves and the height of the community. A saturation function is used to describe the relationship between leaf area per ground area (leaf area index) and light interception. We argue that light interception is less effective when all plants are rather short, because the leaves are more densely packed. Individual plants avoid shading by growing taller (Heger, 2016). Therefore, we include the height of the community in the light interception calculation, also to prevent that a community with short plants can build up a very high biomass. More technically, we use the Beer-Lambert equation to model the non-linear response of the fraction of light intercepted $FPAR_t$ to the total leaf area index $LAI_{tot,t}$ (Monsi, 1953; Monsi and Saeki, 2005). This relationship is governed by the light extinction coefficient $\gamma_{RUE,k}$ $[-]$, which determines how quickly the fraction of absorbed radiation approaches one as the leaf area index increases. Reduction of radiation use efficiency because of densely packaged leaves is a function of the community-weighted mean height and influenced by the parameter $\alpha_{RUE,cwmH} \in [0,1]$ $[-]$, which specifies the growth reduction at $H_{cwm,t} = 0.2\mathrm{m}$. The 0.2 m has been arbitrarily set, and the parameter $\alpha_{RUE,cwmH}$ is inversely calibrated. If $H_{cwm,t}$ is greater than 0.2 m, less self-shading will occur because the leaves are less densely packed and therefore the growth reduction is less than $\alpha_{RUE,cwmH}$:

$$FPAR_t = (1 - \exp\left(-\gamma_{RUE,k} \cdot LAI_{tot,t}\right)) \cdot \exp\left(\frac{\log(\alpha_{RUE,cwmH}) \cdot 0.2\mathrm{m}}{H_{cwm,t}}\right) \tag{7}$$

with the community-weighted mean height, calculated by weighting the height H_{ts} [m] of each species by its share of above-ground biomass $B_{A,ts}$ of the total above-ground biomass $B_{totA,t}$ [kg · ha^{-1}]:

$$H_{cwm,t} = \sum_{s=1}^{S} \frac{B_{A,ts}}{B_{totA,t}} \cdot H_{ts} \tag{8}$$

The total leaf area index $LAI_{tot,t}$ is the sum of the species-specific leaf area indices LAI_{ts}:

$$LAI_{tot,t} = \sum_{s=1}^{S} LAI_{ts}, \tag{9}$$

where LAI_{ts} is defined as

$$LAI_{ts} = B_{A,ts} \cdot sla_s \cdot lbp_s \cdot 0.1, \tag{10}$$

with above-ground biomass $B_{A,ts}$ [kg · ha^{-1}], specific leaf area sla_s [m^2 · g^{-1}], and leaf biomass per above-ground biomass lbp_s [−]. As $B_{A,ts}$ and sla_s must be converted to the same unit, Eq. 10 is multiplied by 0.1.

2.1.2 Species-specific light competition

The proportion of the potential growth of each plant species to the potential growth of the community is based on the leaf area index and height of the species. Species with a higher leaf area index can intercept more light and taller species receive greater light exposure and are less affected by shading from other plant species. The leaf area index of the species considers that plant species which transfer more biomass to their leaves, and have thinner leaves, can build a greater leaf area. This allows them to use the photosynthetic active radiation more efficiently. Being overtopped by other plants or investing more in supporting tissue and less in leaves is a common trade-off in plant strategies (Westoby et al., 2002). The proportion of light intercepted by each species out of the total light intercepted is derived by dividing the sward into vertical height layers of constant width, by default 0.05 m, to account for shading (similar to Taubert et al., 2012). We want to calculate how much light is intercepted in each height layer l $INT_{t,l}$ [−]. Therefore, we need to calculate how much light is intercepted in the layers above and the interception in layer l. We assume that the biomass, and therefore also the leaf area index, is uniformly distributed over the height of the plant. Thus, we can calculate the leaf area index of each species in each height layer $LAI_{ts,l}$ [−] and the total leaf area index of all species in each layer $LAI_{tot,t,l}$ [−]. For each layer we can calculate the total leaf area index above the layer up to the maximum height layer L. The maximum height layer can be reached by the tallest plants with the highest $maxheight$ [m]. The reduction in incoming light based on the total leaf area index of the layers above and the interception of layer l is used to calculate the proportion of light intercepted in layer l $INT_{t,l}$:

$$INT_{t,l} = \exp\left(\gamma_{RUE,k} \cdot \sum_{z=l+1}^{L} LAI_{tot,t,z}\right) \cdot (1 - \exp(\gamma_{RUE,k} \cdot LAI_{tot,t,l})) \tag{11}$$

The proportion of light intercepted in the layer can be used to obtain the proportion of light intercepted for each species in each layer by multiplying $INT_{t,l}$ by the leaf area index proportion of the layer. The sum of all species-specific light
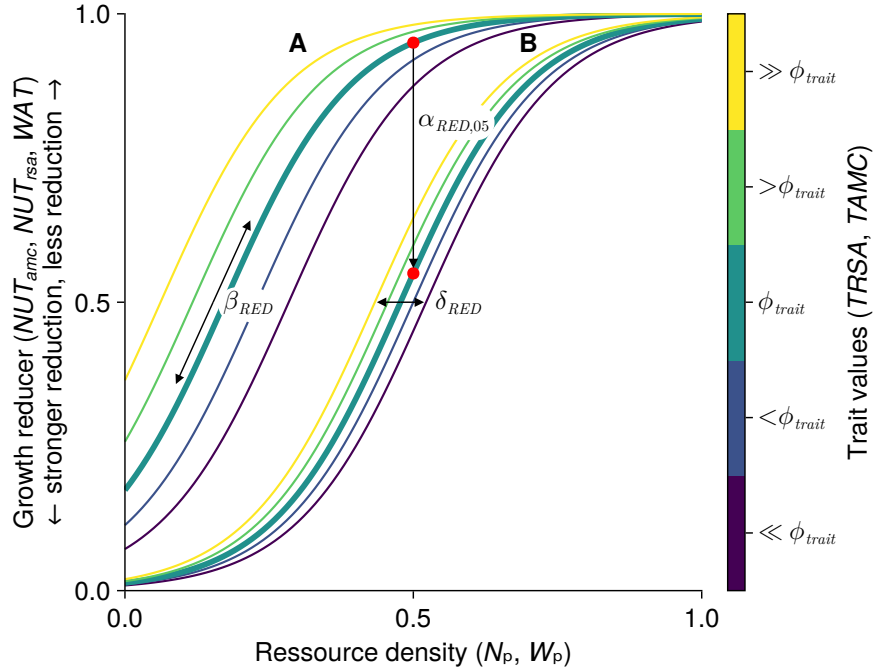
Figure 3. General form of growth reducer as a function of resource density (plant available nutrients and soil water). The function is governed by the four parameters β_{RED} (slope of the logistic function), ϕ_{trait} (usually the mean trait value), $\alpha_{RED,05}$ (growth reduction at half the resource density for species with a trait value of ϕ_{trait}, marked by a red dot), and δ_{RED} (controls how much the species-specific inflection points differ from the inflection point of a species with value of ϕ_{trait}). We show two different curves for different parameter values: A with $\alpha_{RED,05} = 0.95$ and $\delta_{RED} = 0.25$; B with $\alpha_{RED,05} = 0.55$ and $\delta_{RED} = 0.1$. In both cases we used $\beta_R = 9$, $\phi_{trait} = 20$ and the trait values 16, 18, 20, 22 and 24 (from dark purple to yellow). We include dynamic versions with sliders for the parameters for the three growth reducers $NUT_{amc,ts}$, $NUT_{rsa,ts}$, and WAT_{ts} in the supplementary material (see data accessibility statement).

240   interception proportions across all layers can be used to calculate the light competition factor LIG_{ts} $[-]$:

$$LIG_{ts} = \sum_{z=l}^{L} INT_{t,l} \cdot \frac{LAI_{ts,z}}{LAI_{tot,t,z}} \cdot \frac{1}{1 - \exp(\gamma_{RUE,k} \cdot LAI_{tot,t})} \tag{12}$$

We divide the term by the total interception of all layers (compare Eq. 7) to ensure that the sum of all species-specific light competition factors is equal to one. The parameter $\beta_{LIG,H}$ is not used in this method.

2.1.3   General form of the growth reducer for nutrient and water stress

245   We use the same equations with different parameters to relate the plant-available nutrients and plant-available soil water to the growth reducers of nutrient and water stress. Therefore, we show here the general form of the equations (see Fig. 3) to avoid repetition and define the specific variables and parameters used in the next two sections on nutrient and

water stress. The derivation of the equations is shown in more detail in Appendix A. We use a logistic function to relate the resource density R_t (general symbol for the plant-available nutrients $N_{p,ts}$ and the plant-available water $W_{p,t}$) to the growth reducer RED_{ts} (general symbol for the growth reducers for nutrients stress $NUT_{amc,ts}$ and $NUT_{rsa,ts}$ and water stress WAT_{ts}). The growth reducer RED_{ts} lies between zero (no growth possible) and one (no growth reduction at all). While the inflection points of the logistic function $x_{0,RED,ts}$ (general symbol for $x_{0,NUT,rsa,s}$, $x_{0,NUT,amc,s}$, and $x_{0,WAT,s}$) are species-specific depending on the trait values $trait_{ts}$ (general symbol for the root surface area per total biomass $TRSA_{ts}$ and the arbuscular mycorrhizal colonisation rater per total biomass $TAMC_{ts}$), the slope β_{RED} (general symbol for $\beta_{NUT,rsa}$, $\beta_{NUT,amc}$, and $\beta_{WAT,rsa}$) is not species-specific. We assume that if the plant has a trait value equal to the parameter ϕ_{trait} (general symbol for ϕ_{TRSA} and ϕ_{TAMC}), then the growth reduction at 0.5 resource density is $\alpha_{RED,05}$ (general symbol for $\alpha_{NUT,rsa,05}$, $\alpha_{NUT,amc,05}$, and $\alpha_{WAT,rsa,05}$). The parameter ϕ_{trait} can be set to the mean trait of a community, then the parameter $\alpha_{RED,05}$ can be interpreted as the mean response at half the maximum resource density. How much the inflection points deviate from this mean response can be controlled by the parameter δ_{RED} (general symbol for $\delta_{NUT,rsa}$, $\delta_{NUT,amc}$, and $\delta_{WAT,rsa}$). If δ_{RED} is zero, there is no difference in the growth reduction between the species. If δ_{RED} larger than zero, species with higher trait values are less affected by nutrient or water stress:

$$x_{0,RED,ts} = \frac{1}{\beta_{RED}} \cdot \left(-\delta_{RED} \cdot \left(trait_{ts} - \left(\frac{1}{\delta_{RED}} \cdot \log\left(\frac{1-\alpha_{RED,05}}{\alpha_{RED,05}} \right) + \phi_{trait} \right) \right) \right) + 0.5 \tag{13}$$

$$RED_{ts} = \begin{cases} 0 & \text{if } R_t = 0 \\ 1/\left(1 + \exp\left(-\beta_{RED} \cdot (R_t - x_{0,RED,ts})\right)\right) & \text{if } 0 < R_t < 1 \\ 1 & \text{if } R_t >= 1 \end{cases} \tag{14}$$

2.1.4 Species-specific nutrient stress

Plant growth may be reduced when soil nutrient availability is low and plants are inefficient at taking up nutrients. We consider arbuscular mycorrhizal colonisation rate (Marschner and Dell, 1994; George et al., 1995; Van Der Heijden et al., 2015) and root surface area per total biomass (Barber and Silberbush, 1984) as traits that help plants to take up nutrients and reduce nutrient stress. Here, we only consider nutrient deficit as nutrient stress. The growth reducer NUT_{ts} $[-]$ is composed out of the maximum out of two nutrient stress factors that are linked to the arbuscular mycorrhizal colonisation rate $N_{amc,ts}$ $[-]$ and the root surface area per total biomass $N_{rsa,ts}$ $[-]$:

$$NUT_{ts} = \max(NUT_{amc,ts}, NUT_{rsa,ts}) \tag{15}$$

The maximum of the two nutrient stress factors is used because, for simplicity, we assume that plants can invest either in a high root surface area per total biomass or in a high rate of arbuscular mycorrhizal colonisation. Plants with a higher root surface area per total biomass follow the strategy of taking up nutrients themselves, while plants with high arbuscular mycorrhizal colonisation rates follow the strategy of outsourcing nutrient uptake to arbuscular mycorrhizal fungi in the context of the root collaboration gradient (Bergmann et al., 2020). Since growth is reduced by how well plants follow their best strategy, the maximum of the two reduction factors is used to calculate the reduction in growth due to soil nutrients.

For the calculation of the growth reducers for nutrients stress based on the arbuscular mycorrhizal colonisation rate $NUT_{amc,ts}$ [−] we use the parameters ϕ_{TAMC} [−], $\beta_{NUT,amc}$ [−], $\alpha_{NUT,amc,05}$ [−], $\delta_{NUT,amc}$ [−] and for nutrients stress based on the root surface area per total biomass $NUT_{rsa,ts}$ [−] we use ϕ_{TRSA} [m^2 · g^{-1}], $\beta_{NUT,rsa}$ [−], $\alpha_{NUT,rsa,05}$ [−], and $\delta_{NUT,rsa}$ [g · m^{-2}]. Moreover, we still need trait values and the plant available nutrients (to replace $trait_s$ and R_t in Eqs. 13-14).

For the traits that influence the nutrient growth reducer, we consider that plants with high below-ground biomass per total biomass are less affected by low nutrient levels because they have relatively more root tissue to supply nutrients to the above-ground biomass. It has been shown that the root-to-shoot ratio increases in many plants under nitrogen-poor conditions (Jiang et al., 2016; Meurer et al., 2019; Lopez et al., 2023). Therefore, we calculate the root surface area per total biomass $TRSA_{ts}$ [m^2 · g^{-1}] and the arbuscular mycorrhizal colonisation rate per total biomass $TAMC_{ts}$ [−] from the fixed traits root surface area per below-ground biomass rsa_s and arbuscular mycorrhizal colonisation rate per root tissue amc_s with the dynamic proportion of the below-ground biomass $B_{B,ts}$ per total biomass B_{ts}:

$$TAMC_{ts} = \frac{B_{B,ts}}{B_{ts}} \cdot amc_s \tag{16}$$

$$TRSA_{ts} = \frac{B_{B,ts}}{B_{ts}} \cdot rsa_s \tag{17}$$

where the below-ground biomass is cancelled out. $TAMC_{ts}$ and $TRSA_t s$ are used to replace $trait$ in Equation 13 for the calculation of $NUT_{amc,ts}$ and $NUT_{rsa,ts}$.

The nutrients available to plants depend on the total soil nitrogen of a site N [gN · kg^{-1}], the fertilization with nitrogen F [kgN · ha · yr^{-1}] and the density effect, which accounts for stronger competition for nutrients if many plant species have a high biomass. The fertilization rate can vary between years and is the sum of organic and inorganic fertilization with nitrogen per year. More technically, the empirical parameters $\omega_{NUT,N}$ [gN^{-1} · kg] and $\omega_{NUT,F}$ [kgN^{-1} · ha^{-1} · yr] control how strongly the variables total soil nitrogen and the fertilization rate, respectively, contribute to the value of the nutrient index ($\in [0,1]$). The nutrient index is multiplied by the nutrient adjustment factor $NUT_{adj,ts}$ [−], which accounts for the biomass density, to get the plant available nutrients $N_{p,ts}$ [−]:

$$N_{p,ts} = (1 - \exp(-\omega_{NUT,N} \cdot N - \omega_{NUT,F} \cdot F)) \cdot NUT_{adj,ts} \tag{18}$$

The plant available nutrients $N_{p,ts}$ are used in Equation 14 for the resource R_t to calculate the growth reducers of $NUT_{amc,ts}$ and $NUT_{rsa,ts}$. $N_{p,ts}$ can be greater than one, if the total biomass is low, then growth is not reduced (see Eq. 14). In contrast to the plant available water (Eq. 25), the plant available nutrients are species-specific.

Plants are most strongly affected by below-ground competition if conspecifics and plants with similar traits have a high biomass and share the below-ground resources. This is summarized with the nutrient adjustment factor $NUT_{adj,ts}$ [−] that takes into account the biomass and the trait similarity between all species:

$$NUT_{adj,ts} = \alpha_{NUT,maxadj} \cdot \exp\left(\log\left(\frac{1}{\alpha_{NUT,maxadj}}\right) \cdot \sum_{i=1}^{S} TS_{s,i} \cdot B_{ti} \cdot \frac{1}{\alpha_{NUT,TSB}}\right) \tag{19}$$

with the trait similarity $TS_{s,i}$ [−] between species s and i, the biomass of species i B_{ti} [kg · ha^{-1}] and the parameters $\alpha_{NUT,TSB}$ [kg · ha^{-1}] and $\alpha_{NUT,maxadj}$ [−]. A high nutrient adjustment factor $NUT_{adj,ts}$ is favourable for a species because the factor is multiplied by the site nutrients (Eq. 18), which means that the species has to share the resources with fewer competitors. More specifically, a high $NUT_{adj,ts}$ of a species indicates that either the total biomass is low or the plant has traits that are very different from the traits of the abundant plant species. The parameter $\alpha_{NUT,TSB}$ is a reference value for the sum of the product of trait similarity and biomass of all species. If the sum of the product of trait similarity and biomass of all species is equal to $\alpha_{NUT,TSB}$, the nutrient adjustment factor is one. The parameter $\alpha_{NUT,maxadj}$ (≥ 1) controls the maximum of the nutrient adjustment factor. The parameter can be greater than one to allow the plant available nutrients to be increased when the total biomass is low.

The trait similarity is derived by calculating the dissimilarity of the root surface area per above-ground biomass rsa_s [m^2 · g^{-1}] and the arbuscular mycorrhizal colonisation rate amc_s [−] between all species and converting it to a similarity index. These two traits are chosen to calculate the trait dissimilarity index, because both traits encompass unique plant strategies for the acquisition of nutrients and water (Bergmann et al., 2020). The trait dissimilarity $TD_{s,i}$ [−] between species s and species i is calculated with the euclidean distance between the normalized traits of the species:

$$AMC_{\text{norm},s} = \frac{amc_s - \text{mean}(\mathbf{amc})}{\text{sd}(\mathbf{amc})} \tag{20}$$

$$RSA_{\text{norm},s} = \frac{rsa_s - \text{mean}(\mathbf{rsa})}{\text{sd}(\mathbf{rsa})} \tag{21}$$

$$TD_{s,i} = \sqrt{(RSA_{\text{norm},s} - RSA_{\text{norm},i})^2 + (AMC_{\text{norm},s} - AMC_{\text{norm},i})^2} \tag{22}$$

This gives the dissimilarity matrix $\mathbf{TD}$ [−], which is transformed and scaled by the parameter $\beta_{NUT,TS}$ [−] to a trait similarity matrix $\mathbf{TS}$ [−]:

$$\mathbf{TS} = \left(1 - \frac{\mathbf{TD}}{\max(\mathbf{TD})}\right)^{\beta_{NUT,TS}} \tag{23}$$

$$\mathbf{TS} = \begin{bmatrix} 1 & TS_{1,2} & \dots & TS_{1,S} \\ TS_{2,1} & 1 & & \\ \vdots & & \ddots & \\ TS_{S,1} & & & 1 \end{bmatrix} \tag{24}$$

If $\beta_{NUT,TS}$ is zero, the trait similarity has no influence in the calculation of the nutrient adjustment factor in Eq. 19.

2.1.5 Species-specific water stress

Plant growth may be reduced if soil water is low and the plants are poor at taking up water. We consider the root surface area per total biomass $TRSA_{ts}$ [m^2 · g^{-1}] (see Eq. 17) as the trait that influences how strong plants are exposed to the water stress at a certain soil water level. Here, we only consider too little water leading to water stress conditions, not too much water, as our primary goal of our model is not to model systems with regular flooding or waterlogging. We use the

same equations for the water stress reducer WAT_{ts} [−] as for the nutrient reducer (see Eqs. 13-14) with the parameters ϕ_{TRSA} [$m^2 \cdot g^{-1}$], $\beta_{WAT,rsa}$ [−], $\alpha_{WAT,rsa,05}$ [−], and $\delta_{WAT,rsa}$ [$g \cdot m^{-2}$]. The same explanation for the parameters applies as for the nutrient reducer.

The plant available water is the rescaled soil water content (to replace R in Eq. 14): The soil water content W_t [mm] is scaled by the water holding capacity WHC [mm] (Eq. 51) and the permanent wilting point PWP [mm] (Eq. 52) to scale water availability between 0 (soil water content at or below the permanent wilting point) and 1 (soil water content at or above the water holding capacity). The plant available water $W_{p,t}$ [−] is defined as:

$$W_{p,t} = \frac{W_t - PWP}{WHC - PWP} \tag{25}$$

This formulation of plant available water does not take into account some short-term temporal dynamics. For example, after a rainfall event, plants are often not water stressed at all, even if the soil water content is not replenished to the water holding capacity.

2.1.6 Species-specific maintenance costs for roots and mycorrhizae

Maintaining a fine root structure and symbiosis with mycorrhizal fungi costs energy. These costs include respiration (Caldwell, 1979), the production of metabolites for nutrient uptake (Canarini et al., 2019), and the supply of photosynthetic products to the mycorrhizal fungi (Konvalinková et al., 2017). Similarly to Taubert et al. (2012), who consider the costs of maintaining a symbiosis with nitrogen-fixing rhizobia, we include a cost term for root surface area per total biomass $ROOT_{rsa,ts}$ [−] and the mycorrhizal colonisation rate per total biomass $ROOT_{amc,ts}$ [−]. This means that part of the potential growth cannot be used to produce new biomass:

$$ROOT_{ts} = ROOT_{rsa,ts} \cdot ROOT_{amc,ts} \tag{26}$$

where $ROOT_{ts}$ [−] is the root investment factor that lowers the actual growth in (Eq. 5).

$$ROOT_{rsa,ts} = 1 - \kappa_{ROOT,rsa} + \kappa_{ROOT,rsa} \cdot \exp\left(\frac{\log(0.5)}{\phi_{TRSA} \cdot TRSA_{ts}} \right) \tag{27}$$

$$ROOT_{amc,ts} = 1 - \kappa_{ROOT,amc} + \kappa_{ROOT,amc} \cdot \exp\left(\frac{\log(0.5)}{\phi_{TAMC} \cdot TAMC_{ts}} \right) \tag{28}$$

where $TRSA_{ts}$ is the root surface area per total biomass [$m^2 \cdot g^{-1}$] (see Eq. 17) and $TAMC_{ts}$ is the arbuscular mycorrhizal colonisation rate per total biomass [−] (see Eq. 16). Therefore, the cost of maintaining fine and roots and mycorrhizae does change with time depending on the ratio between above-ground and below-ground biomass.

The parameters $\kappa_{ROOT,rsa}$ [−] and $\kappa_{ROOT,amc}$ [−] define the maximum possible growth reduction from zero to one, where zero means no growth reduction at all. The parameters ϕ_{TRSA} [$m^2 \cdot g^{-1}$] and ϕ_{TAMC} [−] define the trait values of $TRSA_{ts}$ and $TAMC_{ts}$ at which the growth reducer is half in between 1 (no growth reduction) and the maximal growth reduction that is defined by $\kappa_{ROOT,rsa}$ and $\kappa_{ROOT,amc}$. Note that the same values for ϕ_{TRSA} and ϕ_{TAMC} are also used for water and nutrient stress reducers.

2.1.7 Community environmental and seasonal factors

The growth is adjusted for environmental and seasonal factors ENV_t that apply in the same way to all species (Eq. 5). For simplicity, we do not consider the effect of specific-specific plant traits on the following functions:

$$ENV_t = RAD_t \cdot TEMP_t \cdot SEA_t \tag{29}$$

with the radiation RAD_t $[-]$ (Eq. 30), temperature $TEMP_t$ $[-]$ (Eq. 31), and seasonal SEA_t $[-]$ (Eq. 32) growth adjustment factors.

Plant growth increases with photosynthetically active radiation (as formulated in Eq. 6), but excess radiation can lead to oxidative damage and photoinhibition (Long et al., 1994). We have therefore included the equation and parametrisation from Schapendonk et al. (1998) that reduces the growth due to excess radiation. The radiation adjustment factor RAD_t $[-]$ is calculated as follows:

$$RAD_t = \min\left(1, 1 - \gamma_{RAD,1}\left(PAR_t - \gamma_{RAD,2}\right)\right) \tag{30}$$

with the photosynthetic active radiation PAR_t $[\mathrm{MJ} \cdot \mathrm{ha}^{-1}]$ and the parameters $\gamma_{RAD,1}$ $[\mathrm{MJ}^{-1} \cdot \mathrm{ha}]$ and $\gamma_{RAD,2}$ $[\mathrm{MJ} \cdot \mathrm{ha}^{-1}]$. A linear decrease of radiation use efficiency with a steepness of $\gamma_{RAD,1}$ is assumed if the photosynthetic active radiation is above $\gamma_{RAD,2}$.

Temperature is one of the fundamental environmental factors that influence plant growth (Went, 1953). Thus, a temperature adjustment factor $TEMP_t$ $[-]$ is included in the model. The temperature adjustment factor is based on the empirical step functions by Schapendonk et al. (1998) that were adjusted by Jouven et al. (2006):

$$TEMP_t = \begin{cases} 0 & \text{if } T_t < \omega_{TEMP,T_1} \\ \frac{T_t - \omega_{TEMP,T_1}}{\omega_{TEMP,T_2} - \omega_{TEMP,T_1}} & \text{if } \omega_{TEMP,T_1} < T_t < \omega_{TEMP,T_2} \\ 1 & \text{if } \omega_{TEMP,T_2} < T_t < \omega_{TEMP,T_3} \\ \frac{\omega_{TEMP,T_4} - T_t}{\omega_{TEMP,T_4} - \omega_{TEMP,T_3}} & \text{if } \omega_{TEMP,T_3} < T_t < \omega_{TEMP,T_4} \\ 0 & \text{if } T_t > \omega_{TEMP,T_4} \end{cases} \tag{31}$$

with the minimum temperature requirement for growth ω_{TEMP,T_1} $[^\circ\mathrm{C}]$, the optimum temperature for growth between ω_{TEMP,T_2} $[^\circ\mathrm{C}]$ and ω_{TEMP,T_3} $[^\circ\mathrm{C}]$ and the maximum temperature for growth ω_{TEMP,T_4} $[^\circ\mathrm{C}]$. The temperature adjustment factor increases linearly from zero to one between ω_{TEMP,T_1} and ω_{TEMP,T_2}, stays at one between ω_{TEMP,T_2} and ω_{TEMP,T_3}, decreases linearly from one to zero between ω_{TEMP,T_3} and ω_{TEMP,T_4} and stays at zero above ω_{TEMP,T_4}.

A seasonal factor accounts for growth patterns that would not be expected from an analysis of daily abiotic conditions alone. Plants usually grow more strongly in spring than in autumn, even if the radiation and temperature values are similar. Therefore, in addition to the influence of radiation (Eqs. 6, 30) and temperature (Eq. 31) a seasonality factor is added. Jouven et al. (2006) build the following empirical step functions for the seasonal factor SEA_t $[-]$ based on the yearly accumulated degree days ST_t $[^\circ\mathrm{C}]$ and the parameters $\zeta_{SEA\min}$ $[-]$, $\zeta_{SEA\max}$ $[-]$, ζ_{SEA,ST_1} $[^\circ\mathrm{C}]$, and ζ_{SEA,ST_2} $[^\circ\mathrm{C}]$:

$$
SEA_t =
\begin{cases}
\zeta_{SEA\min} & \text{if } ST_t < 200\,^{\circ}\text{C} \\
\zeta_{SEA\min} + (\zeta_{SEA\max} - \zeta_{SEA\min}) \cdot \frac{ST_t - 200\,^{\circ}\text{C}}{\zeta_{SEA,ST_1} - 400\,^{\circ}\text{C}} & \text{if } 200\,^{\circ}\text{C} < ST_t < \zeta_{SEA,ST_1} - 200\,^{\circ}\text{C} \\
\zeta_{SEA\max} & \text{if } \zeta_{SEA,ST_1} - 200\,^{\circ}\text{C} < ST_t < \zeta_{SEA,ST_1} - 100\,^{\circ}\text{C} \\
\zeta_{SEA\min} + (\zeta_{SEA\min} - \zeta_{SEA\max}) \cdot \frac{ST_t - \zeta_{SEA,ST_2}}{\zeta_{SEA,ST_2} - \zeta_{SEA,ST_1} - 100\,^{\circ}\text{C}} & \text{if } \zeta_{SEA,ST_1} - 100\,^{\circ}\text{C} < ST_t < \zeta_{SEA,ST_2} \\
\zeta_{SEA\min} & \text{if } ST_t > \zeta_{SEA,ST_2}
\end{cases}
\tag{32}
$$

$$
ST_t = \sum_{i=t \bmod 365}^{t} \max\left(0\,^{\circ}\text{C}, T_i\right)
\tag{33}
$$

The seasonality factor starts to increases from $\zeta_{SEA\min}$ to $\zeta_{SEA\max}$ with a yearly accumulated temperature of above 200 $^{\circ}$C and reaches the maximum at $\zeta_{SEA,ST_1} - 200$ $^{\circ}$C. From $\zeta_{SEA,ST_1} - 100$ $^{\circ}$C to ζ_{SEA,ST_2} of the yearly accumulated the temperature the seasonality factor decreases from $\zeta_{SEA\max}$ to $\zeta_{SEA\min}$.

2.1.8 Species-specific senescence

Removal of plant biomass occurs through senescence and through management. The biomass removed by senescence S_{ts} [$\text{kg} \cdot \text{ha}^{-1}$] depends on the basic senescence rate α_{SEN} [month^{-1}], a seasonality factor SEN_t [$-$], an effect of specific leaf area of the species sla_s [$\text{m}^2 \cdot \text{g}^{-1}$], and the biomass of the species B_{ts} [$\text{kg} \cdot \text{ha}^{-1}$]:

$$
S_{ts} = \left(1 - (1 - \alpha_{SEN})^{1/30.44}\right) \cdot SEN_t \cdot \left(\frac{sla_s}{\phi_{sla}}\right)^{\beta_{SEN,sla}} \cdot B_{ts}
\tag{34}
$$

While the basic senescence rate and seasonality factor are consistent across the plant community, the contribution of specific leaf area and biomass to the senescence rate varies between species. To facilitate interpretation, we have chosen to use the basic senescence rate per month α_{SEN}. Consequently, α_{SEN} has been converted to a senescence rate per day, assuming a monthly duration of 30.44 days. The influence of specific leaf area on senescence is controlled by two parameters: ϕ_{sla} [$\text{m}^2 \cdot \text{g}^{-1}$] and $\beta_{SEN,sla}$ [$-$]. $\beta_{SEN,sla}$ controls how much the senescence rate differs between species. If $\beta_{SEN,sla}$ is zero, there is no difference, and if $\beta_{SEN,sla}$ is large, there is a large difference in senescence rate between species. ϕ_{sla} is used as a reference for the specific leaf area values: if $sla_s < \phi_{sla}$ the senescence rate is less than α_{SEN}, if $sla_s = \phi_{sla}$ the senescence rate is equal to α_{SEN} and if $sla_s > \phi_{sla}$ the senescence rate is greater than α_{SEN}. We included the effect of specific leaf on senescence rate because plant species with high specific leaf area are at the fast end of the leaf economic spectrum. This means that they tend to be highly photosynthetically efficient, modelled here with a higher leaf area index per biomass, but have a short leaf lifespan and therefore a high senescence rate (Reich et al., 1992; Wright et al., 2004; Onoda et al., 2017).

A seasonality factor is used to account for the higher senescence in autumn. Depending on the cumulative temperate since the beginning of the current year ST_t [$^{\circ}$C] (Eq. 33) the seasonality factor increases from one [$-$] to a maximum

$\psi_{SEN\,max}$ [$-$]:

$$SEN_t = \begin{cases} 1 & \text{if } ST_t < \psi_{SEN,ST_1} \\ 1 + (\psi_{SEN\,max} - 1)\frac{ST_t - \psi_{SEN,ST_1}}{\psi_{SEN,ST_2} - \psi_{SEN,ST_1}} & \text{if } \psi_{SEN,ST_1} < ST_t < \psi_{SEN,ST_2} \\ \psi_{SEN\,max} & \text{if } ST_t > \psi_{SEN,ST_2} \end{cases} \tag{35}$$

where ψ_{SEN,ST_1} [$°C$] and ψ_{SEN,ST_2} [$°C$] are the temperature thresholds at which the seasonality factor starts to increase and reaches its maximum, respectively. The equation and the parameter values are based on Moulin et al. (2021) which is turn based on Jouven et al. (2006).

2.1.9 Biomass removal due to management

Biomass losses M_{ts} [$kg \cdot ha^{-1}$] due to management are caused by mowing MOW_{ts} [$kg \cdot ha^{-1}$] (Eq. 37) and grazing GRZ_{ts} [$kg \cdot ha^{-1}$] (Eq. 38) :

$$M_{ts} = MOW_{ts} + GRZ_{ts} \tag{36}$$

The biomass removed by mowing MOW_{ts} [$kg \cdot ha^{-1}$] depends on the cutting height of the mowing machine and the height of the plant species. The proportion of above-ground plant biomass removed by mowing is defined by calculating the fraction of the plant height H_{ts} [m] above the cutting height CUT_t [m] (see Table A3):

$$MOW_{ts} = \frac{\max(H_{ts} - CUT_t, 0)}{H_{ts}} \cdot B_{A,ts}, \tag{37}$$

thereby assuming a uniform distribution of the biomass along the height of the plant.

The amount of biomass of one species that is fed by grazers depends on the livestock density, the palatability of the plant species that is linked to the leaf nitrogen content and the height of the plants. The grazing function GRZ_{ts} [$kg \cdot ha^{-1}$] is divided into two parts: the first part defines the total grazed biomass and the second part the proportion between the grazed biomass of each species and the total grazed biomass:

$$GRZ_{ts} = \frac{\kappa_{GRZ} \cdot LD_t \cdot (B_{F,t})^2}{(\kappa_{GRZ} \cdot LD_t \cdot \eta_{GRZ})^2 + (B_{F,t})^2} \cdot \frac{LNC_{GRZ,ts} \cdot H_{GRZ,ts} \cdot B_{F,ts}}{\sum_{i=1}^{S} LNC_{GRZ,ti} \cdot H_{GRZ,ti} \cdot B_{F,ti}} \tag{38}$$

The variables and parameters are explained in the following two paragraphs.

For the total grazed biomass, we assume that grazers can only feed on plant biomass that is above a certain height $\epsilon_{GRZ,\min H}$ [m] (usually set to $0.05\,m$), because it has been shown that the intake rate of cattle decreases strongly with low sward height (Hirata et al., 2010; Silva et al., 2018; Kunrath et al., 2020; Boval and Sauvant, 2021). Therefore, we calculate the above-ground biomass that can be fed by grazers $B_{F,ts}$ [$kg \cdot ha^{-1}$] with the proportion of the above-ground biomass that is above the height $\epsilon_{GRZ,\min H}$:

$$B_{F,ts} = \max\left(1 - \frac{\epsilon_{GRZ,\min H}}{H_{ts}}, 0\right) \cdot B_{A,ts} \tag{39}$$

$$B_{F,t} = \sum_{s=1}^{S} B_{F,ts} \tag{40}$$

where $B_{F,t}$ [kg $\cdot$ ha^{-1}] is the total above-ground biomass that can be consumed by grazers. Furthermore, we assume that
if the overall reachable above-ground biomass is low, the farmers will gradually increase the supply of additional fodder
resulting in less grazed biomass. If no reachable above-ground biomass is left, the farmers will fully compensate the
requirements of the livestock animals. We do not include the fodder supply as an input in the model, but rather calculate it
based on the above-ground biomass that is available to grazers. To incorporate this, we use a function that works similarly
to a Holling type III response curve. The consumption of the grazers is determined by the product of the livestock density
LD_t [LU $\cdot$ ha^{-1}] (see Table A3) and the consumption per livestock and day κ_{GRZ} [kg $\cdot$ ha^{-1}]. We assume that the fodder
supply equals half of the consumption of the grazers if the reachable above-ground biomass is equal to $LD_t \cdot \kappa_{GRZ} \cdot \eta_{GRZ}$.
The parameter η_{GRZ} [$-$] is a scaling parameter in the term. For example, if η_{GRZ} equals two, the total grazed biomass is
reduced to half of the consumption at a reachable above-ground biomass that equals two times the consumption of the
grazers.

The distribution of grazed biomass among plant species depends on their leaf nitrogen content, height, and the biomass
accessible to grazers. The leaf nitrogent content factor $LNC_{GRZ,ts}$ [$-$] is based on the trait leaf nitrogen content per leaf
mass lnc_s [mg $\cdot$ g^{-1}] relative to the community-weighted mean leaf nitrogen content per leaf mass $LNC_{cwm,t}$ [mg $\cdot$ g^{-1}]

$$LNC_{GRZ,ts} = \left(\frac{lnc_s}{LNC_{cwm,t}} \right)^{\beta_{GRZ,lnc}} \tag{41}$$

$$LNC_{cwm,t} = \sum_{s=1}^{S} \frac{B_{F,ts}}{B_{F,t}} \cdot lnc_s \tag{42}$$

with $\beta_{GRZ,lnc}$ [$-$] acting as a scaling exponent that defines how strongly the $LNC_{GRZ,ts}$ values deviate from one. This
parameter thus controls the strength of the grazer's preference for plant species with high leaf nitrogen content. Empirical
studies have demonstrated that cattle prefer plant species with high leaf nitrogen content (Pauler et al., 2020; Atkinson
et al., 2024) and a high carbon to nitrogen ratio in leaves is associated with a grazing avoidance strategy (Archibald et al.,
2019). Furthermore, we include a height factor because grazers feed more on plants that are tall and easily reachable
(Hodgson et al., 1994). The height factor $H_{GRZ,ts}$ follows a similar equation as the leaf nitrogen factor, utilizing plant
species H_{ts} in place of leaf nitrogen content relative to the community-weighted mean height $H_{cwm,t}$ [m] and scaled by
the exponent $\beta_{GRZ,H}$ [$-$]. In summary, the distribution of grazed biomass among plant species is driven by the biomass
of the plant species, but can be altered by their relative leaf nitrogen content and height.

2.2 Plant height dynamics

Plant height H_{ts} increases due to growth but decreases with mowing and grazing. The height can increase until the plant
reaches the maximum height $maxheight_s$ [m]. The growth rate is the ratio of above-ground biomass growth $A_{ts} \cdot G_{act,ts}$
(Eq. 3) to above-ground biomass $B_{A,ts}$. We consider the proportion of mown MOW_{ts} (Eq. 37) or grazed biomass GRZ_{ts}
(Eq. 38) on the above-ground biomass as the proportion of height lost, assuming an even distribution of biomass along
the height of the plant. Since leaves can die without reducing height, we assume that senescence has no effect on plant

height:

$$H_{t+1s} = H_{ts} \cdot \left(1 + \frac{A_{ts} \cdot G_{act,ts}}{B_{A,ts}} - \frac{MOW_{ts}}{B_{A,ts}} - \frac{GRZ_{ts}}{B_{A,ts}} \right) \tag{43}$$

2.3 Soil water dynamics

The change in the soil water content is influenced by multiple factors, including precipitation, evaporation, transpiration, and drainage and surface run-off. The equations follow Moulin et al. (2021) that are based on Schapendonk et al. (1998). The change in the soil water content W_t [mm] is described by

$$W_{t+1} = W_t + P_t - AET_t - R_t \tag{44}$$

where P_t is the precipitation [mm], AET_t is the actual evapotranspiration [mm], and R_t is the surface run-off and drainage of water from the soil [mm].

How strongly the soil surface is covered by vegetation influence whether more evaporation or transpiration occurs. This is modelled by the total leaf area index $LAI_{tot,t}$ (Eqs. 9,10). If the soil is barely covered with vegetation, evaporation is higher than transpiration. Conversely, if the soil is well covered with vegetation, transpiration is higher than evaporation. Water can continue to evaporate from the soil as long as it contains water. Therefore, the potential evapotranspiration PET_t [mm], which is a forcing function influencing both evaporation and transpiration (see Table A3), is multiplied by the fraction between the soil water content W_t and the water holding capacity WHC [mm] (Eq. 51) to obtain the evaporation E_t:

$$E_t = \frac{W_t}{WHC} \cdot PET_t \cdot \left[1 - \min\left(1, \frac{LAI_{tot,t}}{3} \right) \right] \tag{45}$$

On the other hand, plants can only transpire water that is available to them, so transpiration can only deplete the soil water content to the permanent wilting point. Therefore, the soil water content is rescaled by the permanent wilting point PWP [mm] (Eq. 52) and the water holding capacity WHC [mm] (Eq. 51) to a factor between zero and one that influences the amount of transpiration TR_t:

$$TR_t = \max\left(0, \frac{W_t - PWP}{WHC - PWP} \right) \cdot PET_t \cdot \min\left(1, \frac{LAI_{tot,t}}{3} \right) \tag{46}$$

Additionally, in contrast to Moulin et al. (2021), the transpiration depends here on a factor of the community-weighted mean specific leaf area SLA_t [m$^2 \cdot$ g^{-1}]. It was shown that species reduce the specific leaf area under drought stress (Wright et al., 1993; Liu and Stützel, 2004) most likely to reduce transpiration. Therefore, it is here assumed that thinner leaves transpire more water. This relationship is modelled by the parameter $\alpha_{TR,sla}$ [m$^2 \cdot$ g^{-1}] that is the community-weighted mean specific leaf area where the factor equals one and $\beta_{TR,sla}$ [$-$] that simulates how strongly the factor deviates from one if the community-weighted mean specific leaf area is below or above $\alpha_{TR,sla}$.

The actual evapotranspiration AET_t [mm] is the sum of the evaporation E_t [mm] and the transpiration TR_t [mm] but cannot exceed the soil water content W_t [mm]:

$$AET_t = \min\left(W_t, E_t + TR_t \right) \tag{47}$$

and any excess water above the water holding capacity WHC [mm] (Eq. 51) is removed by surface run-off and drainage R_t [mm]:

$$R_t = \max\left(0\,\mathrm{mm}, W_t + P_t - AET_t - WHC\right) \tag{48}$$

Water holding capacity and permanent wilting point are derived from soil properties. Gupta and Larson (1979) show how the fraction of soil that can be filled with water F can be related to particle size distribution, organic matter content and bulk density for different matrix potentials. This fraction was calculated for a matrix potential of -7 kPa for the water holding capacity ($F_{WHC,}$) and for a matrix potential of -1500 kPa for the permanent wilting point ($F_{PWP,}$). The respective fraction was multiplied by the rooting depth to derive the water holding capacity and the permanent wilting point for the part of the soil that plants can reach with their roots:

$$F_{WHC} = \beta_{SND,WHC} \cdot SND + \beta_{SLT,WHC} \cdot SLT + \beta_{CLY,WHC} \cdot CLY +$$
$$\beta_{OM,WHC} \cdot OM + \beta_{BLK,WHC} \cdot BLK \tag{49}$$

$$F_{PWP} = \beta_{SND,PWP} \cdot SND + \beta_{SLT,PWP} \cdot SLT + \beta_{CLY,PWP} \cdot CLY +$$
$$\beta_{OM,PWP} \cdot OM + \beta_{BLK,PWP} \cdot BLK \tag{50}$$

$$WHC = F_{WHC} \cdot RD \tag{51}$$

$$PWP = F_{PWP} \cdot RD \tag{52}$$

3 Calibration and validation of the model

We calibrated and evaluated the model performance independently using two datasets. Firstly, we used an experimental dataset on the biomass production of a single species to compare intraannual observations and simulations (see Section 3.1). Secondly, we compared the observed and simulated interannual dynamics in terms of both the biomass production and the plant functional composition in plant communities, using a dataset of real managed grasslands (see Section 3.2).

3.1 FAO dataset - seasonal dynamics of productivity
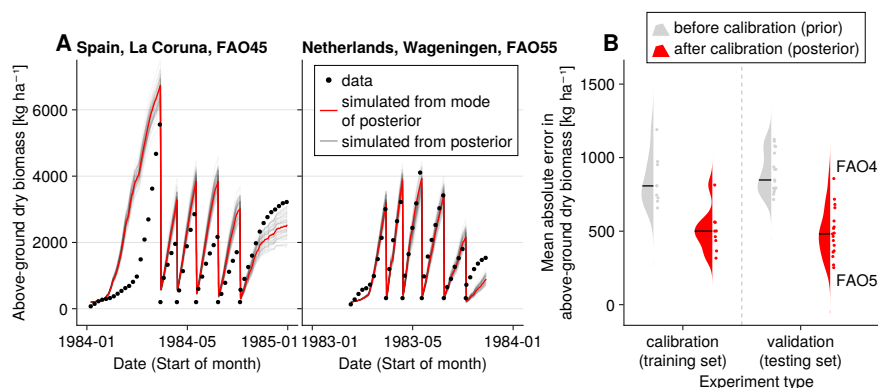
Figure 4. Time series from the independent validation experiments with the highest (FAO45) and the lowest (FAO55) mean absolute error in predicting the above-ground dry biomass of the FAO dataset (panel A). Predictions from the mode of the posterior distribution (maximum a posteriori estimate) and predictions from draws of the posterior distribution are shown to compare them with the measured above-ground biomass. In addition, the mean absolute error between the predicted and observed biomass is shown separately for the calibration (training set) and validation (testing set) experiments, both before and after calibration (panel B). The mean absolute error is calculated for each observation and then averaged across each experiment. The improvement in prediction before calibration, based on the mean error calculated with 50 draws from the prior distribution, is compared to the error after calibration, based on the mean error calculated with 50 draws from the posterior distribution.

First, we used the dataset of the project "Predicting production from grassland" in the framework of an FAO Subnetwork for lowland grassland, which was carried out from 1982 to 1986. The dataset was used to calibrate the LINGRA grassland model (Schapendonk et al., 1998) and is described in detail in Bouman et al. (1996). The project consisted of several sites across Europe in which the productivity of the grass *Lolium perenne* L. was measured weekly over one year. For some sites, experiments were repeated over several years. All experiments were fertilized and we only used the irrigated experiments to evaluate whether our model can predict for one species the seasonal patterns under growth conditions with high water and nutrient supply. No site-specific soil data was measured, nor is it required for the model simulation without water and nutrient limitation. We used site-specific climate data that was supplied with the dataset. We used the trait data for *Lolium perenne* that we prepared for the Biodiversity Exploratories dataset (for details see Appendix C). We used initial

values for *Lolium perenne* of 200 $\mathrm{kg \cdot ha^{-1}}$ and 250 $\mathrm{kg \cdot ha^{-1}}$ for above-ground and below-ground biomass, respectively, as well as an initial height of 0.4 $\mathrm{kg \cdot ha^{-1}}$. We selected the initial values so that the simulated above-ground biomass is close to the first data point. The 26 experiments were split into nine experiments for calibration and 17 experiments for validation (see Table A7). We calibrated the parameters for senescence (α_{SEN}, $\psi_{SEN\,max}$, ϕ_{SEN,ST_1}, and ϕ_{SEN,ST_2}),

540   seasonality in growth ($\zeta_{SEA\,min}$, $\zeta_{SEA\,max}$, ζ_{SEA,ST_1}, and ζ_{SEA,ST_2}) and for the reduction factor of radiation use efficiency based on the community height ($\alpha_{RUE,cwmH}$). All other parameters were kept constant (for their parameter values see Table A4).

We applied the Haario-Bardenet Adaptive Markov Chain Monte Carlo method (Haario et al. 2001; Johnstone et al. 2016, as implemented in Clerx et al. 2019) for calibrating our parameters given the priors and the experimental data (for

545   technical details see Appendix E). We set moderately informative priors (for details see Table A6) that were based on the values used by Jouven et al. (2006) and Moulin et al. (2021). We used a likelihood function based on a normal distribution, where the mean is given by the simulated above-ground biomass, the measured above-ground biomass is treated as the data, and the variance is a parameter estimated during calibration. We calculated the total likelihood as the product of the likelihoods over all time points and all nine experiments. During the calibration, we reset the simulated above-ground

550   biomass after evaluating the likelihood for one time point to the measured above-ground biomass (see Figure 5 step 3). This approach allowed us to assess how well the model can predict changes in biomass from one data point to the next, given a set of parameters.

After the calibration, our model can reproduce the seasonal patterns for the species *Lolium perenne* for independent validation sites across Europe satisfactory well (see Figure 4). The mean absolute error in above-ground biomass was

555   reduced from approximately 750 $\mathrm{kg \cdot ha^{-1}}$ of the prior to 500 $\mathrm{kg \cdot ha^{-1}}$ of the mode of the posterior (respectively the median of all validation experiments). The uncertainty in the posterior estimates of parameters was reduced greatly compared to the prior (see Figures A1 and A2). Therefore, also the uncertainty in the prediction from the prior compared to predictions from the posterior was lowered clearly (see Figure A3).

We identified the parameter groups to which the above-ground biomass of *Lolium perenne* is most sensitive to small

560   changes in parameter values (local sensitivity analysis, for details see Table A12). These groups are about the radiation use efficiency (γ_{RUEmax}, $\gamma_{RUE,k}$, $\gamma_{RAD,1}$ and $\alpha_{RUE,cwmH}$), the seasonal adjustment for growth ($\zeta_{SEA\,min}$ and $\zeta_{SEA\,max}$) and senescence ($\beta_{SEN,sla}$ and α_{SEN}).

3.2   Biodiversity Exploratories dataset - dynamics of community traits and biomass

Second, we used data from the Biodiversity Exploratories project (Fischer et al., 2010). It is an observational dataset

565   of permanent grassland sites from three different regions in Germany, and we used the subset from 2006 to 2022. Farmers documented their land use practices, and vegetation composition and above-ground biomass were documented annually by researchers. We assessed whether our model could reproduce patterns in total biomass production and in the development of the community trait distribution. We used site-specific climate, management and soil data (for details on data preparation and references see Appendix C). In total, 150 sites are included the project. We selected those that
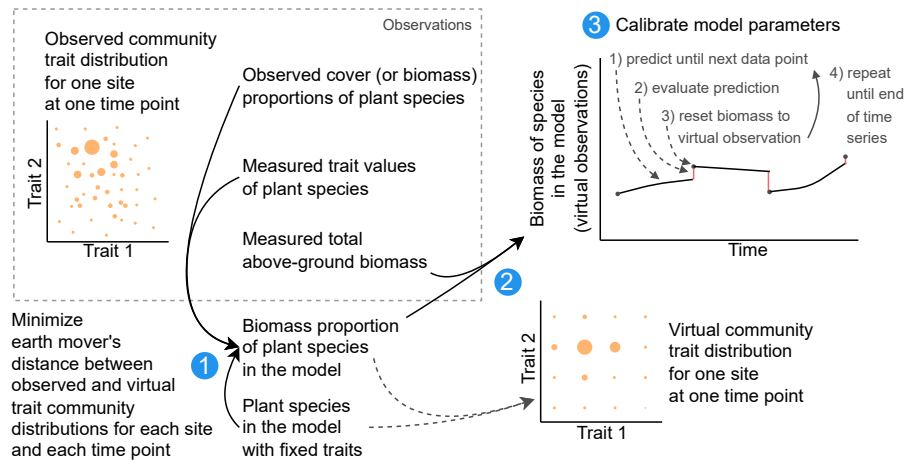
Figure 5. Calibration workflow. For the Biodiversity Exploratories dataset, we reduced the number of species from 70 to 25 to lower the computation time in the calibration. We created virtual observations for the 25 species by finding the biomass proportion of the 25 species so that the community trait distribution closely resembles the trait distribution of the community with 70 species (step 1). The biomass proportion of the 25 species can be multiplied with the measured total biomass to create virtual observations for our modelled species (step 2). For the calibration of the global model parameters, the model can be used to simulate a trajectory for one parameter combination. The simulated trajectory is compared with the virtual observation to calculate the likelihood and then reset to the virtual observation. Due to the resetting, we can evaluate how good is the model in predicting from one observation to another. We evaluate the likelihood starting from the second data point to minimise the influence of the initial values, which were not calibrated (step 3). The resetting is not used for the evaluation of the model after the calibration. For the calibration with the FAO dataset, only one species was grown and is simulated and therefore we only used step 3 for the calibration.

570 were mainly used as meadows (mown) or a mixture of pasture (grazed) and meadow and excluded those that were used as pasture only, resulting in 92 sites over all three regions. We decided to exclude the pasture sites because farmers often decided to provide supplementary feeding on these sites and the information on supplementary feeding is not detailed enough to be included in the simulation model. The 82 sites were split into 12 sites for calibration and 70 sites for validation (see Tables A9, A10, and A11). For calibration, we selected four sites from each of the three regions, some 575 of which were mown only, while others were grazed and mown. We calibrated parameters of the water growth reducers ($\alpha_{WAT,rsa,05}$ and $\delta_{WAT,rsa}$), nutrient growth reducers ($\alpha_{NUT,rsa,05}$, $\alpha_{NUT,amc,05}$, $\delta_{NUT,rsa}$ and $\delta_{NUT,amc}$), investment into roots ($\kappa_{ROOT,rsa}$ and $\kappa_{ROOT,amc}$) and the reference traits that influence all just mentioned processes (ϕ_{TRSA} and ϕ_{TAMC}). All other parameters were kept constant and are based on literature, based on the calibration with the FAO dataset, or are set manually by comparing simulated trajectories with measured data of the calibration sites.

580 We compiled trait data for 70 plant species that occurred on the Biodiversity Exploratories sites partly from measurements from the project and partly from trait databases (for details see Appendix C). For the calibration, we wanted to lower the computation time. That is why we reduced the number of plant species to 25 by applying hierarchical clustering and
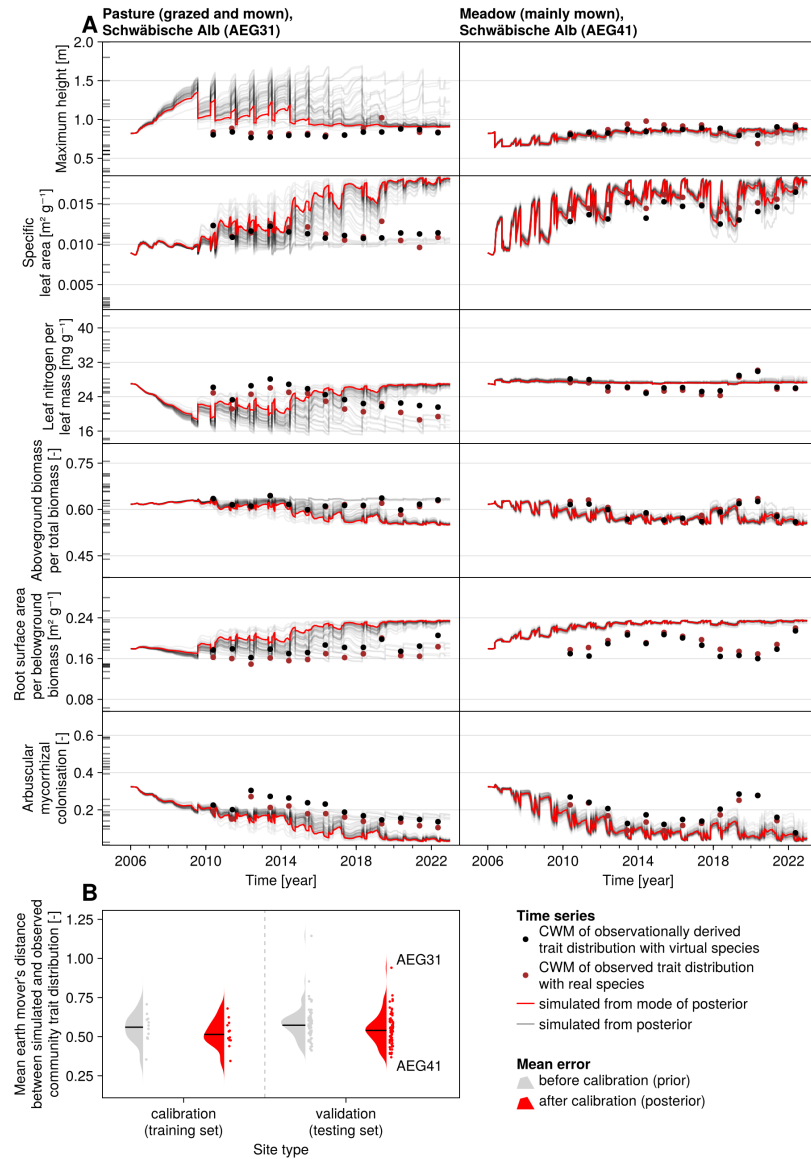
Figure 6. Time series of the community weighted mean (CWM) trait values for the independent validation sites with the highest (AEG31) and the lowest (AEG41) mean absolute error for the distance between simulated and observationally derived community trait distribution (panel A). Predictions from the mode of the posterior (maximum a posteriori estimate) and from draws from the posterior distribution are shown to compare them with the observationally derived community weighted mean traits. In addition, the mean absolute error between predicted and observationally derived community trait distribution is shown separately for the calibration (training set) and validation (testing set) sites, both before and after calibration (panel B). The mean absolute error is calculated for each observation and then averaged across each site. The predictive performance before calibration, based on the mean error calculated with 50 draws from the prior distribution, is compared to the error after calibration, based on the mean error calculated with 50 draws from the posterior distribution.
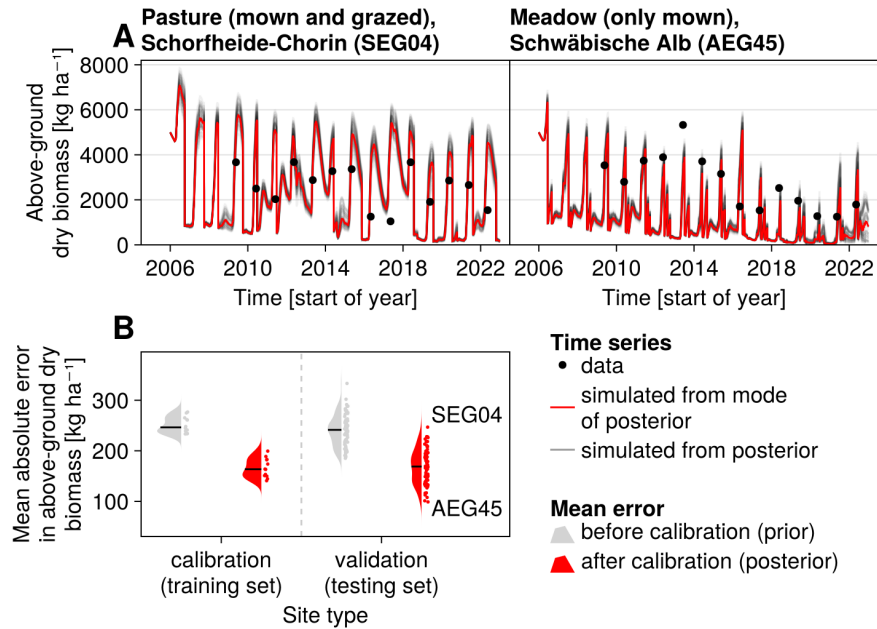
Figure 7. Time series from the independent validation sites with the highest (SEG04) and the lowest (AEG45) mean absolute error in predicting the above-ground dry biomass of the Biodiversity Exploratories dataset (panel A). Predictions from the mode of the posterior distribution (maximum a posteriori estimate) and draws from the posterior distribution are shown to compare them with the measured above-ground biomass. In addition, the mean absolute error between predicted biomass and measured biomass is shown separately for the calibration (training set) and validation (testing test) sites, both before and after calibration (panel B). The mean absolute error is calculated for each observation and then averaged across each site. The predictive performance before calibration, based on the mean error calculated with 50 draws from the prior distribution, is compared to the error after calibration, based on the mean error calculated with 50 draws from the posterior distribution.

calculating the mean trait values for the 25 groups (for details see Appendix C1). Lowering the number of species did not change the general patterns in community dynamics (see Figure A4). We derived virtual observations for these 25 virtual

585   plant species by finding a community trait distribution with the 25 virtual species that closely ressembles the community trait distribution with the 70 species by minimizing the earth mover's distance (also called Wasserstein distance, Rubner et al. 2000) between these two community trait distributions (for details about distance between community trait distributions see Appendix D). Thereby, we optimized the relative abundance of the 25 virtual species (see step 1 in Figure 5) and calculated the biomass of each virtual species by multiplying the relative abundance with the total biomass (see step

590   2 in Figure 5). These virtual observations help to reset the biomass of the simulated species after the evaluation of the likelihood for one time point (see step 3 in Figure 5). We used a likelihood function based on a normal distribution with zero mean, where the distance between the simulated and the observationally derived community trait distribution (our virtual observations), as calculated by the earth mover's distance, is treated as the data, and the variance is a parameter

estimated during calibration. We did not use the total above-ground biomass in the calibration, but evaluated it after the calibration. We used the same Markov Chain Monte Carlo method as for the calibration with FAO dataset to derive the posterior distribution for the parameters.

Each species is initialised with the same above- and below-ground biomass (200 $\mathrm{kg \cdot ha^{-1}}$) and a height equal to half of their maximum height. This sets the total biomass at a rather high initial value (5000 $\mathrm{kg \cdot ha^{-1}}$ of above-ground biomass in winter; see Figure 7). Environmental conditions, management practices and biotic interactions with other plant species lead to the site-specific community assembly. While the biomass of most simulated species decreases rapidly due to their functional traits, the biomass of a few species increases over time.

The calibration resulted in a slight decrease in the mean absolute error for predicting the community trait distribution (see Figure 6) and greatly reduced the mean absolute error for predicting the above-ground biomass (see Figure 7). The time series of the community weighted mean traits for the independent validation sites with the lowest distance between predicted and observationally derived community trait distribution (AEG41 in Figure 6) show that the general trends are captured well for all traits except the root surface area per below-ground biomass. For the site with highest error in predicting the community trait distribution (AEG31 in Figure 6), the trend for for most community weighted mean traits are not well captured. The development of the whole community trait distribution over time for the same sites show that the simulated functional diversity is lower than the observed functional diversity (variance in the community trait distributions, see Figures A8, A9 and A10). For most data points, the simulated and measured total above-ground biomass at the independent validation sites with the highest and lowest predictive error correspond closely (see Figure 7).

We applied a local sensitivity analysis and calculated the sensitivity of the total above-ground biomass to small changes of parameter values (for details see Table A13). We identified that the total above-ground biomass is most sensitive to changes in parameters dealing with senescence (ϕ_{sla}, α_{SEN} and $\beta_{SEN,sla}$), the calculation of the permanent wilting point and the water holding capacity ($\beta_{CLY,PWP}$, $\beta_{SLT,WHC}$ and $\beta_{CLY,WHC}$), radiation use efficiency (γ_{RUEmax}, $\gamma_{RUE,k}$ and $\alpha_{RUE,cwmH}$) and seasonal growth adjustment ($\zeta_{SEA\max}$ and $\zeta_{SEA\min}$).

4 Discussion

4.1 Validation of GrasslandTraitSim.jl

The validation of the GrasslandTraitSim.jl model demonstrated its ability to relate the morphological traits of plant species to their species-specific physiological and demographic rates. Changes in these rates lead to changes in species biomass and, consequently, changes in plant community composition. We proved that the model could satisfactorily reconstruct seasonal biomass production for one species, biomass production of plant communities, and with minor limitations, functional community composition for various grassland sites.

One of the key advantages of our modelling approach is that we can compare the simulated morphological trait distributions with measured morphological trait distributions at the community level. In contrast to previous grassland models (e.g., DynaGraM; Moulin et al. 2021 or GRASSMIND; Taubert et al. 2012) that require demographic or physiological rates as species-specific parameters, our model only requires commonly measured morphological traits (compare Figure 2). In this way, our model can be applied to a much larger set of species and communities for which such trait data are available from on-site measurements or databases.

In our model, we tried to keep a balance between a model that can reproduce the basic patterns in biomass production and functional community composition, but does not have too many global parameters, so that it is possible to calibrate all parameters with datasets that are readily available. However, already with the complexity that we presented here, it was not possible to calibrate all global parameters by the Markov Chain Monte Carlo method at once. We had to fix some parameter values beforehand manually, and we had to set informative priors on the parameters so that all chains from random starting positions of the prior distribution converged to the posterior distribution within a reasonable number of iterations.

In general, it was much easier to calibrate the model parameters with the FAO dataset, because biomass was measured weekly rather than annually, as was the case with the Biodiversity Exploratories' observations of biomass and composition. Annual observations are not optimal because many different trajectories, simulated by sets of parameter values, can lead to the same simulated point after one year. This highlights the need for datasets with several measurements per year for the calibration of process-based grassland models (Taubert et al., 2020). These detailed datasets could also reduce the widespread problem of parameter identifiability in the calibration of ecosystem models (Luo et al., 2009).

Another limitation of the Biodiversity Exploratories dataset is that we used species mean traits derived from the project or trait databases to calculate the community trait distribution (see Appendix C). However, using species mean traits results in the loss of intra-specific trait variability from the observations. We expect the realised community trait distributions to vary more between sites than is reflected in the dataset (Violle et al., 2012; Siefert et al., 2015).

We included grazing in our model because grazing is an important land use factor in semi-natural grasslands. Some of the grassland models did not take this factor into account (see Table 1 or A2). However, in this study, we were not able to fully calibrate and evaluate grazing in our model, as the sites of the Biodiversity Exploratories lack accurate data to quantify supplementary feeding. Supplementary feeding is an important factor, for example, on year-round grazing sites.

For the independent validation site with the highest error of the FAO dataset (FAO45 in Spain, see Figure 4), our model predicts too high above-ground biomass in spring. Thereby, we see that the model is not flexible enough to simulate production in a very wide range of regions. Our step function for seasonal growth adjustment assumes that the growth increases in spring after 200 °C have been accumulated (see Eq. 32). This might be a reasonable assumption for *Lolium perenne* in the Netherlands, but not for sites in Spain. The strong growth starts too early for the site in Spain. For the calibration of the LINGRA model with the same dataset, it was assumed that species-specific parameters are different for the northern and southern sites (Bouman et al., 1996). We did not calibrate the model here for spatial subsets of the sites, as we wanted to analyse whether our model is in general applicable to a variety of sites.

4.2 Discussion of the concept

We chose the morphological functional traits that represent main trade-offs in plant physiology. Rather than reflecting one process in detail with many traits (e.g., more traits dealing with water stress, such as stomatal conductance and rooting depth), we aimed to represent the following main trade-offs of plants: (1) The slow-fast continuum of the leaf economic spectrum states that plants with thinner leaves have a higher light use efficiency per unit of biomass, but also a higher senescence rates (as reflected by specific leaf area; Reich et al. 1992; Wright et al. 2004). (2) Taller plant species can overtop other plant species and are therefore less affected by shading. However, they are more susceptible to mowing and grazing (as reflected by maximum plant height; Díaz et al. 2007; Klimešová et al. 2008). (3) Investing in roots and mycorrhizae enhances nutrient and water uptake, but this comes at the cost of maintaining fine roots and the collaboration with mycorrhiza (as reflected by above-ground biomass per plant biomass, root surface per below-ground biomass, arbuscular mycorrhizal colonisation rate; Reich 2014; Prieto et al. 2015; Bergmann et al. 2020).

To some extent, our model can simulate intra-specific trait variability based on the functional representation rather than species identity. In our model, two simulated species can represent one species in the real world that exhibits different traits on different sites. However, this approach is not applicable to plant species whose traits change dynamically depending on variable environmental conditions. Furthermore, our model does not reflect changes in traits during the life stages of plant species.

The number of coexisting species (e.g., with biomass > 2 %) is rather low, with three to five species accounting for most of the biomass in most scenario analyses. This is a common challenge in grassland models. For example, in a model comparison study with the GRASSMIND and LPJmL models, it was noted that in a two-species simulation always one species always accounted for most of the biomass (Wirth et al., 2021). We noticed that by including a density-dependent senescence rate (not shown in the model equations above), the simulated functional diversity is increased, and the distance between modelled and observed community trait distributions can be lowered. A density-dependent senescence rate can be explained, for example, by negative plant-soil feedbacks (Bonanomi et al., 2005; Liu et al., 2022; Goossens et al., 2023). This shows the potential to explore in future studies how the incorporation of coexistence mechanisms can lead to more realistic predictions of functional community composition.

We argue that our model is well suited for analysing the effects of management (grazing, mowing and fertilization), of

685 edaphic factors (soil nitrogen, permanent wilting point and water holding capacity), and of climatic factors (temperature, radiation, potential evapotranspiration and precipitation) on the productivity and the functional composition of diverse plant communities of temperate semi-natural grasslands. We envisage the model as a useful tool for conducting scenario analyses (e.g., what would happen if the input X were to change, and why?), rather than as a model with superior predictive performance compared to conventional statistical models. For example, the influence of management type and

690 intensity on achieving a balance between creating highly productive grasslands and maintaining plant diversity could be analysed. Furthermore, the influence of the initial species composition on the productivity under fluctuating climate conditions (e.g., years with drought) could be studied by answering the question whether a more diverse community can buffer extreme climatic events. Moreover, we consider the potential application of including or excluding certain processes (e.g., a specific transfer function, which links traits to demographic rates) and analyse whether the agreement between

695 simulations and measured data improves.

5   Conclusions

700 We presented GrasslandTraitSim.jl, a process-based model that can be used to simulate the effects of land use and climate change on the plant functional composition and biomass production of permanent semi-natural grasslands. We have extended the approach of Chalmandrier et al. (2021) by linking measurements of morphological plant traits with demographic and physiological species-specific processes. Our model uses only morphological traits as species-specific inputs to simulate the biomass of many plant species over time. Therefore, the study is a step towards modelling highly diverse plant communities in grasslands. We hope that the accompanying documentation, tutorials, and open-source code will encourage collaboration and discussion on this topic.

Appendix A: Derivation of the species-specific water and nutrient growth reducers

705 The response curves (growth reducers) RED_{ts} for different nutrient and water availabilities, denoted as R_t, are implemented via logistic equations with a minimum of zero (no growth is possible) and a maximum of one (no growth reduction). While the species-specific part of the response curves is implemented by different inflection points $x_{0,RED,ts}$, the slope β_{RED} is the same for all species:

$$RED_{ts} = \frac{1}{1 + \exp\left(-\beta_{RED} \cdot (R_t - x_{0,RED,ts})\right)} \tag{A1}$$

710 We then used another logistic equation that relates the trait values to the inflection point of the response curve. We wanted to control how much the response curves should differ when the trait values differ from $x_{0,prep,s}$, this is implemented with the parameter δ_{RED}. The equation could be written as:

$$x_{0,RED,ts} = x_{0,RED,\min} + \frac{x_{0,RED,\max} - x_{0,RED,\min}}{1 + \exp\left(-\delta_{RED} \cdot (trait_{ts} - x_{0,prep,s})\right)} \tag{A2}$$

However, this equations and their parameter $x_{0,prep,s}$, $x_{0,RED,\min}$, and $x_{0,RED,\max}$ are hard to understand and to inter-
715 pret, therefore we reformulated the equation. Instead of calculating the inflection point $x_{0,RED,ts}$ directly, we calculated the growth reduction at 0.5 of the maximal resource availability:

$$RED_{05,ts} = \frac{1}{1 + \exp\left(-\delta_{RED} \cdot (trait_{ts} - x_{0,RED,05})\right)} \tag{A3}$$

This has the advantage that we have natural boundaries $\in [0, 1]$, because the growth reduction cannot be larger than one ($RED_{ts} = 0$) or lower than zero ($RED_{ts} = 1$). We introduce one parameter $\alpha_{RED,05}$ that is the growth reducer for the
720 mean trait ϕ_{trait} at half of the maximal resource availability:

$$\alpha_{RED,05} = \frac{1}{1 + \exp\left(-\delta_{RED} \cdot (\phi_{trait} - x_{0,R,05})\right)} \tag{A4}$$

and rearranged the equation to:

$$x_{0,R,05} = \frac{1}{\delta_{RED}} \cdot \log\left(\frac{1 - \alpha_{RED,05}}{\alpha_{RED,05}}\right) + \phi_{trait} \tag{A5}$$

This leads to an equation that we can use to calculate the growth reducer for all trait values at half of the maximal resource
725 availability:

$$RED_{05,ts} = \frac{1}{1 + \exp\left(-\delta_{RED} \cdot \left(trait_{ts} - \left(\frac{1}{\delta_{RED}} \cdot \log\left(\frac{1-\alpha_{RED,05}}{\alpha_{RED,05}}\right) + \phi_{trait}\right)\right)\right)} \tag{A6}$$

Now, we need again the full equation to calculate the growth reducer for any resource availability. We use the Equation A1 and solve for $x_{0,RED,ts}$ with $RED_{ts} = 0.5$:

$$RED_{05,ts} = \frac{1}{1 + \exp\left(-\beta_{RED} \cdot (0.5 - x_{0,RED,ts})\right)} \tag{A7}$$

730   to get the inflection point $x_{0,RED,ts}$:

$$x_{0,RED,ts} = \frac{1}{\beta_R} \cdot \log\left(\frac{1 - RED_{05,ts}}{RED_{05,ts}}\right) + 0.5 \tag{A8}$$

Thus, the full equation to calculate the growth reducer for any resource availability is:

$$RED_{ts} = \frac{1}{1 + \exp\left(-\beta_{RED} \cdot \left(R_t - \left(\frac{1}{\beta_{RED}} \cdot \log\left(\frac{1 - RED_{05,ts}}{RED_{05,ts}}\right) + 0.5\right)\right)\right)} \tag{A9}$$

and with everything combined and simplified:

735   $$RED_{ts} = \frac{1}{1 + \exp\left(-\beta_{RED} \cdot \left(R_t - \left[\frac{1}{\beta_{RED}} \cdot \left(-\delta_{RED} \cdot \left(trait_{ts} - \left(\frac{1}{\delta_{RED}} \cdot \log\left(\frac{1 - \alpha_{RED,05}}{\alpha_{RED,05}}\right) + \phi_{trait}\right)\right)\right) + 0.5\right]\right)\right)} \tag{A10}$$

Note the species-specific inflection point $x_{0,RED,ts}$ in square brackets.

Appendix B: Technical details of the GrasslandTraitSim.jl model

The model is implemented as a Julia package and can be used with the Julia programming language (Bezanson et al., 2017). It can be used on all major operating systems (Linux, MacOS, Windows). The model can be run on computers with low hardware requirements. For example, a 10-year simulation involving 70 species typically takes less than half a second to run on a standard personal computer. A graphical user interface allows you to manually change parameter values and see the influence of each parameter on the simulation results (explained in more detail in the online documentation, see data accessibility statement). The model can be run on headless systems, but then the graphical user interface is not available. Throughout the model, units are used directly in the programming code using Unitful.jl, making the model easier to understand and debug. The outputs of the model have labelled axes using DimensionalData.jl, making it easy to know which is the space, time or species axis. The package has extensive online documentation with all the equations, tutorials on how to set up the input data and how to analyse the output (see data accessibility statement). For each equation there are interactive plots to visualise the relationship between the variables and the influence of the parameters. Flowcharts are also available online to give a quick overview of the sub-processes. The model version described here can be installed in Julia using `import Pkg; Pkg.add("GrasslandTraitSim", version = "1.0.0")`. The newest version can be installed using the same command without the version argument. All dependencies will be installed with this command. The model is open-source and licensed under the GNU GPLv3. Contributions are welcome and can be made via GitHub. The development of the model is hosted at https://github.com/felixnoessler/GrasslandTraitSim.jl and new versions will be published in the General Julia package registry.

Appendix C: Detailed description and data preparation for the Biodiversity Exploratories dataset

We compiled input data for the model from different sources. Management data was used directly from the Biodiversity Exploratories project (timing and intensity of grazing and timing and height of mowing events and total fertilization of nitrogen per year, Vogt et al. 2024). The exact dates of grazing were not available, only the type of grazing, the number of days and the start and end month of a grazing period. We assumed different numbers of consecutive grazing days (2 for rotational grazing type I - "Portionsweide", rotational grazing, 5 for rotational grazing type II - "Umtriebsweide" and all days for permanent grazing) and distributed them equally over the whole grazing period. Potential evapotranspiration was used from AMBAV, an agro-meteorological model that outputs "potential evaporation over grass" from weather stations are in the three regions (DWD Climate Data Center, 2019) and is therefore the same for all sites of one region. Air temperature and precipitation were obtained for each site from the Biodiversity Exploraties project (Wöllauer et al., 2023). Photosynthetic activate radiation (PAR) was download with a three hours resolution from Wang (2021), the daily sum of PAR was obtained by calculating the integral of a quadratic regression to the PAR values. We calculated the PAR values per region. We created region-specific PAR inputs due to the coarse resolution of the PAR data. Soil texture (Schöning et al., 2021c), rooting depth (Herold et al., 2021), bulk density (Schöning et al., 2021d) and organic matter content (Schöning et al., 2021b) were used from soil sampling campaigns of the Biodiversity Exploratories project. The total nitrogen concentration was aggregated from four years to get a mean overall total nitrogen concentration (Schöning et al., 2021b, e, a; Schöning, 2023). The trait data was compiled from species that are present in grasslands of the Biodiversity Exploratories project. Leaf area and leaf dry weight was sampled from individuals from sites of the Exploratories (Prati et al., 2021) to calculate the specific leaf area. The root surface area per below-ground biomass, arbuscular mycorrhizal colonisation rate and above-ground biomass per total biomass were obtained from individuals that were grown in a greenhouse experiment on sand (Bergmann and Rillig, 2022). The maximum height was obtained from Jäger et al. (2017) and the leaf nitrogen per leaf mass from the TRY database (Kattge et al. 2020, mainly from Gubsch et al. 2010; Pakeman et al. 2008; Schroeder-Georgi et al. 2016). We decided to set leaf biomass per above-ground biomass to 80 % for all species, as values for the trait leaf biomass per plant biomass were not available for many species. For 70 species we had values for all the traits. We used a reduced set of 25 species as input for the simulation (see Appendix C1). During initialisation, the initial above-ground and below-ground biomass of 5000 $\mathrm{kg \cdot ha^{-1}}$ was evenly distributed across all species. The initial height was set to half of the maximum height of each plant species. The initial soil water content was set to 180 mm, which assumes no drought stress in the beginning of the simulation. For the calibration and validation data we used the cut above-ground biomass and the cover to compare observed and simulated community trait distributions. The biomass was cut once per year on every site at 4 cm height (Hinderling et al., 2024). Each year, the cover of plant species was estimated on an area of 16 $\mathrm{m^2}$ (Hinderling and Keller, 2023). Whereas we used input data from 2006 to 2022, we only used calibration data from 2010 to 2022 to allow for an initialisation phase of the grassland model.

C1 Reducing the number of species from 70 to 25 for the Biodiversity Exploratories dataset

For calibration, we reduced the number of simulated species from 70 to 25. We calculated new trait values for the 25 species by forming groups of species with similar trait values and calculating the mean trait values within each of the 25 groups. To do this, we first standardised the trait values by min-max normalisation to a range of [0, 1] to give each trait value equal weight in the distance calculation. We then calculated the Manhattan distance between all 70 species. We applied hierarchical clustering ("hclust" function from "stats" package, R Core Team 2024) and formed 25 groups and calculated the mean of the non-standardised trait values to obtain the trait values for 25 virtual species. A comparison of the simulated community dynamics with 70 and 25 species showed that lowering the number of species did not change the general community patterns (see Figure A4).

Appendix D: Calculating the distance between two community trait distributions

The earth mover's distance, which is also called Wasserstein distance, can be used to calculate the distance between two discrete distributions (Rubner et al. 2000; Villani 2009; Bernton et al. 2019, for applications in movement ecology see Potts et al. 2014; Kranstauber et al. 2017). The cost is computed as the product of the amount of probability mass transported and the distance it is moved. We used the implementation in the Python package "scipy" ("wasserstein_distance_nd" function, Virtanen et al. 2020). With this function the trait values of both distributions are given as "u_values" and "v_values" (matrices, each row with trait values for one species) and the respective cover or biomass proportions are given as "u_weights" and "v_weights". Always, when we write in the text, that we calculate the earth mover's distance, we standardise the trait value by z-score normalisation ($(x - \bar{x})/\text{std}(x)$) to give all traits an equal weight in the calculation.

Appendix E: Technical details on running the MCMC routine

For both datasets, we used the Haario-Bardenet Markov Chain Monte Carlo with the Python software package PINTS (Clerx et al., 2019). We called our Julia package GrasslandTraitSim.jl from Python. We ran four independent chains for 810 75 thousand iterations (150 thousand for FAO dataset) and discarded the first half of the iterations as warm-up. The first five thousand iterations were used as an adaption free initial phase. We checked that all four chains converged to the same posterior region by visually examining the trace plots (see Figures A2 and A7) and by checking that all rhat values were less than 1.01 (not shown, Vehtari et al. 2021). We compared how much the posterior shifted in comparison to the prior densities and interpreted it as how much uncertainty was reduced. We also compared how much uncertainty was 815 reduced while simulating trajectories with GrasslandTraitSim.jl from the prior and from the posterior (comparing the prior predictive with the posterior predictive distribution).

For both datasets, we used the one step ahead prediction method (predict until next datapoint, evaluate prediction, reset state variables to data point and repeat procedure). By using this method and not explicitly estimating the hidden state of the above-ground biomass (e.g., by a state space model), we ignored the observational error and only considered 820 the process error. We assumed that the observational error is small and decided to keep the calibration method simpler by not estimating the hidden states.
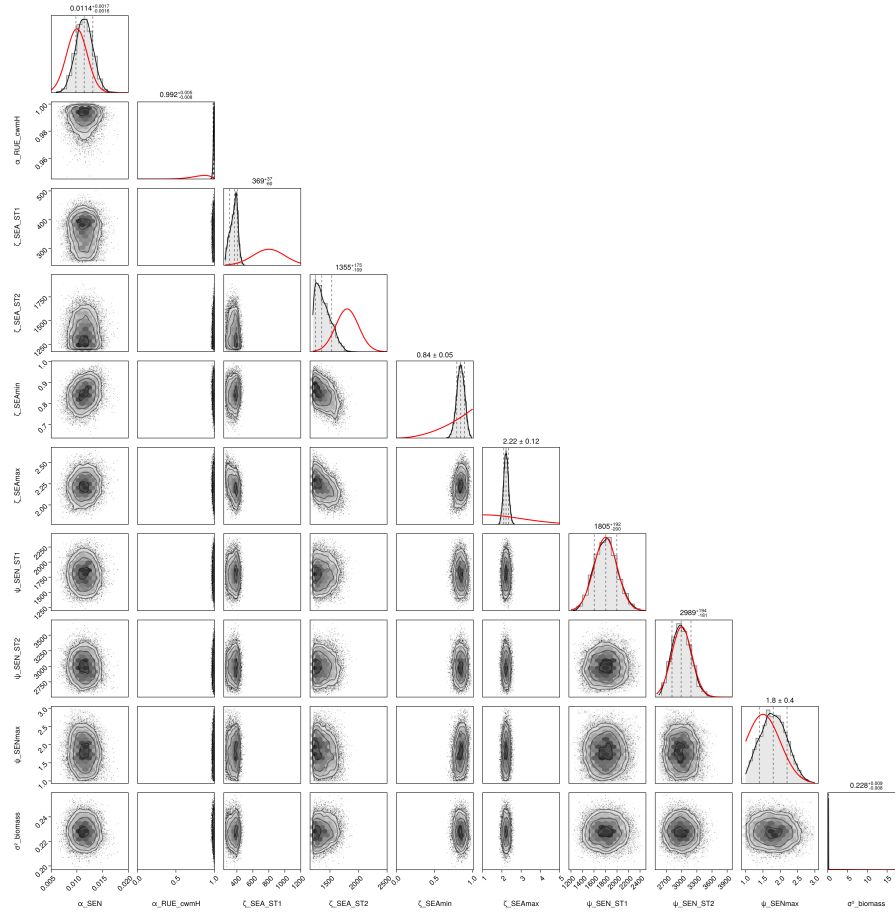
Figure A1. Pair plot of the posterior densities for the calibration with the FAO dataset. In the right upper plots, the marginal posterior densities (histograms) are shown together with the prior densities (red lines). The first half of the iterations were discarded as warm-up.
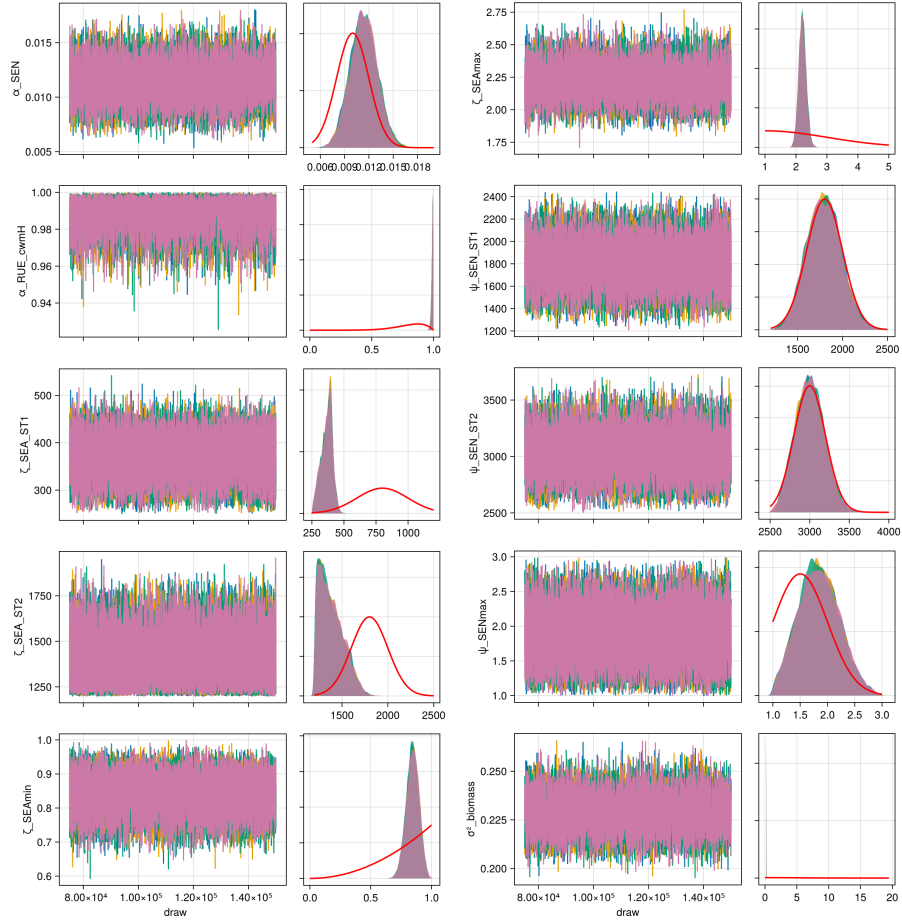
Figure A2. Trace plot, prior and posterior densities for the calibration with the FAO dataset. Different colours represent the different MCMC chains. In the density plot, the prior density (red line) and the posterior densities are visible. The first half of the iterations were discarded as warm-up.
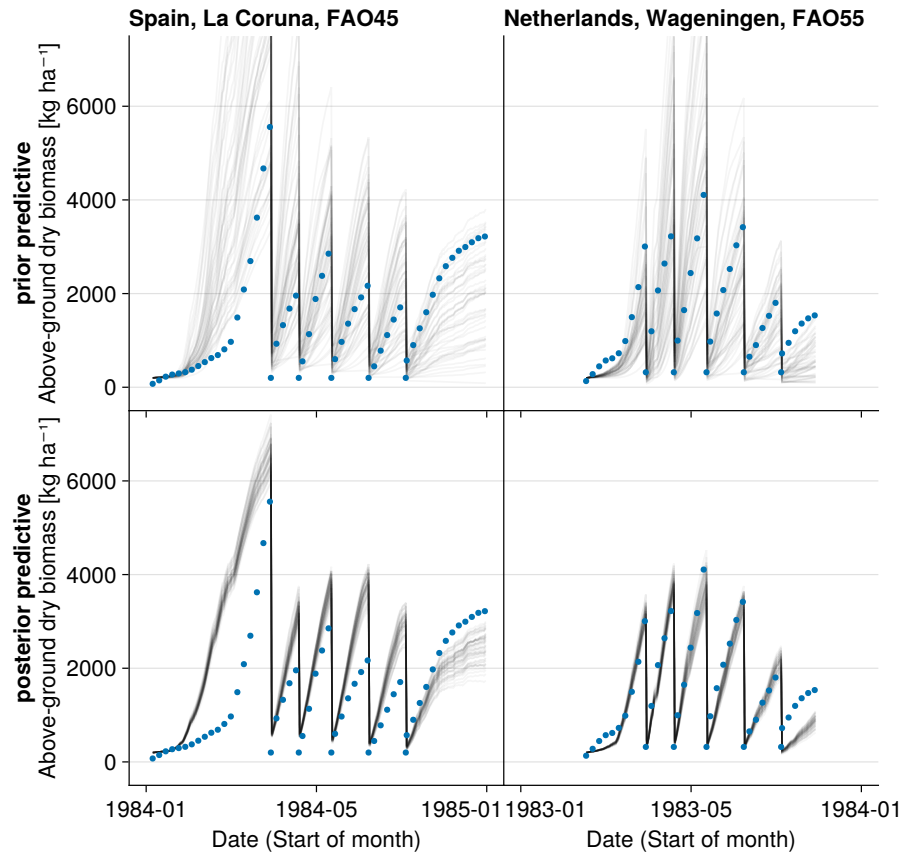
Figure A3. Prior and posterior predictive checks for the FAO dataset. Simulations with parameters drawn from the prior distribution or from the posterior distribution (grey lines) are compared to measured above-ground biomass (blue dots).
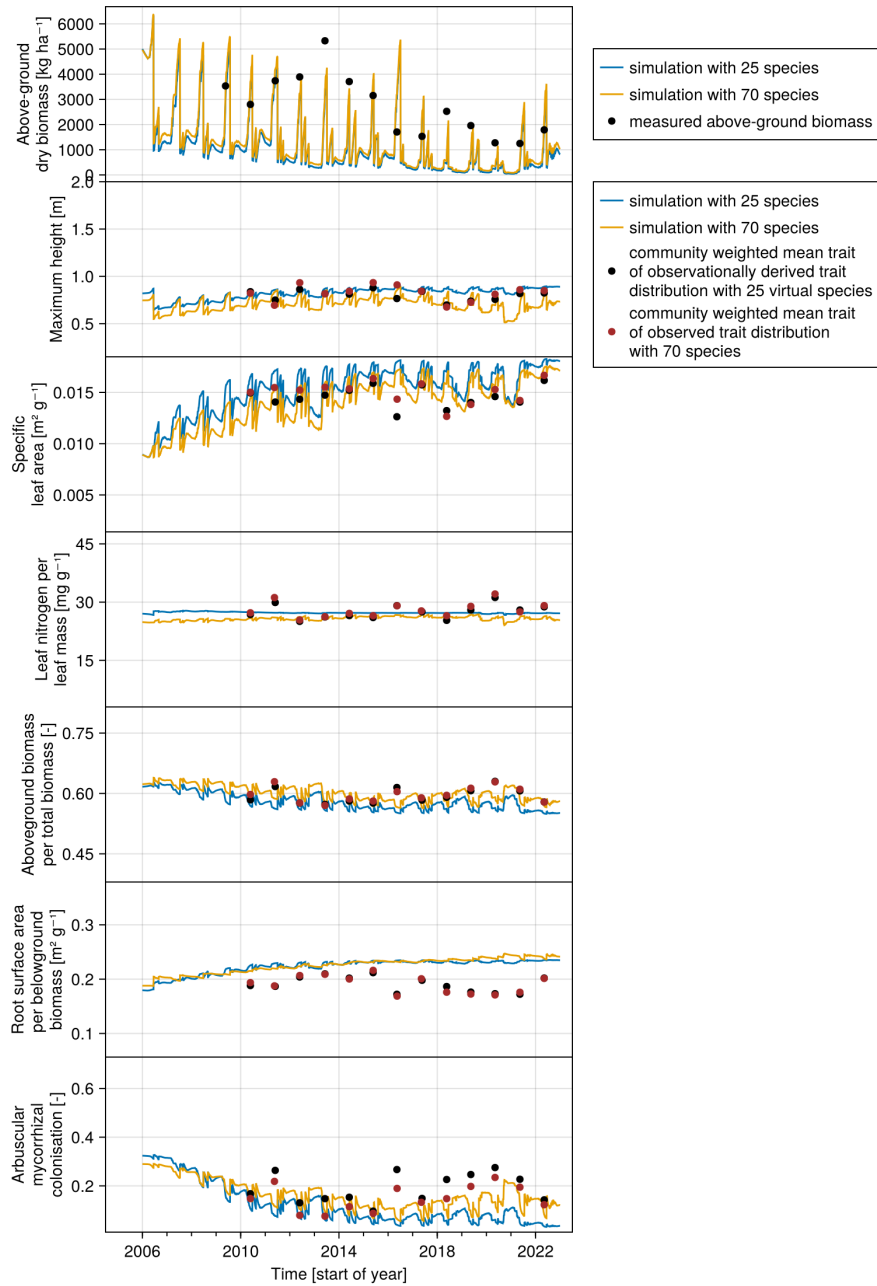
Figure A4. Comparison of community dynamics (above-ground biomass and community weighted mean traits) with 70 species and with the reduced set of 25 species. The trait values of the 25 species were derived by calculating mean trait values of 25 groups that were built from the dataset with the trait values of all 70 species (see Appendix C1).
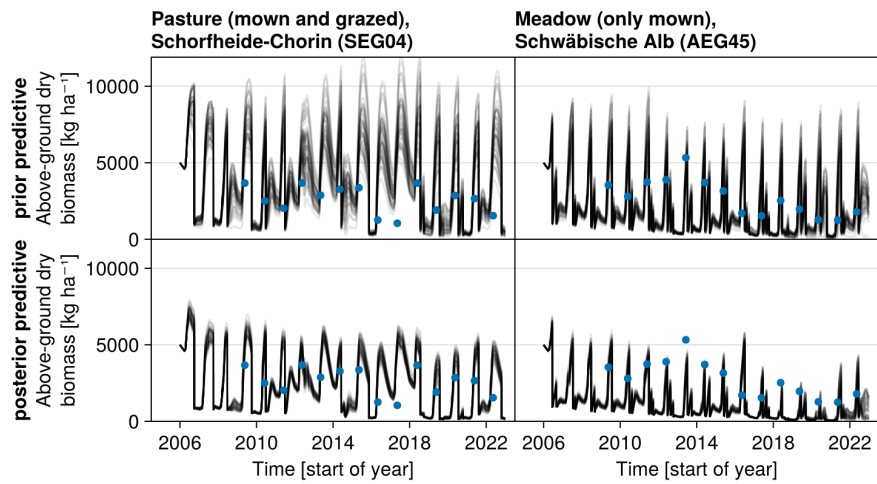
Figure A5. Prior and posterior predictive checks for two sites of the Biodiversity Exploratories dataset. The predicted above-ground biomass, based on simulations with parameters drawn from either the prior or posterior distributions, is compared to the measured above-ground biomass.
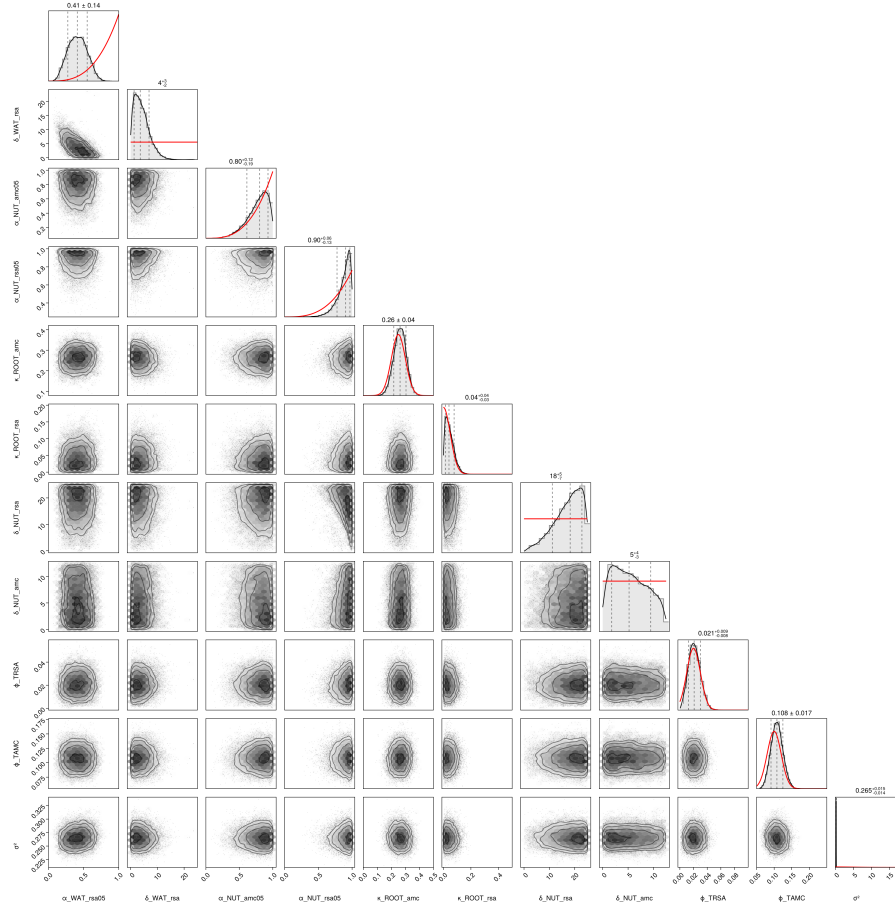
Figure A6. Pair plot of the posterior densities for the calibration with the Biodiversity Exploratories dataset. In the right upper plots, the marginal posterior densities (histograms) are shown together with the prior densities (red lines). The first half of the iterations were discarded as warm-up.
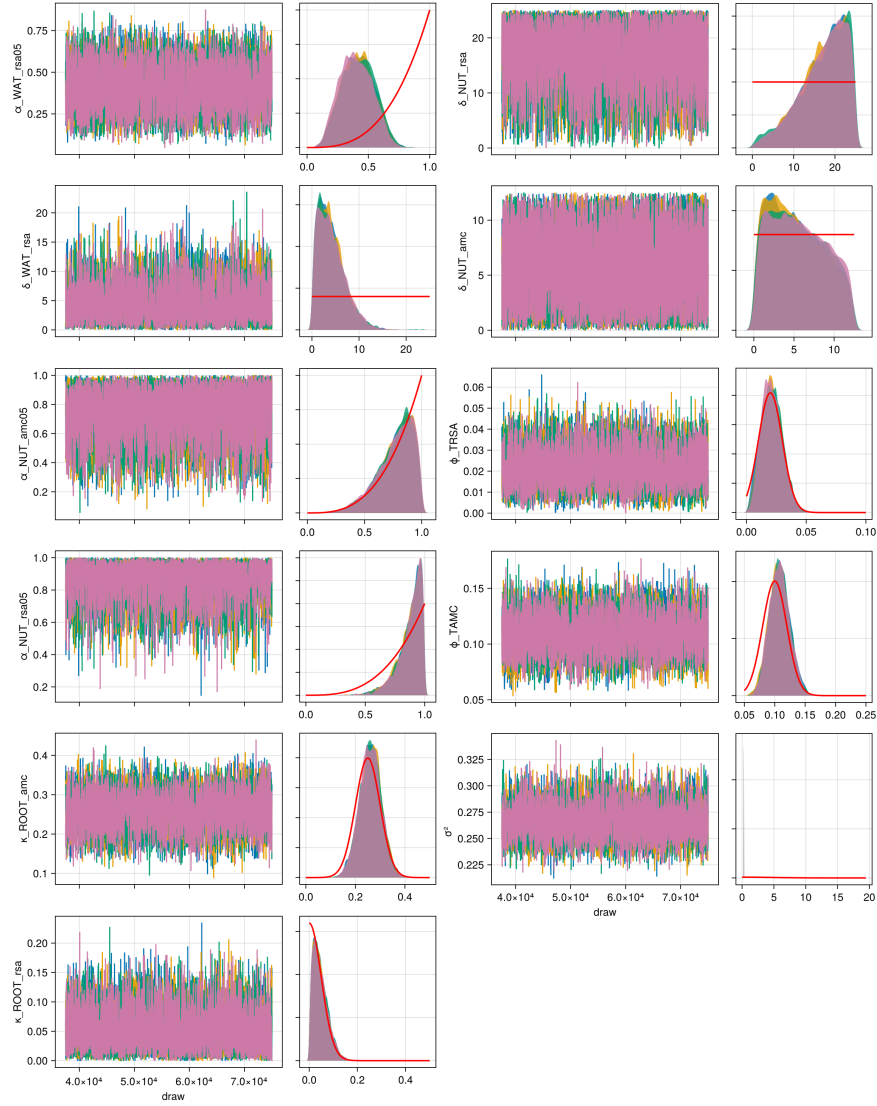
Figure A7. Trace plot, prior and posterior densities for the calibration with the Biodiversity Exploratories dataset. Different colours represent the different MCMC chains. In the density plot, the prior density (red line) and the posterior densities are visible. The first half of the iterations were discarded as warm-up.
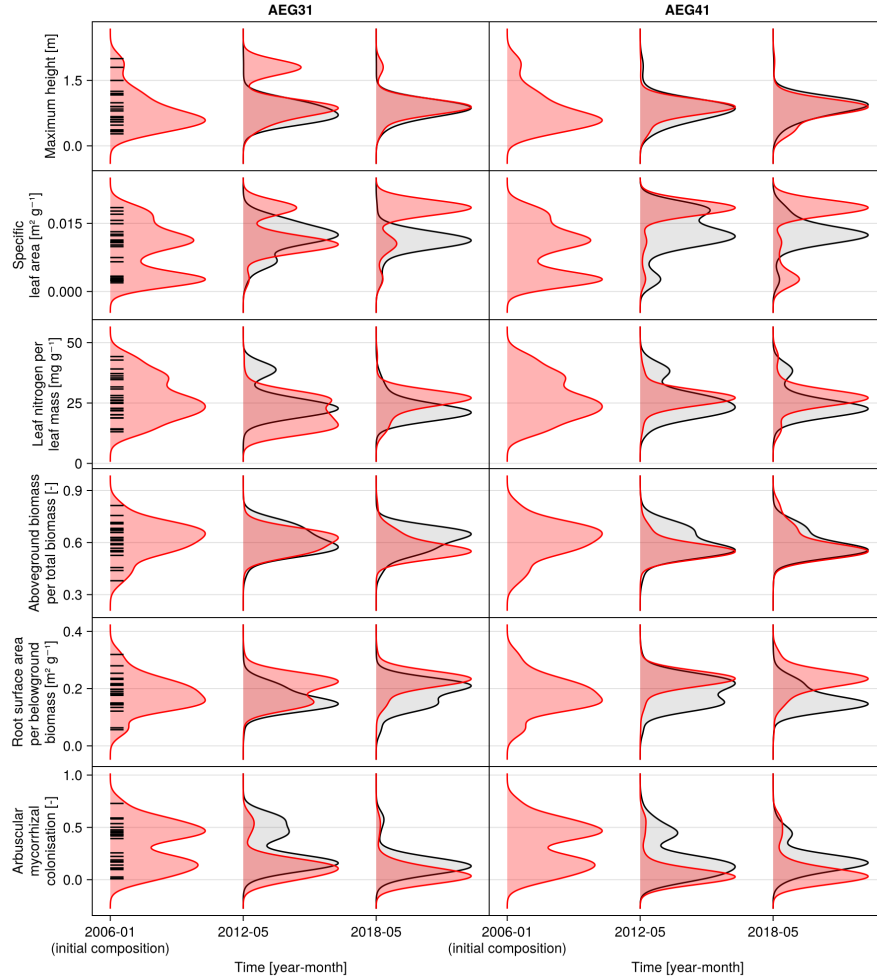
Figure A8. Development of the community trait distribution over time for validation sites with the highest (SEG20) and the lowest (HEG47) mean absolute error for the distance between simulated and observed community trait distribution (for the selection, see Figure 6). The simulated (red) and observed (grey) densities are calculated by kernel density estimation by including the biomass proportion of the species as weights. The trait values of the species are constant (black horizontal lines on the left). To analyse correlations between traits, the observed and simulated trait distributions are shown in a pair plot for 2018 in Figure A9 and A10.
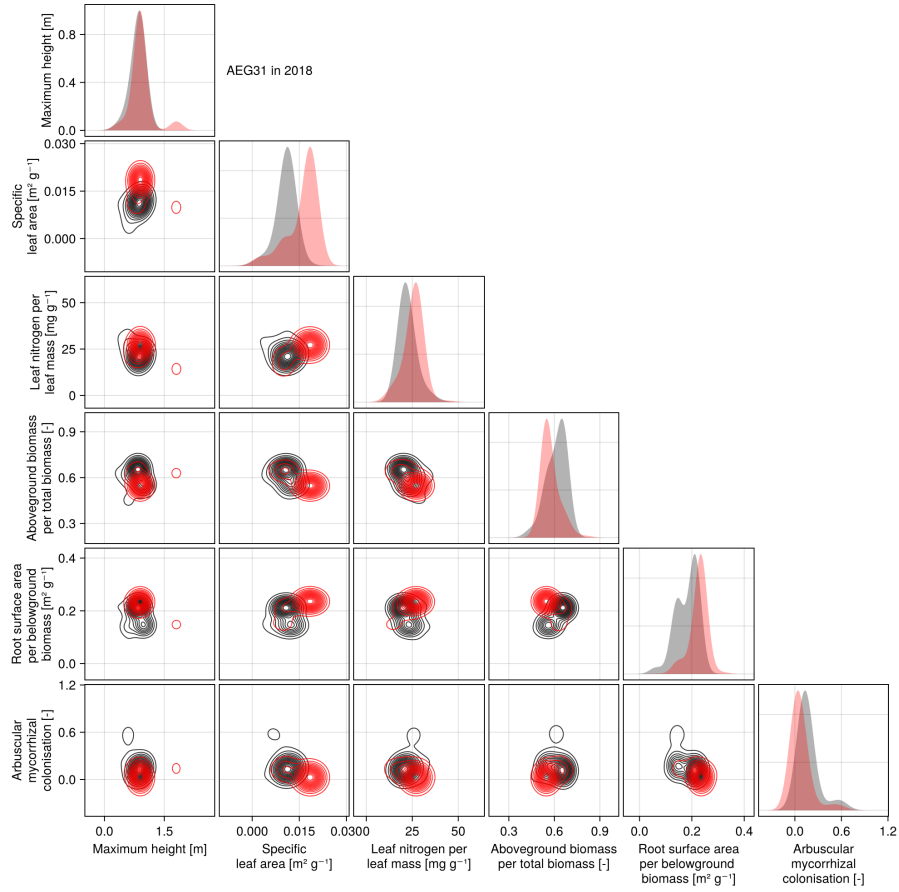
Figure A9. Simulated (red) and observationally derived (black) community trait distribution for the grassland site AEG31 of the Schwäbische Alb region (Germany) in 2018. The AEG31 site has the highest distance between the simulated and observationally derived community trait distribution over all years (see Figure 6).
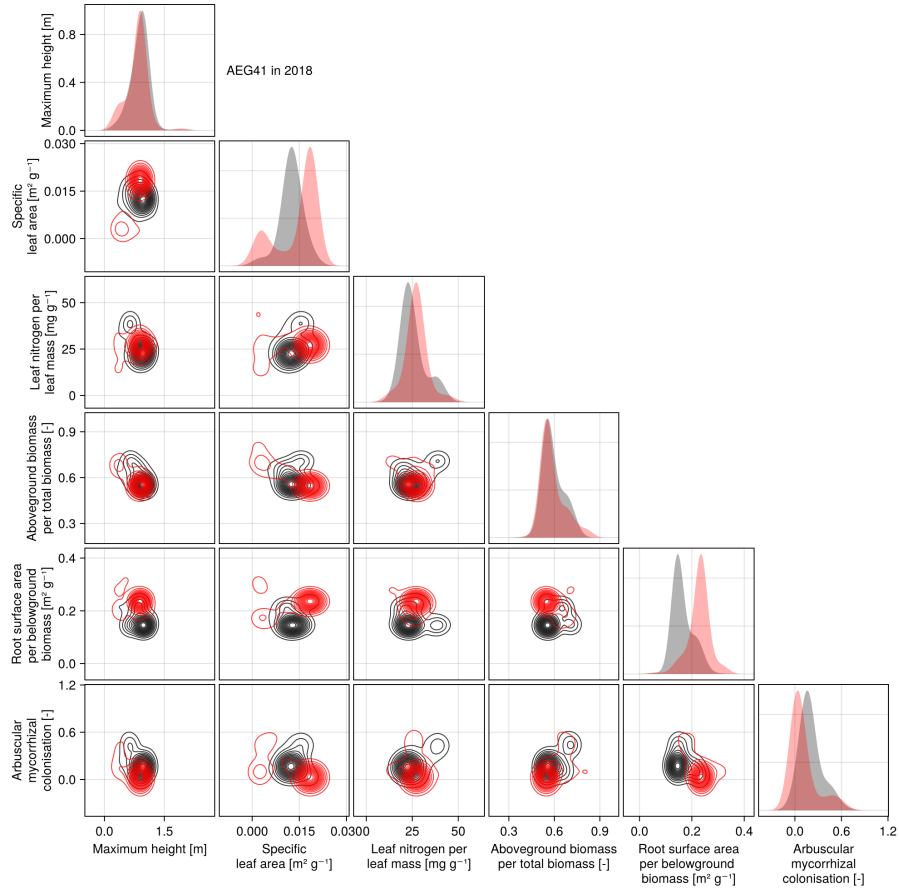
Figure A10. Simulated (red) and observationally derived (black) community trait distribution for the grassland site AEG41 of the Schwäbische Alb region (Germany) in 2018. The AEG41 site has the lowest distance between the simulated and observationally derived community trait distribution over all years (see Figure 6).

Table A1. Grassland model overview – general characteristics.

Model name with reference	Primary goal of given publication(s)	Simulation of ...	Spatial representation and resolution	Calibration of ...[1]	Number of species/PFTs simulated	Number of global parameters
GrasslandTraitSim.jl, presented here	predict plant functional community composition and production for different management and climatic conditions	populations	point simulation	transfer functions	25-70	54
LV-competition model, Chalmandrier et al. 2021	determine the relationship between plant functional morphological traits and species demography	populations	point simulation	transfer functions	118	< 25
DynaGraM, Moulin et al. 2021	predict plant functional community composition and production for different management and climatic conditions	populations	point simulation	species parameters	15	25-50
GraS, Siehoff et al. 2011	predict vegetation types given the management in a spatial explicit landscapes	populations	population in 10 × 10 m²	species parameters	10	< 25
LPJmL-CSR, Wirth et al. 2024	predict the share of the C, S, R strategies in line with the CSR-model in a dynamic global vegetation model	populations	population in 0.5° × 0.5°²	species parameters	3	> 100
LINGRA, Schapendonk et al. 1998	predict productivity of *Lolium perenne*	single population	point simulation	species parameters	1	< 25
ModVege, Jouven et al. 2006a/b	predict production, structure and digestibility of permanent grassland in various sites under different defoliation regimes	single population	point simulation	species parameters	1 aggr.	< 25
ModVege-CoSMo, Confalonieri 2014, Piseddu 2022	predict community composition, production, structure and digestibility of permanent grassland in various sites under different defoliation regimes	populations	point simulation	species parameters	8	< 25
PaSim, Riedo et al. 1998	predict the annual production of a mainly mown under cutting and fertilization in relationship to biochemical cycles.	single populations	point simulation	species parameters	1 aggr.	> 100
PROGRASS, Lazzarotto et al. 2009	predict dynamics of productive, cut grass/clover mixtures in response to management, and the role of root development on grass/clover interactions	populations	point simulation	species parameters	2	50-100
GRASSMIND, Taubert et al. 2012	predict grassland community dynamics and biogeochemical cycles under different management and climate	individuals	individuals within 1 × 1 m²	species parameters	3–5	50-100
IBC-grass, May et al. 2009	predict the influence of grazing on different plant functional types under different assumptions about plant-plant competition	individuals	resource competition on 1 × 1 cm²	species parameters	81	< 25

[1]We distinguish between models in which parameters of transfer functions mapping morphological functional traits to species demographic rates are calibrated, and models in which species demographic parameters are calibrated directly (Chalmandrier et al. 2021). ²LPJmL-CSR can be applied on a global scale, but was also used on higher spatial resolution for smaller areas, e.g. with grid cells of 1 × 1 km².

Table A2. Grassland model overview – ecological and technical details

Model name with reference	State variables of vegetation	Number and type of species-specific parameters	Plant competition	Simulation of soil water (W) and nitrogen (N) cycle	Management factors	Climate variables[1]
GrasslandTraitSim.jl, presented here	above- and below-ground biomass, height	7 morphological	water, nitrogen, light	W[2]	mowing, grazing, fertilization	T, PAR, P, PET
LV-competition model, Chalmandrier et al. 2021	above-ground biomass	8 morphological	-	-	-	T
DynaGraM, Moulin et al. 2021	above-ground biomass	9 morphological / demographic / indicator values	water, nitrogen, light	W, N	mowing, grazing, fertilization	T, PAR, P, PET
GraS, Siehoff et al. 2011	cover	5 demographic, indicator values	space	-	mowing, grazing, trampling	-
LPJmL-CSR, Wirth et al. 2024	above- and below-ground biomass, number of individuals	8 morphological / demographic	water, nitrogen, ligth, space	W, N	mowing, grazing, fertilization, irrigation	T, PAR, P, PET
LINGRA, Schapendonk et al. 1998	above- and below-ground biomass, leaf area index	10 morphological / demographic	-	W	mowing	T, PAR, P
ModVege, Jouven et al. 2006a/b	reproductive and vegetative above-ground biomass with age	26 morphological / demographic	-	W	mowing, grazing, fertilization	T, PAR, P, PET
ModVege-CoSMo, Confalonieri 2014, Piseddu et al. 2022	reproductive and vegetative above-ground biomass with age	26 + 7 morphological / demographic	water, nitrogen, light	W	mowing, grazing, fertilization	T, PAR, P, PET
PaSim, Riedo et al. 1998	laminae, sheath and stem, ear, and below-ground biomass, leaf area index	61 morphological / demographic	water, nitrogen, light	W, N	mowing, fertilization	T, PAR, P, PET
PROGRASS, Lazzarotto et al. 2009	above- and below-ground biomass, leaf area index	27 morphological / demographic	water, nitrogen, light	W, N	mowing, fertilization	T, PAR, P, PET
GRASSMIND, Taubert et al. 2012	reproductive and vegetative above-ground and below-ground biomass, height	30 morphological / demographic	water, nitrogen, light	W, N	mowing, fertilization, irrigation	T, PAR, P, PET
IBC-grass, May et al. 2009	reproductive and vegetative above-ground and below-ground biomass	15 morphological / demographic	generic above-ground and below-ground resource	-	grazing	-

[1]We have reviewed whether air temperature (T), photosynthetically active radiation (PAR), precipitation (P), and potential evapotranspiration (PET) are used in a model. Other external climate drivers, even if used in the specific model, are not shown in the table. [2]While the soil nutrient index can change with time and the amount of biomass, the soil nitrogen cycle is not simulated explicitly in GrasslandTraitSim.jl. [3]We define the number of global parameters as all parameters that are not species-specific.

Table A3. Input variables of the GrasslandTraitSim.jl model. The dimensions of the variables are given in the subscript of the symbols: t per day and s per species.

Symbol	Variable description	Unit
Climate		
PAR_t	Photosynthetic active radiation	$\mathrm{MJ \cdot ha^{-1}}$
T_t	Mean air temperature	$\mathrm{^\circ C}$
P_t	Precipitation	mm
PET_t	Potential evapotranspiration	mm
Management		
CUT_t	Cutting height for mowing	m or NaN
LD_t	Livestock density	$\mathrm{ha^{-1}}$ or NaN
F	Fertilization (may vary from year to year)	$\mathrm{kgN \cdot ha^{-1} \cdot yr^{-1}}$
Soil		
SND	Sand content (proportion $\in [0,1]$)	–
SLT	Silt content (proportion $\in [0,1]$)	–
CLY	Clay content (proportion $\in [0,1]$)	–
OM	Organic matter content (proportion $\in [0,1]$)	–
BLK	Bulk density	$\mathrm{g \cdot cm^{-3}}$
RD	Rooting depth of plants	mm
N	Total nitrogen in the soil	$\mathrm{gN \cdot kg^{-1}}$
Morphological plant traits		
$maxheight_s$	Maximum plant height	m
sla_s	Specific leaf area	$\mathrm{m^2 \cdot kg^{-1}}$
lnc_s	Leaf nitrogen content per leaf mass	$\mathrm{mg \cdot g^{-1}}$
rsa_s	Root surface area per below-ground biomass	$\mathrm{m^2 \cdot g^{-1}}$
amc_s	Arbuscular mycorrhizal colonisation rate	–
abp_s	Above-ground biomass per total biomass	–
lbp_s	Leaf biomass per above-ground biomass	–

Table A4. Parameters of the model and the references for the parameter values. In the reference column we denote whether a parameter is calibrated with the Biodiversity Exploratories (BE) or the FAO dataset, whether the parameter is set manually by comparing time series with data or if the parameter value is derived from literature. For the parameters calibrated using the FAO dataset, we set prior distributions based on the literature, as shown in Table A6.

Symbol	Parameter	Value	Unit	Reference
Reference traits				
ϕ_{TRSA}	Reference root surface area per total biomass, used in nutrient stress function and maintenance costs for roots function	≈ 0.023	$\mathrm{m}^2 \cdot \mathrm{g}^{-1}$	calibrated with BE dataset
ϕ_{TAMC}	Reference arbuscular mycorrhiza colonisation rate per total biomass, used in nutrient stress function and maintenance costs for mycorrhizae function	≈ 0.11	–	calibrated with BE dataset
ϕ_{sla}	Reference specific leaf area, used in senescence function	0.012	$\mathrm{m}^2 \cdot \mathrm{g}^{-1}$	manually adjusted for BE dataset, close to community mean
Light interception and competition				
γ_{RUEmax}	Maximum radiation use efficiency	0.003	$\mathrm{kg} \cdot \mathrm{MJ}^{-1}$	Schapendonk et al. (1998)
$\gamma_{RUE,k}$	Light extinction coefficient	0.6	–	Schapendonk et al. (1998)
$\alpha_{RUE,cwmH}$	Reduction factor of radiation use efficiency at a height of 0.2 m $\in [0,1]$	≈ 0.989	–	calibrated with FAO dataset
Water stress				
$\alpha_{WAT,rsa,05}$	Water stress growth reduction factor for species with mean trait: $TRSA = \phi_{TRSA}$, when the plant available water equals: $W_{p,t} = 0.5$	≈ 0.41	–	calibrated with BE dataset
$\beta_{WAT,rsa}$	Slope of the logistic function that relates the plant available water to the water stress growth reduction factor	7.5	–	manually adjusted for BE dataset
$\delta_{WAT,rsa}$	Controls how strongly species differ in their water stress growth reduction from the mean response	≈ 4.1	$\mathrm{g} \cdot \mathrm{m}^{-2}$	calibrated with BE dataset
Nutrient stress				
$\omega_{NUT,F}$	Controls the influence of the fertilization rate on the nutrient index	0.4	$\mathrm{kgN}^{-1} \cdot \mathrm{ha}^{-1} \cdot \mathrm{yr}$	manually adjusted for BE dataset
$\omega_{NUT,N}$	Controls the influence of the total soil nitrogen on the nutrient index	2	$\mathrm{gN}^{-1} \cdot \mathrm{kg}$	manually adjusted for BE dataset

Symbol	Parameter	Value	Unit	Reference
$\alpha_{NUT,TSB}$	Reference value, if the sum of the product of trait similarity and biomass of all species equals: $\sum TS \cdot B < 1, \sum TS \cdot B = 1, \sum TS \cdot B > 1$ the nutrient adjustment factor $NUT_{adj,ts}$ is higher than one, one and lower than one, respectively	5000	$\mathrm{kg \cdot ha^{-1}}$	manually adjusted for the BE dataset
$\alpha_{NUT,maxadj}$	Maximum of the nutrient adjustment factor	2	–	manually adjusted for BE dataset
$\beta_{NUT,TS}$	Scaling factor for the trait similarity matrix	2	–	manually adjusted for BE dataset
$\alpha_{NUT,amc,05}$	Nutrient stress based on arbuscular mycorrhiza colonisation growth reduction factor for species with mean trait: $TAMC = \phi_{TAMC}$, when the plant available nutrients equal: $N_{p,ts} = 0.5$	≈ 0.79	–	calibrated with BE dataset
$\alpha_{NUT,rsa,05}$	Nutrient stress based on root surface area growth reduction factor for species with mean trait: $TRSA = \phi_{TRSA}$, when the plant available nutrients equal: $N_{p,ts} = 0.5$	≈ 0.76	–	calibrated with BE dataset
$\beta_{NUT,amc}$	Slope of the logistic function that relates the plant available nutrients to the nutrient stress growth reduction factor based on arbuscular mycorrhiza colonisation	7.5	–	manually adjusted for BE dataset
$\beta_{NUT,rsa}$	Slope of the logistic function that relates the plant available nutrients to the nutrient stress growth reduction factor based on root surface area	7.5	–	manually adjusted for BE dataset
$\delta_{NUT,amc}$	Controls how strongly species differ in their nutrients stress growth reduction based on arbuscular mycorrhiza colonisation from the mean response	≈ 6.1	–	calibrated with BE dataset
$\delta_{NUT,rsa}$	Controls how strongly species differ in their nutrient stress growth reduction based on root surface area from the mean response	≈ 19.2	$\mathrm{g \cdot m^{-2}}$	calibrated with BE dataset

Maintenance costs for roots and mycorrhizae

Symbol	Parameter	Value	Unit	Reference
$\kappa_{ROOT,amc}$	Maximum growth reduction due to maintenance costs for mycorrhizae based on arbuscular mycorrhiza colonisation rate	≈ 0.28	–	calibrated with BE dataset

Symbol	Parameter	Value	Unit	Reference
$\kappa_{ROOT,rsa}$	Maximum growth reduction due to maintenance costs for fine roots based on root surface area	≈ 0.07	–	calibrated with BE dataset

Environmental and seasonal growth adjustment

Symbol	Parameter	Value	Unit	Reference
$\gamma_{RAD,1}$	Controls the steepness of the linear decrease in radiation use efficiency for high PAR_t values	$4.45 \cdot 10^{-6}$	$\mathrm{MJ}^{-1} \cdot \mathrm{ha}$	Schapendonk et al. (1998)
$\gamma_{RAD,2}$	Threshold value of PAR_t from which starts a linear decrease in radiation use efficiency	$5 \cdot 10^{4}$	$\mathrm{MJ} \cdot \mathrm{ha}^{-1}$	Schapendonk et al. (1998)
ω_{TEMP,T_1}	Minimum temperature for growth	4	$^{\circ}\mathrm{C}$	Jouven et al. (2006)
ω_{TEMP,T_2}	Lower limit of optimum temperature for growth	10	$^{\circ}\mathrm{C}$	Schapendonk et al. (1998)
ω_{TEMP,T_3}	Upper limit of optimum temperature for growth	20	$^{\circ}\mathrm{C}$	Jouven et al. (2006)
ω_{TEMP,T_4}	Maximum temperature for growth	35	$^{\circ}\mathrm{C}$	Moulin et al. (2021)
ζ_{SEA,ST_1}	Threshold of the cumulative temperature since the beginning of the current year, the seasonality factor starts to decrease from $\zeta_{SEA\,max}$ to $\zeta_{SEA\,min}$ above $\zeta_{SEA,ST_1} - 100\ ^{\circ}\mathrm{C}$	≈ 400	$^{\circ}\mathrm{C}$	calibrated with FAO dataset
ζ_{SEA,ST_2}	Threshold of the cumulative temperature since the beginning of the current year, above which the seasonality factor is set to $\zeta_{SEA\,min}$	≈ 1460	$^{\circ}\mathrm{C}$	calibrated with FAO dataset
$\zeta_{SEA\,min}$	Minimum value of the seasonal growth effect	≈ 0.84	–	calibrated with FAO dataset
$\zeta_{SEA\,max}$	Maximum value of the seasonal growth effect	≈ 2.16	–	calibrated with FAO dataset

Senescence

Symbol	Parameter	Value	Unit	Reference
α_{SEN}	Basic senescence rate	≈ 0.012	month^{-1}	calibrated with FAO dataset
$\beta_{SEN,sla}$	Controls the influence of the specific leaf area on the senescence rate	2.5	–	manually adjusted for BE dataset
ψ_{SEN,ST_1}	Threshold of the cumulative temperature since the beginning of the current year above which the senescence begins to increase	≈ 1731	$^{\circ}\mathrm{C}$	calibrated with FAO dataset
ψ_{SEN,ST_2}	Threshold of the cumulative temperature since the beginning of the current year above which the senescence reaches the maximum senescence rate $\psi_{SEN\,max}$	≈ 2933	$^{\circ}\mathrm{C}$	calibrated with FAO dataset
$\psi_{SEN\,max}$	Maximum senescence rate	≈ 1.77	–	calibrated with FAO dataset

Management

Symbol	Parameter	Value	Unit	Reference
$\beta_{GRZ,lnc}$	Controls the influence of leaf nitrogen per leaf mass on grazer preference	3	–	manually adjusted for BE dataset

825

Symbol	Parameter	Value	Unit	Reference
$\beta_{GRZ,H}$	Controls the influence of height on grazer preference	1	—	manually adjusted for BE dataset
η_{GRZ}	Scaling factor that controls at which biomass density additional feed is supplied by farmers, fixed for calibration	2	—	manually adjusted for BE dataset
κ_{GRZ}	Consumption of dry biomass per livestock and day	22	$kg \cdot ha^{-1}$	Gillet (2008)
$\epsilon_{GRZ,\min H}$	Minimum height that is reachable by grazers	0.05	m	cf. Hirata et al. (2010)
Water dynamics				
$\beta_{SND,WHC}$,	Slope parameter relating the sand, silt, clay,	0.5678,	—,	Gupta and Larson (1979) for
$\beta_{SLT,WHC}$,	organic matter content and the bulk density to the	0.9228,	—,	all five parameter values
$\beta_{CLY,WHC}$,	soil water content at the water holding capacity	0.9135,	—,	
$\beta_{OM,WHC}$,		0.6103,	—,	
$\beta_{BLK,WHC}$		-0.2696	$cm^3 \cdot g^{-1}$	
$\beta_{SND,PWP}$,	Slope parameter relating the sand, silt, clay,	-0.0059,	—,	Gupta and Larson (1979) for
$\beta_{SLT,PWP}$,	organic matter content and the bulk density to the	0.1142,	—,	all five parameter values
$\beta_{CLY,PWP}$,	soil water content at the permanent wilting point	0.5766,	—,	
$\beta_{OM,PWP}$,		0.2228,	—,	
$\beta_{BLK,PWP}$		0.02671	$cm^3 \cdot g^{-1}$	

Table A5. Overview of the model equations and their references. New means that the equations are newly composed for the grassland model and were not adopted from other grassland models.

Eq.	Topic	References
Main biomass dynamic		
1	main biomass dynamic	similar to Schapendonk et al. (1998); Moulin et al. (2021)
2	ratio between above-ground and below-ground biomass	new
3	change in above-ground biomass	new
4	change in below-ground biomass	new
5	actual growth	similar to Schapendonk et al. (1998); Moulin et al. (2021)
Light interception and competition		
6	potential growth	Eq. (1) of Lacasa et al. (2021), Monsi and Saeki (2005)
7	fraction of the radiation that is intercepted	for Beer-Lambert equation see Monsi and Saeki (2005); Lacasa et al. (2021), added the influence of the community height
8	community-weighted mean height	general equation
9	total leaf area index	general equation
10	leaf area index	Watson (1947)
11	light interception in vertical layers of the sward	similar to Taubert et al. (2012)
12	vertical layers method for light competition	similar to Taubert et al. (2012)
General form of the growth reducer for nutrient and water stress		
13	species-specific inflection point of logistic growth reduction function for nutrient and water stress	new
14	logistic growth reduction function for nutrient and water stress	new
Nutrient stress		
15	nutrient stress growth reduction factor	new
16	arbuscular mycorrhizal colonisation rate per total biomass	new
17	root surface area per total biomass	new
18	plant available nutrients	
19	nutrient adjustment factor based on biomass and trait similarity	new

Eq.	Topic	References
20	normalized arbuscular mycorrhizal colonisation rate	general equation
21	normalized root surface area per below-ground biomass	general equation
22	trait dissimilarity index	new
23	trait similarity calculation	new
24	trait similarity as matrix	new

Water stress

25	plant available water	Moulin et al. (2021)

Maintenance costs for roots and mycorrhizae

26	costs for roots and mycorrhizae growth reduction factor	new
27	costs for fine roots reduction factor	new
28	costs for mycorrhizae growth reduction factor	new

Environmental and seasonal growth adjustment

29	environmental and seasonal growth adjustment	Moulin et al. (2021)
30	growth reduction based on too high radiation	Schapendonk et al. (1998)
31	temperature growth reducer function	Schapendonk et al. (1998), Jouven et al. (2006), Moulin et al. (2021)
32	seasonal growth adjustment	Jouven et al. (2006), Moulin et al. (2021)
33	yearly accumulated temperature	Jouven et al. (2006), Moulin et al. (2021)

Senescence

34	senescence rate	Moulin et al. (2021), added influence of specific leaf area
35	seasonality of senescence	Moulin et al. (2021)

Management

36	biomass losses due to management	similar to Moulin et al. (2021)
37	mown biomass	influence of plant height to mowing tolerance similar to the λ in Moulin et al. (2021)
38	grazed biomass	partly based on Moulin et al. (2021); added influence of leaf nitrogen content and height on grazer preference
41	influence of leaf nitrogen per leaf mass on grazer preference	new
42	community-weighted mean leaf nitrogen content	general equation

Plant height dynamics

43	change in the plant height	new

Water dynamic

Eq.	Topic	References
44	main soil water dynamic	Schapendonk et al. (1998), Moulin et al. (2021)
45	evaporation	Moulin et al. (2021)
46	transpiration	simplified/modified from Moulin et al. (2021)
47	actual evapotranspiration	Moulin et al. (2021)
48	water drainage and run-off	Moulin et al. (2021)
49	fraction of the soil that can be filled with water at the water holding capacity	Gupta and Larson (1979)
50	fraction of the soil that can be filled with water at the permanent wilting point	Gupta and Larson (1979)
51	water holding capacity in the rooting zone	Gupta and Larson (1979)
52	permanent wilting point in the rooting zone	Gupta and Larson (1979)

830

Table A6. Prior distributions for the calibration with the FAO dataset.

Parameter	Prior Distribution	Reference for Prior
α_{SEN}	truncated(Normal(0.01, 0.002); lower = 0.005, upper = 0.02)	we assumed a relatively low basis senescence rate per month
$\psi_{SEN\max}$	truncated(Normal(1.5, 0.5); lower = 1, upper = 3)	Moulin et al. (2021) used 3 $[-]$
ψ_{SEN,ST_1}	truncated(Normal(1800, 200); lower = 1200, upper = 2500)[1]	Moulin et al. (2021) used 775 $[°C]$
ψ_{SEN,ST_2}	truncated(Normal(3000, 200); lower = 2500, upper = 4000)	Moulin et al. (2021) used 3000 $[°C]$
$\zeta_{SEA\min}$	Beta(3, 1)	Jouven et al. (2006) used 0.67 $[-]$
$\zeta_{SEA\max}$	truncated(Normal(1, 2); lower = 1, upper = 5)	Jouven et al. (2006) used 1.33 $[-]$
ζ_{SEA,ST_1}	truncated(Normal(800, 200); lower = 250, upper = 1200)	Jouven et al. (2006) used 775 $[°C]$
ζ_{SEA,ST_2}	truncated(Normal(1800, 200); lower = 1200, upper = 2500)	Jouven et al. (2006) used 1450 $[°C]$
$\alpha_{RUE,cwmH}$	Beta(8, 2)	we assumed a small effect, if the parameter is one, the process would have no effect
σ^2	truncated(Normal(0, 5); lower = 0.0)	wide prior, we compared measured and simulated biomass in $[\mathrm{t} \cdot \mathrm{ha}^{-1}]$

[1]Note that we assumed higher values for ϕ_{SEN,ST_1} because we calibrated our model for lower altitudes compared to Moulin et al. (2021), as more heat is accumulated over the year before the senescence starts to increase in autumn.

Table A7. Overview of experiments with location, year and whether an experiment is used for calibration for the FAO dataset. If an experiment is not used for calibration, it is used for validation. We only used the subset of the experiments that were irrigated.

experiment number	location (lat, lon)	year	used for calibration?
FAO01	UK, Crossnacreevy (54.53, -5.85)	1982	x
FAO05	Switzerland, Changins (46.4, 6.23)	1983	x
FAO07	Switzerland, Changins (46.4, 6.23)	1984	x
FAO09	Switzerland, Changins (46.4, 6.23)	1985	x
FAO19	France, Rennes (48.12, -1.68)	1984	x
FAO21	France, Rennes (48.12, -1.68)	1985	x
FAO28	Romania, Cluj-Napoca (46.77, 23.6)	1986	x
FAO33	Belgium, Michamps (50.05, 5.8)	1984	x
FAO35	Belgium, Michamps (50.05, 5.8)	1985	x
FAO43	Spain, La Coruna (43.37, -8.4)	1983	
FAO45	Spain, La Coruna (43.37, -8.4)	1984	
FAO47	Spain, La Coruna (43.37, -8.4)	1985	
FAO51	Italy, Carmagnola (44.85, 7.72)	1983	
FAO53	Italy, Carmagnola (44.85, 7.72)	1984	
FAO55	Netherlands, Wageningen (51.97, 5.67)	1983	
FAO57	Netherlands, Wageningen (51.97, 5.67)	1984	
FAO59	Italy, Lodi (45.32, 9.5)	1983	
FAO61	Italy, Lodi (45.32, 9.5)	1984	
FAO63	Italy, Lodi (45.32, 9.5)	1985	
FAO65	UK, North Wyke (50.77, -3.9)	1983	
FAO67	UK, North Wyke (50.77, -3.9)	1984	
FAO69	UK, North Wyke (50.77, -3.9)	1985	
FAO71	Netherlands, Zegveld (52.12, 4.85)	1984	
FAO73	Netherlands, Zegveld (52.12, 4.85)	1985	
FAO75	UK, Crossnacreevy (54.53, -5.85)	1983	
FAO77	UK, Crossnacreevy (54.53, -5.85)	1984	

Table A8. Prior distributions for the calibration with the Biodiversity Exploratories dataset. The prior distributions for the parameters, which are rather theoretical, were set so that the simulated trajectories were close to the measured above-ground biomass and to the community weighted mean traits.

Parameter	Prior Distribution
$\alpha_{WAT,rsa,05}$	Beta(4, 1)
$\delta_{WAT,rsa}$	Uniform(0, 25)
$\alpha_{NUT,rsa,05}$	Beta(4, 1)
$\alpha_{NUT,amc,05}$	Beta(4, 1)
$\delta_{NUT,rsa}$	Uniform(0, 25)
$\delta_{NUT,amc}$	Uniform(0, 12.5)
$\kappa_{ROOT,rsa}$	truncated(Normal(0.0, 0.05); lower = 0, upper = 0.5)
$\kappa_{ROOT,amc}$	truncated(Normal(0.25, 0.05); lower = 0, upper = 0.5)
ϕ_{TRSA}	truncated(Normal(0.02, 0.01); lower = 0.0, upper = 0.1)
ϕ_{TAMC}	truncated(Normal(0.1, 0.02); lower = 0.05, upper = 0.25)
$\sigma^2_{wasserstein}$	truncated(Normal(0, 5); lower = 0.0)

Table A9. Overview of sites with location, dominant land use and whether a site is used for calibration of the Biodiversity Exploratories dataset from the Schwäbische Alb region. If a site is not used for calibration, it is used for validation.

Site code	Location (lat, lon)	Dominant land use	Used for calibration?
AEG01	Schwäbische Alb (48.4, 9.34)	mainly mown	x
AEG02	Schwäbische Alb (48.38, 9.47)	mainly mown	x
AEG03	Schwäbische Alb (48.41, 9.53)	mainly mown	x
AEG04	Schwäbische Alb (48.38, 9.42)	mown and grazed	x
AEG05	Schwäbische Alb (48.4, 9.44)	mown and grazed	
AEG06	Schwäbische Alb (48.4, 9.44)	mown and grazed	
AEG08	Schwäbische Alb (48.42, 9.49)	mown and grazed	
AEG10	Schwäbische Alb (48.38, 9.21)	mainly mown	
AEG11	Schwäbische Alb (48.49, 9.35)	mainly mown	
AEG12	Schwäbische Alb (48.39, 9.35)	mainly mown	
AEG13	Schwäbische Alb (48.39, 9.36)	mainly mown	
AEG14	Schwäbische Alb (48.38, 9.52)	mainly mown	
AEG15	Schwäbische Alb (48.49, 9.45)	mainly mown	
AEG17	Schwäbische Alb (48.4, 9.52)	mainly mown	
AEG18	Schwäbische Alb (48.38, 9.52)	mainly mown	
AEG22	Schwäbische Alb (48.4, 9.51)	mainly mown	
AEG23	Schwäbische Alb (48.42, 9.51)	mainly mown	
AEG24	Schwäbische Alb (48.4, 9.49)	mown and grazed	
AEG29	Schwäbische Alb (48.42, 9.36)	mown and grazed	
AEG31	Schwäbische Alb (48.46, 9.46)	mown and grazed	
AEG35	Schwäbische Alb (48.48, 9.29)	mainly mown	
AEG36	Schwäbische Alb (48.48, 9.3)	mainly mown	
AEG37	Schwäbische Alb (48.4, 9.41)	mainly mown	
AEG38	Schwäbische Alb (48.44, 9.43)	mainly mown	
AEG39	Schwäbische Alb (48.39, 9.43)	mainly mown	
AEG40	Schwäbische Alb (48.41, 9.57)	mainly mown	
AEG41	Schwäbische Alb (48.37, 9.4)	mainly mown	
AEG42	Schwäbische Alb (48.4, 9.38)	mown and grazed	
AEG45	Schwäbische Alb (48.4, 9.46)	mainly mown	
AEG50	Schwäbische Alb (48.41, 9.47)	mainly mown	

Table A10. Overview of sites with location, dominant land use and whether a site is used for calibration of the Biodiversity Exploratories dataset from the Hainich region. If a site is not used for calibration, it is used for validation.

Site code	Location (lat, lon)	Dominant land use	Used for calibration?
HEG01	Hainich (50.97, 10.41)	mainly mown	x
HEG02	Hainich (51.0, 10.43)	mown and grazed	x
HEG03	Hainich (51.0, 10.43)	mown and grazed	x
HEG06	Hainich (51.21, 10.39)	mown and grazed	x
HEG04	Hainich (51.11, 10.44)	mainly mown	
HEG05	Hainich (51.22, 10.32)	mown and grazed	
HEG10	Hainich (51.28, 10.45)	mainly mown	
HEG11	Hainich (51.28, 10.46)	mainly mown	
HEG13	Hainich (51.26, 10.38)	mown and grazed	
HEG14	Hainich (51.29, 10.44)	mown and grazed	
HEG15	Hainich (51.07, 10.49)	mown and grazed	
HEG22	Hainich (51.03, 10.32)	mown and grazed	
HEG23	Hainich (51.13, 10.34)	mown and grazed	
HEG24	Hainich (51.1, 10.35)	mown and grazed	
HEG26	Hainich (51.28, 10.37)	mainly mown	
HEG27	Hainich (51.09, 10.6)	mainly mown	
HEG28	Hainich (51.27, 10.5)	mainly mown	
HEG29	Hainich (51.26, 10.5)	mown and grazed	
HEG30	Hainich (51.2, 10.36)	mainly mown	
HEG31	Hainich (51.17, 10.22)	mown and grazed	
HEG32	Hainich (51.08, 10.57)	mown and grazed	
HEG33	Hainich (51.11, 10.43)	mown and grazed	
HEG34	Hainich (51.21, 10.39)	mown and grazed	
HEG37	Hainich (51.03, 10.51)	mown and grazed	
HEG47	Hainich (51.28, 10.37)	mown and grazed	
HEG48	Hainich (51.29, 10.38)	mainly mown	
HEG49	Hainich (51.28, 10.39)	mainly mown	
HEG50	Hainich (51.28, 10.42)	mown and grazed	

Table A11. Overview of sites with location, dominant land use and whether a site is used for calibration of the Biodiversity Exploratories dataset from the Schorfheide-Chorin region. If a site is not used for calibration, it is used for validation.

Site code	Location (lat, lon)	Dominant land use	Used for calibration?
SEG01	Schorfheide-Chorin (53.09, 13.97)	mainly mown	x
SEG02	Schorfheide-Chorin (53.09, 13.98)	mown and grazed	x
SEG03	Schorfheide-Chorin (53.1, 13.99)	mainly mown	x
SEG08	Schorfheide-Chorin (53.11, 14.02)	mown and grazed	x
SEG04	Schorfheide-Chorin (53.11, 14.0)	mainly mown	
SEG05	Schorfheide-Chorin (53.11, 14.0)	mainly mown	
SEG10	Schorfheide-Chorin (53.11, 14.0)	mainly mown	
SEG11	Schorfheide-Chorin (53.11, 13.99)	mainly mown	
SEG12	Schorfheide-Chorin (53.09, 13.97)	mainly mown	
SEG13	Schorfheide-Chorin (52.97, 13.82)	mainly mown	
SEG14	Schorfheide-Chorin (53.09, 13.98)	mown and grazed	
SEG15	Schorfheide-Chorin (53.11, 14.01)	mainly mown	
SEG17	Schorfheide-Chorin (53.1, 13.63)	mown and grazed	
SEG18	Schorfheide-Chorin (53.14, 13.88)	mainly mown	
SEG19	Schorfheide-Chorin (53.12, 14.01)	mown and grazed	
SEG23	Schorfheide-Chorin (53.11, 14.03)	mainly mown	
SEG24	Schorfheide-Chorin (53.09, 14.0)	mainly mown	
SEG25	Schorfheide-Chorin (53.11, 13.62)	mainly mown	
SEG26	Schorfheide-Chorin (53.11, 14.02)	mainly mown	
SEG27	Schorfheide-Chorin (53.12, 13.71)	mainly mown	
SEG28	Schorfheide-Chorin (53.09, 14.01)	mainly mown	
SEG29	Schorfheide-Chorin (53.09, 14.0)	mainly mown	
SEG30	Schorfheide-Chorin (53.15, 13.83)	mainly mown	
SEG31	Schorfheide-Chorin (53.15, 13.84)	mainly mown	
SEG32	Schorfheide-Chorin (53.15, 13.83)	mainly mown	
SEG39	Schorfheide-Chorin (52.98, 13.82)	mown and grazed	
SEG41	Schorfheide-Chorin (53.12, 13.85)	mainly grazed	

Table A12. Sensitivity of above-ground biomass of *Lolium perenne* to changes in parameter values for all experiments in the FAO dataset. The default parameter values are listed in Table A4. We decreased (θ^-) and increased (θ^+) each parameter one-at-a-time by 1 % (local sensitivity analysis). We calculated the output variable (denoted by Y) with one parameter decreased, one parameter increased and the default parameters to calculate the following quotient: $\left(Y(\theta^+) - Y(\theta^-)\right)/(2 \cdot 0.01 \cdot Y(\theta))$. We calculated the ratio for each time point and for all the experiments and took the overall average. All parameters not listed here have no influence on the biomass dynamic without soil water and nutrient growth limitation. The parameters are ordered from positive, to small positive/negative effect, to negative effect on the above-ground biomass.

Parameter	Sensitivity of above-ground biomass to parameter changes
γ_{RUEmax}	1.465
$\alpha_{RUE,cwmH}$	1.251
$\zeta_{SEA\,min}$	0.836
$\gamma_{RUE,k}$	0.680
$\zeta_{SEA\,max}$	0.628
ϕ_{sla}	0.454
ζ_{SEA,ST_2}	0.354
$\gamma_{RAD,2}$	0.339
ϕ_{TAMC}	0.124
ω_{TEMP,T_3}	0.047
ψ_{SEN,ST_2}	0.043
ψ_{SEN,ST_1}	0.031
ω_{TEMP,T_4}	0.015
ϕ_{TRSA}	0.004
ζ_{SEA,ST_1}	-0.012
ω_{TEMP,T_1}	-0.012
ω_{TEMP,T_2}	-0.047
$\psi_{SEN\,max}$	-0.066
$\kappa_{ROOT,rsa}$	-0.076
$\kappa_{ROOT,amc}$	-0.152
α_{SEN}	-0.183
$\gamma_{RAD,1}$	-0.283
$\beta_{SEN,sla}$	-0.333

Table A13. Sensitivity of the total above-ground biomass to changes in parameter values for all sites in the Biodiversity Exploratories dataset. The default parameter values are listed in Table A4. We decreased (θ^-) and increased (θ^+) each parameter one-at-a-time by 1 % (local sensitivity analysis). We calculated the output variable (denoted by Y) with one parameter decreased, one parameter increased and the default parameters to calculate the following quotient: $\left(Y(\theta^+) - Y(\theta^-)\right) / \left(2 \cdot 0.01 \cdot Y(\theta)\right)$. We calculated the ratio for each time point and for all the sites and took the overall average. The parameters are sorted into positive (left columns) and negative effect or almost no effect (right columns) on the total above-ground biomass.

Parameter	Sensitivity of total above-ground biomass to parameter changes	Parameter	Sensitivity of total above-ground biomass to parameter changes
ϕ_{sla}	2.91	$\beta_{CLY,PWP}$	-1.26
γ_{RUEmax}	2.32	α_{SEN}	-1.23
$\alpha_{RUE,cwmH}$	1.84	$\beta_{SEN,sla}$	-1.11
$\gamma_{RUE,k}$	1.49	$\beta_{BLK,WHC}$	-0.69
$\beta_{SLT,WHC}$	1.46	$\psi_{SEN\max}$	-0.67
$\zeta_{SEA\max}$	1.41	$\omega_{TEMP,T2}$	-0.39
$\beta_{CLY,WHC}$	1.26	$\gamma_{RAD,1}$	-0.39
$\alpha_{WAT,rsa,05}$	1.11	$\beta_{WAT,rsa}$	-0.3
$\zeta_{SEA\min}$	0.9	$\beta_{SLT,PWP}$	-0.28
$\gamma_{RAD,2}$	0.45	$\kappa_{ROOT,rsa}$	-0.17
$\zeta_{SEA,ST2}$	0.45	$\kappa_{ROOT,amc}$	-0.16
$\delta_{WAT,rsa}$	0.44	$\omega_{TEMP,T1}$	-0.13
ψ_{SEN,ST_2}	0.24	$\beta_{BLK,PWP}$	-0.11
$\zeta_{SEA,ST1}$	0.22	κ_{GRZ}	-0.09
$\epsilon_{GRZ,\min H}$	0.18	ϕ_{TRSA}	-0.06
ψ_{SEN,ST_1}	0.12	$\beta_{OM,PWP}$	-0.05
ϕ_{TAMC}	0.1	$\alpha_{NUT,maxadj}$	-0.05
$\beta_{SND,WHC}$	0.1	$\beta_{GRZ,lnc}$	-0.02
$\beta_{OM,WHC}$	0.09	$\beta_{NUT,rsa}$	-0.01
$\alpha_{NUT,rsa,05}$	0.07	ω_{TEMP,T_4}	0.0
$\alpha_{NUT,TSB}$	0.07	$\delta_{NUT,amc}$	0.0
η_{GRZ}	0.07	$\alpha_{NUT,amc,05}$	0.0
$\delta_{NUT,rsa}$	0.05	$\beta_{NUT,amc}$	0.0
$\omega_{TEMP,T3}$	0.01	$\omega_{NUT,F}$	0.0
$\omega_{NUT,N}$	0.01	$\beta_{SND,PWP}$	0.0
$\beta_{NUT,TS}$	0.01		
$\beta_{GRZ,H}$	0.01		

Code and data availability. The model code, scripts for calibration, and raw and processed data for the calibration and validation can be found on Zenodo with DOI: 10.5281/zenodo.14011849 (Nößler, 2025). This work is partly based on data of the Biodiversity Exploratories program (DFG Priority Program 1374). These datasets are publicly available in the Biodiversity Exploratories Information System (http://doi.org/10.17616/R32P9Q), with links to the specific datasets in the reference section, and are included in the Zenodo
835   repository. The documentation of the model with installation instructions and tutorials can be found online at https://felixnoessler.github. io/GrasslandTraitSim.jl/.

Author contributions. Conceptualization: FN, FM, TM, and OB. Methodology: FN and TM. Software, Formal analysis, Visualization, and Writing - original draft: FN. Writing - review and editing: FN, BT, TM, FM, and OB. Supervision: FM, OB, BT, and TM.

Competing interests. The contact author has declared that none of the authors has any competing interests.

840   *Acknowledgements.* We would like to thank Florian Hartig for the discussion on calibration and Joana Bergmann for the discussion on below-ground plant traits. We acknowledge support by the Open Access Publication Fund of Freie Universität Berlin. We thank the managers of the three Exploratories, Julia Bass, Miriam Teuscher, Franca Marian and all former managers for their work in maintaining the plot and project infrastructure; Victoria Grießmeier for giving support through the central office, Andreas Ostrowski for managing the central data base, and Markus Fischer, Eduard Linsenmair, Dominik Hessenmöller, Daniel Prati, Ingo Schöning, François Buscot,
845   Ernst-Detlef Schulze, Wolfgang W. Weisser and the late Elisabeth Kalko for their role in setting up the Biodiversity Exploratories project. We thank the administration of the Hainich national park, the UNESCO Biosphere Reserve Swabian Alb and the UNESCO Biosphere Reserve Schorfheide-Chorin as well as all land owners for the excellent collaboration. The work has been (partly) funded by the DFG Priority Program 1374 "Biodiversity- Exploratories". Field work permits were issued by the responsible state environmental offices of Baden-Württemberg, Thüringen, and Brandenburg.

References

Adler, P. B., Seabloom, E. W., Borer, E. T., Hillebrand, H., Hautier, Y., Hector, A., Harpole, W. S., O'Halloran, L. R., Grace, J. B., Anderson, T. M., Bakker, J. D., Biederman, L. A., Brown, C. S., Buckley, Y. M., Calabrese, L. B., Chu, C.-J., Cleland, E. E., Collins, S. L., Cottingham, K. L., Crawley, M. J., Damschen, E. I., Davies, K. F., DeCrappeo, N. M., Fay, P. A., Firn, J., Frater, P., Gasarch, E. I., Gruner, D. S., Hagenah, N., Hille Ris Lambers, J., Humphries, H., Jin, V. L., Kay, A. D., Kirkman, K. P., Klein, J. A., Knops, J. M. H., La Pierre, K. J., Lambrinos, J. G., Li, W., MacDougall, A. S., McCulley, R. L., Melbourne, B. A., Mitchell, C. E., Moore, J. L., Morgan, J. W., Mortensen, B., Orrock, J. L., Prober, S. M., Pyke, D. A., Risch, A. C., Schuetz, M., Smith, M. D., Stevens, C. J., Sullivan, L. L., Wang, G., Wragg, P. D., Wright, J. P., and Yang, L. H.: Productivity Is a Poor Predictor of Plant Species Richness, Science, 333, 1750–1753, https://doi.org/10.1126/science.1204498, 2011.

Archibald, S., Hempson, G. P., and Lehmann, C.: A unified framework for plant life-history strategies shaped by fire and herbivory, New Phytologist, 224, 1490–1503, https://doi.org/10.1111/nph.15986, 2019.

Atkinson, J., Gallagher, R., Czyżewski, S., Kerr, M., Trepel, J., Buitenwerf, R., and Svenning, J.: Integrating functional traits into trophic rewilding science, Journal of Ecology, https://doi.org/10.1111/1365-2745.14307, 2024.

Barber, S. A. and Silberbush, M.: Plant Root Morphology and Nutrient Uptake, in: Roots, Nutrient and Water Influx, and Plant Growth, pp. 65–87, Soil Sci. Soc. Amer., Crop Sci. Soc. Amer., Amer. Soc. Agron., https://doi.org/10.2134/asaspecpub49.c4, 1984.

Bergmann, J. and Rillig, M.: Fine root and mycorrhizal traits of 82 grassland species measured in a greenhouse experiment on sand, 2018, https://www.bexis.uni-jena.de/ddm/data/Showdata/26546?version=2, dataset ID: 26546, 2022.

Bergmann, J., Weigelt, A., van der Plas, F., Laughlin, D. C., Kuyper, T. W., Guerrero-Ramirez, N., Valverde-Barrantes, O. J., Bruelheide, H., Freschet, G. T., Iversen, C. M., Kattge, J., McCormack, M. L., Meier, I. C., Rillig, M. C., Roumet, C., Semchenko, M., Sweeney, C. J., van Ruijven, J., York, L. M., and Mommer, L.: The fungal collaboration gradient dominates the root economics space in plants, Science Advances, 6, eaba3756, https://doi.org/10.1126/sciadv.aba3756, 2020.

Bernton, E., Jacob, P. E., Gerber, M., and Robert, C. P.: On parameter estimation with the Wasserstein distance, Information and Inference: A Journal of the IMA, 8, 657–676, https://doi.org/10.1093/imaiai/iaz003, 2019.

Bezanson, J., Edelman, A., Karpinski, S., and Shah, V. B.: Julia: A fresh approach to numerical computing, SIAM Rev. Soc. Ind. Appl. Math., 59, 65–98, https://doi.org/10.1137/141000671, 2017.

Bonanomi, G., Giannino, F., Mazzoleni, S., and Setälä, H.: Negative Plant-Soil Feedback and Species Coexistence, Oikos, 111, 311–321, https://doi.org/10.1111/j.0030-1299.2005.13975.x, 2005.

Bouman, B., Schapendonk, A., Stol, W., and van Kraalingen, D.: Description of the growth model LINGRA as implemented in CGMS, Quantitative approaches in systems analysis, 7, 1996.

Boval, M. and Sauvant, D.: Ingestive behaviour of grazing ruminants: Meta-analysis of the components linking bite mass to daily intake, Animal Feed Science and Technology, 278, 115 014, https://doi.org/10.1016/j.anifeedsci.2021.115014, 2021.

Buzhdygan, O. Y., Meyer, S. T., Weisser, W. W., Eisenhauer, N., Ebeling, A., Borrett, S. R., Buchmann, N., Cortois, R., De Deyn, G. B., de Kroon, H., Gleixner, G., Hertzog, L. R., Hines, J., Lange, M., Mommer, L., Ravenek, J., Scherber, C., Scherer-Lorenzen, M., Scheu, S., Schmid, B., Steinauer, K., Strecker, T., Tietjen, B., Vogel, A., Weigelt, A., and Petermann, J. S.: Biodiversity increases multitrophic energy use efficiency, flow and storage in grasslands, Nature Ecology & Evolution, 4, 393–405, https://doi.org/10.1038/s41559-020-1123-8, 2020.

Caldwell, M. M.: Root Structure: The Considerable Cost of Belowground Function, in: Topics in Plant Population Biology, edited by Solbrig, O. T., Jain, S., Johnson, G. B., and Raven, P. H., pp. 408–427, Macmillan Education UK, London, ISBN 978-1-349-04627-0, https://doi.org/10.1007/978-1-349-04627-0_18, 1979.

Canarini, A., Kaiser, C., Merchant, A., Richter, A., and Wanek, W.: Root Exudation of Primary Metabolites: Mechanisms and Their Roles in Plant Responses to Environmental Stimuli, Frontiers in Plant Science, 10, https://doi.org/10.3389/fpls.2019.00157, 2019.

Chalmandrier, L., Hartig, F., Laughlin, D. C., Lischke, H., Pichler, M., Stouffer, D. B., and Pellissier, L.: Linking functional traits and demography to model species-rich communities, Nature Communications, 12, https://doi.org/10.1038/s41467-021-22630-1, 2021.

Chen, S., Wang, W., Xu, W., Wang, Y., Wan, H., Chen, D., Tang, Z., Tang, X., Zhou, G., Xie, Z., Zhou, D., Shangguan, Z., Huang, J., He, J.-S., Wang, Y., Sheng, J., Tang, L., Li, X., Dong, M., Wu, Y., Wang, Q., Wang, Z., Wu, J., Chapin, F. S., and Bai, Y.: Plant diversity enhances productivity and soil carbon storage, Proceedings of the National Academy of Sciences, 115, 4027–4032, https://doi.org/10.1073/pnas.1700298114, 2018.

Clark, J. S., Carpenter, S. R., Barber, M., Collins, S., Dobson, A., Foley, J. A., Lodge, D. M., Pascual, M., Pielke Jr, R., and Pizer, W.: Ecological forecasts: an emerging imperative, science, 293, 657–660, https://doi.org/10.1126/science.293.5530.657, 2001.

Clerx, M., Robinson, M., Lambert, B., Lei, C. L., Ghosh, S., Mirams, G. R., and Gavaghan, D. J.: Probabilistic Inference on Noisy Time Series (PINTS), Journal of Open Research Software, 7, 23, https://doi.org/10.5334/jors.252, 2019.

Confalonieri, R.: CoSMo: A simple approach for reproducing plant community dynamics using a single instance of generic crop simulators, Ecological Modelling, 286, 1–10, https://doi.org/10.1016/j.ecolmodel.2014.04.019, 2014.

Dee, L. E., Ferraro, P. J., Severen, C. N., Kimmel, K. A., Borer, E. T., Byrnes, J. E. K., Clark, A. T., Hautier, Y., Hector, A., Raynaud, X., Reich, P. B., Wright, A. J., Arnillas, C. A., Davies, K. F., MacDougall, A., Mori, A. S., Smith, M. D., Adler, P. B., Bakker, J. D., Brauman, K. A., Cowles, J., Komatsu, K., Knops, J. M. H., McCulley, R. L., Moore, J. L., Morgan, J. W., Ohlert, T., Power, S. A., Sullivan, L. L., Stevens, C., and Loreau, M.: Clarifying the effect of biodiversity on productivity in natural ecosystems with longitudinal data and methods for causal inference, Nature Communications, 14, 2607, https://doi.org/10.1038/s41467-023-37194-5, 2023.

DWD Climate Data Center: Calculated daily values for different characteristic elements of soil and crops., https://opendata.dwd.de/climate_environment/CDC/derived_germany/soil/daily/historical/, version v19.3. Accessed on 09.03.2023, 2019.

Díaz, S., Lavorel, S., McIntyre, S., Falczuk, V., Casanoves, F., Milchunas, D. G., Skarpe, C., Rusch, G., Sternberg, M., Noy-Meir, I., Landsberg, J., Zhang, W., Clark, H., and Campbell, B. D.: Plant trait responses to grazing – a global synthesis, Global Change Biology, 13, 313–341, https://doi.org/10.1111/j.1365-2486.2006.01288.x, 2007.

European Environment Agency, Kühn, E., Pettersson, L., Strien, A., Õunap, E., Warren, M., Settele, J., Švitra, G., Botham, M., Regan, E., Prokofev, I., Swaay, C., Stefanescu, C., Heliölä, J., Popov, S., Roth, T., Leopold, P., Verovnik, R., Fontaine, B., Musche, M., Julliard, R., Collins, S., Goloshchapova, S., Öberg, S., Cornish, N., Brereton, T., Titeux, N., Harpke, A., and Roy, D.: The European grassland butterfly indicator - 1990-2011, Publications Office of the European Union, https://doi.org/10.2800/89760, 2013.

Eurostat: Main farm land use by NUTS 2 regions, https://doi.org/10.2908/ef_lus_main, 2020.

Fartmann, T.: Routledge Handbook of Insect Conservation, chap. Insect Conservation in Grasslands, Routledge, ISBN 9781003285793, https://doi.org/10.4324/9781003285793, 2024.

Fischer, M., Bossdorf, O., Gockel, S., Hänsel, F., Hemp, A., Hessenmöller, D., Korte, G., Nieschulze, J., Pfeiffer, S., Prati, D., Renner, S., Schöning, I., Schumacher, U., Wells, K., Buscot, F., Kalko, E. K. V., Linsenmair, K. E., Schulze, E.-D., and Weisser, W. W.: Implementing large-scale and long-term functional biodiversity research: The Biodiversity Exploratories, Basic and Applied Ecology, 11, 473–485, https://doi.org/10.1016/j.baae.2010.07.009, 2010.

Fort, H.: On predicting species yields in multispecies communities: Quantifying the accuracy of the linear Lotka-Volterra generalized model, Ecological Modelling, 387, 154–162, https://doi.org/10.1016/j.ecolmodel.2018.09.009, 2018.

Funk, J. L., Larson, J. E., Ames, G. M., Butterfield, B. J., Cavender-Bares, J., Firn, J., Laughlin, D. C., Sutton-Grier, A. E., Williams, L., and Wright, J.: Revisiting the Holy Grail: using plant functional traits to understand ecological processes, Biological Reviews, 92, 1156–1173, https://doi.org/10.1111/brv.12275, 2017.

Geijzendorffer, I. R., van der Werf, W., Bianchi, F. J. J. A., and Schulte, R. P. O.: Sustained dynamic transience in a Lotka-Volterra competition model system for grassland species, Ecological Modelling, 222, 2817–2824, https://doi.org/10.1016/j.ecolmodel.2011.05.029, 2011.

George, E., Marschner, H., and Jakobsen, I.: Role of Arbuscular Mycorrhizal Fungi in Uptake of Phosphorus and Nitrogen From Soil, Critical Reviews in Biotechnology, 15, 257–270, https://doi.org/10.3109/07388559509147412, 1995.

Gillet, F.: Modelling vegetation dynamics in heterogeneous pasture-woodland landscapes, Ecological Modelling, 217, 1–18, https://doi.org/10.1016/j.ecolmodel.2008.05.013, 2008.

Goossens, E. P., Minden, V., Van Poucke, F., and Olde Venterink, H.: Negative plant-soil feedbacks disproportionly affect dominant plants, facilitating coexistence in plant communities, npj Biodiversity, 2, 27, https://doi.org/10.1038/s44185-023-00032-4, 2023.

Gossner, M. M., Lewinsohn, T. M., Kahl, T., Grassein, F., Boch, S., Prati, D., Birkhofer, K., Renner, S. C., Sikorski, J., Wubet, T., Arndt, H., Baumgartner, V., Blaser, S., Blüthgen, N., Börschig, C., Buscot, F., Diekötter, T., Jorge, L. R., Jung, K., Keyel, A. C., Klein, A.-M., Klemmer, S., Krauss, J., Lange, M., Müller, J., Overmann, J., Pašalić, E., Penone, C., Perović, D. J., Purschke, O., Schall, P., Socher, S. A., Sonnemann, I., Tschapka, M., Tscharntke, T., Türke, M., Venter, P. C., Weiner, C. N., Werner, M., Wolters, V., Wurst, S., Westphal, C., Fischer, M., Weisser, W. W., and Allan, E.: Land-use intensification causes multitrophic homogenization of grassland communities, Nature, 540, 266–269, https://doi.org/10.1038/nature20575, 2016.

Griffin-Nolan, R. J., Blumenthal, D. M., Collins, S. L., Farkas, T. E., Hoffman, A. M., Mueller, K. E., Ocheltree, T. W., Smith, M. D., Whitney, K. D., and Knapp, A. K.: Shifts in plant functional composition following long-term drought in grasslands, Journal of Ecology, 107, 2133–2148, https://doi.org/10.1111/1365-2745.13252, 2019.

Grime, J. P.: Evidence for the Existence of Three Primary Strategies in Plants and Its Relevance to Ecological and Evolutionary Theory, The American Naturalist, 111, 1169–1194, 1977.

Gubsch, M., Buchmann, N., Schmid, B., Schulze, E.-D., Lipowsky, A., and Roscher, C.: Differential effects of plant diversity on functional trait variation of grass species, Annals of Botany, 107, 157–169, https://doi.org/10.1093/aob/mcq220, 2010.

Gupta, S. C. and Larson, W. E.: Estimating soil water retention characteristics from particle size distribution, organic matter percent, and bulk density, Water Resources Research, 15, 1633–1635, https://doi.org/10.1029/WR015i006p01633, 1979.

Haario, H., Saksman, E., and Tamminen, J.: An Adaptive Metropolis Algorithm, Bernoulli, 7, 223–242, https://doi.org/10.2307/3318737, 2001.

Heger, T.: Light availability experienced in the field affects ability of following generations to respond to shading in an annual grassland plant, Journal of Ecology, 104, 1432–1440, https://doi.org/10.1111/1365-2745.12607, 2016.

Hejcman, M., Hejcmanová, P., Pavlů, V., and Beneš, J.: Origin and history of grasslands in Central Europe - a review, Grass and Forage Science, 68, 345–363, https://doi.org/10.1111/gfs.12066, 2013.

Herold, N., Schöning, I., and Schrumpf, M.: Soil Survey 2008 Subplot Description, https://www.bexis.uni-jena.de/ddm/data/Showdata/4761?version=3, dataset ID: 4761, 2021.

Hilpold, A., Seeber, J., Fontana, V., Niedrist, G., Rief, A., Steinwandter, M., Tasser, E., and Tappeiner, U.: Decline of rare and specialist species across multiple taxonomic groups after grassland intensification and abandonment, Biodiversity and Conservation, 27, 3729–3744, https://doi.org/10.1007/s10531-018-1623-x, 2018.

Hinderling, J. and Keller, S.: Vegetation records for grassland EPs, 2008 - 2022, https://www.bexis.uni-jena.de/ddm/data/Showdata/965   31389?version=7, dataset ID: 31389, 2023.

Hinderling, J., Penone, C., Prati, D., Bolliger, R., Schäfer, D., Boch, S., and Schmitt, B.: Biomass data for grassland EPs, 2009 - 2023, https://www.bexis.uni-jena.de/ddm/data/Showdata/31581?version=5, dataset ID: 31581, 2024.

Hirata, M., Kunieda, E., and Tobisa, M.: Short-term ingestive behaviour of cattle grazing tropical stoloniferous grasses with contrasting growth forms, The Journal of Agricultural Science, 148, 615–624, https://doi.org/10.1017/S0021859610000353, 2010.

970   Hodgson, J., Clark, D., and Mitchell, R.: Foraging Behavior in Grazing Animals and Its Impact on Plant Communities, in: Forage Quality, Evaluation, and Utilization, pp. 796–827, John Wiley & Sons, Ltd, https://doi.org/10.2134/1994.foragequality.c19, 1994.

Jeltsch, F., Moloney, K. A., Schurr, F. M., Köchy, M., and Schwager, M.: The state of plant population modelling in light of environmental change, Perspectives in Plant Ecology, Evolution and Systematics, 9, 171–189, https://doi.org/10.1016/j.ppees.2007.11.004, 2008.

Jiang, Y., Li, Y., Nie, G., and Liu, H.: Leaf and Root Growth, Carbon and Nitrogen Contents, and Gene Expression of Perennial Ryegrass 975   to Different Nitrogen Supplies, Journal of the American Society for Horticultural Science J. Amer. Soc. Hort. Sci., 141, 555 – 562, https://doi.org/10.21273/JASHS03883-16, 2016.

Johnstone, R. H., Chang, E. T., Bardenet, R., de Boer, T. P., Gavaghan, D. J., Pathmanathan, P., Clayton, R. H., and Mirams, G. R.: Uncertainty and variability in models of the cardiac action potential: Can we build trustworthy models?, Journal of Molecular and Cellular Cardiology, 96, 49–62, https://doi.org/10.1016/j.yjmcc.2015.11.018, special Issue: Computational Modelling of the Heart, 980   2016.

Jouven, M., Carrère, P., and Baumont, R.: Model predicting dynamics of biomass, structure and digestibility of herbage in managed permanent pastures. 1. Model description, Grass and Forage Science, 61, 112–124, https://doi.org/10.1111/j.1365-2494.2006.00515.x, 2006.

Jäger, E. J., Müller, F., Ritz, C., Welk, E., and Wesche, K., eds.: Rothmaler - Exkursionsflora von Deutschland, Gefäßpflanzen: Atlas-985   band, Springer Berlin Heidelberg, ISBN 9783662497104, https://doi.org/10.1007/978-3-662-49710-4, 2017.

Kattge, J., Bönisch, G., Díaz, S., Lavorel, S., Prentice, I. C., Leadley, P., Tautenhahn, S., Werner, G. D. A., et al.: TRY plant trait database - enhanced coverage and open access, Global Change Biology, 26, 119–188, https://doi.org/10.1111/gcb.14904, 2020.

Kipling, R. P., Virkajärvi, P., Breitsameter, L., Curnel, Y., De Swaef, T., Gustavsson, A.-M., Hennart, S., Höglind, M., Järvenranta, K., Minet, J., Nendel, C., Persson, T., Picon-Cochard, C., Rolinski, S., Sandars, D. L., Scollan, N. D., Sebek, L., Seddaiu, G., Topp, C. 990   F. E., Twardy, S., Van Middelkoop, J., Wu, L., and Bellocchi, G.: Key challenges and priorities for modelling European grasslands under climate change, Science of The Total Environment, 566-567, 851–864, https://doi.org/10.1016/j.scitotenv.2016.05.144, 2016.

Klimešová, J., Latzel, V., de Bello, F., and van Groenendael, J. M.: Plant functional traits in studies of vegetation changes in response to grazing and mowing: towards a use of more specific traits, Preslia, 80, 245–253, 2008.

Konvalinková, T., Püschel, D., Řezáčová, V., Gryndlerová, H., and Jansa, J.: Carbon flow from plant to arbuscular mycorrhizal fungi is 995   reduced under phosphorus fertilization, Plant and Soil, 419, 319–333, https://doi.org/10.1007/s11104-017-3350-6, 2017.

Kranstauber, B., Smolla, M., and Safi, K.: Similarity in spatial utilization distributions measured by the earth mover's distance, Methods in Ecology and Evolution, 8, 155–160, https://doi.org/10.1111/2041-210X.12649, 2017.

Kunrath, T. R., Nunes, P. A. d. A., de Souza Filho, W., Cadenazzi, M., Bremm, C., Martins, A. P., and Carvalho, P. C. d. F.: Sward height determines pasture production and animal performance in a long-term soybean-beef cattle integrated system, Agricultural Systems,

1000   177, 102 716, https://doi.org/10.1016/j.agsy.2019.102716, 2020.

Lacasa, J., Hefley, T. J., Otegui, M. E., and Ciampitti, I. A.: A practical guide to estimating the light extinction coefficient with nonlinear models—a case study on maize, Plant Methods, 17, https://doi.org/10.1186/s13007-021-00753-2, 2021.

Liu, F. and Stützel, H.: Biomass partitioning, specific leaf area, and water use efficiency of vegetable amaranth (Amaranthus spp.) in response to drought stress, Scientia Horticulturae, 102, 15–27, https://doi.org/https://doi.org/10.1016/j.scienta.2003.11.014, 2004.

1005   Liu, X., Parker, I. M., Gilbert, G. S., Lu, Y., Xiao, Y., Zhang, L., Huang, M., Cheng, Y., Zhang, Z., and Zhou, S.: Coexistence is stabilized by conspecific negative density dependence via fungal pathogens more than oomycete pathogens, Ecology, 103, https://doi.org/10.1002/ecy.3841, 2022.

Long, S. P., Humphries, S., and Falkowski, P. G.: Photoinhibition of Photosynthesis in Nature, Annual Review of Plant Physiology and Plant Molecular Biology, 45, 633–662, https://doi.org/10.1146/annurev.pp.45.060194.003221, 1994.

1010   Lopez, G., Ahmadi, S. H., Amelung, W., Athmann, M., Ewert, F., Gaiser, T., Gocke, M. I., Kautz, T., Postma, J., Rachmilevitch, S., Schaaf, G., Schnepf, A., Stoschus, A., Watt, M., Yu, P., and Seidel, S. J.: Nutrient deficiency effects on root architecture and root-to-shoot ratio in arable crops, Frontiers in Plant Science, 13, https://doi.org/10.3389/fpls.2022.1067498, 2023.

Luo, W., Ishii, N. I., Muraina, T. O., Song, L., Te, N., Griffin-Nolan, R. J., Slette, I. J., Ross, S. R. P. J., Sasaki, T., Rudgers, J. A., Smith, M. D., Knapp, A. K., and Collins, S. L.: Extreme Drought Increases the Temporal Variability of Grassland Productivity by Suppressing

1015   Dominant Grasses, Ecology Letters, 28, e70 127, https://doi.org/10.1111/ele.70127, 2025.

Luo, Y., Weng, E., Wu, X., Gao, C., Zhou, X., and Zhang, L.: Parameter Identifiability, Constraint, and Equifinality in Data Assimilation with Ecosystem Models, Ecological Applications, 19, 571–574, https://doi.org/10.1890/08-0561.1, 2009.

Marschner, H. and Dell, B.: Nutrient uptake in mycorrhizal symbiosis, Plant and Soil, 159, 89–102, https://doi.org/10.1007/bf00000098, 1994.

1020   May, F., Grimm, V., and Jeltsch, F.: Reversed effects of grazing on plant diversity: the role of below-ground competition and size symmetry, Oikos, 118, 1830–1843, https://doi.org/10.1111/j.1600-0706.2009.17724.x, 2009.

Meurer, K. H. E., Bolinder, M. A., Andrén, O., Hansson, A.-C., Pettersson, R., and Kätterer, T.: Shoot and root production in mixed grass ley under daily fertilization and irrigation: validating the N productivity concept under field conditions, Nutrient Cycling in Agroecosystems, 115, 85–99, https://doi.org/10.1007/s10705-019-10006-3, 2019.

1025   Monsi, M.: Uber den Lichtfaktor in den Pflanzengesellschaften und seine Bedeutung fur die Stoffproduktion, Jap. J. Bot., 14, 22–52, 1953.

Monsi, M. and Saeki, T.: On the Factor Light in Plant Communities and its Importance for Matter Production, Annals of Botany, 95, 549–567, https://doi.org/10.1093/aob/mci052, 2005.

Monteith, J. L.: Solar Radiation and Productivity in Tropical Ecosystems, Journal of Applied Ecology, 9, 747–766,

1030   https://doi.org/10.2307/2401901, 1972.

Moulin, T., Perasso, A., Calanca, P., and Gillet, F.: DynaGraM: A process-based model to simulate multi-species plant community dynamics in managed grasslands, Ecological Modelling, 439, 109 345, https://doi.org/10.1016/j.ecolmodel.2020.109345, 2021.

Nagy, S.: Grasslands as a bird habitat, in: Grasslands in Europe: Of High Nature Value, pp. 35–41, KNNV Publishing, ISBN 9789004278103, https://doi.org/10.1163/9789004278103_005, 2009.

1035 Nößler, F.: Supplementary material: A trait-based model to describe plant community dynamics in managed grasslands (Grassland-TraitSim.jl v1.0.0), https://doi.org/10.5281/zenodo.14011849, 2025.

Onoda, Y., Wright, I. J., Evans, J. R., Hikosaka, K., Kitajima, K., Niinemets, Ü., Poorter, H., Tosens, T., and Westoby, M.: Physiological and structural tradeoffs underlying the leaf economics spectrum, New Phytologist, 214, 1447–1463, https://doi.org/10.1111/nph.14496, 2017.

1040 Pakeman, R. J., Garnier, E., Lavorel, S., Ansquer, P., Castro, H., Cruz, P., Doležal, J., Eriksson, O., Freitas, H., Golodets, C., Kigel, J., Kleyer, M., Lepš, J., Meier, T., Papadimitriou, M., Papanastasis, V. P., Quested, H., Quétier, F., Rusch, G., Sternberg, M., Theau, J.-P., Thébault, A., and Vile, D.: Impact of abundance weighting on the response of seed traits to climate and land use, Journal of Ecology, 96, 355–366, https://doi.org/10.1111/j.1365-2745.2007.01336.x, 2008.

Parton, W.: The CENTURY model, in: Evaluation of soil organic matter models: Using existing long-term datasets, pp. 283–291,
1045 Springer, https://doi.org/10.1007/978-3-642-61094-3_23, 1996.

Parton, W. J., Hartman, M., Ojima, D., and Schimel, D.: DAYCENT and its land surface submodel: description and testing, Global and Planetary Change, 19, 35–48, https://doi.org/10.1016/S0921-8181(98)00040-X, 1998.

Pauler, C. M., Isselstein, J., Suter, M., Berard, J., Braunbeck, T., and Schneider, M. K.: Choosy grazers: Influence of plant traits on forage selection by three cattle breeds, Functional Ecology, 34, 980–992, https://doi.org/10.1111/1365-2435.13542, 2020.

1050 Pei, Y., Dong, J., Zhang, Y., Yuan, W., Doughty, R., Yang, J., Zhou, D., Zhang, L., and Xiao, X.: Evolution of light use efficiency models: Improvement, uncertainties, and implications, Agricultural and Forest Meteorology, 317, 108 905, https://doi.org/10.1016/j.agrformet.2022.108905, 2022.

Petermann, J. S. and Buzhdygan, O. Y.: Grassland biodiversity, Current Biology, 31, R1195–R1201, https://doi.org/10.1016/j.cub.2021.06.060, 2021.

1055 Piseddu, F., Bellocchi, G., and Picon-Cochard, C.: Mowing and warming effects on grassland species richness and harvested biomass: meta-analyses, Agronomy for Sustainable Development, 41, https://doi.org/10.1007/s13593-021-00722-y, 2021.

Piseddu, F., Martin, R., Movedi, E., Louault, F., Confalonieri, R., and Bellocchi, G.: Simulation of Multi-Species Plant Communities in Perturbed and Nutrient-Limited Grasslands: Development of the Growth Model ModVege, Agronomy, 12, https://doi.org/10.3390/agronomy12102468, 2022.

1060 Potts, J. R., Auger-Méthé, M., Mokross, K., and Lewis, M. A.: A generalized residual technique for analysing complex movement models using earth mover's distance, Methods in Ecology and Evolution, 5, 1012–1022, https://doi.org/10.1111/2041-210X.12253, 2014.

Prati, D., Goßner, M., and Neff, F.: Leaf traits of most abundant plant species from all EPs, 2017/2018, https://www.bexis.uni-jena.de/ddm/data/Showdata/24807?version=2, dataset ID: 24807, 2021.

Prieto, I., Roumet, C., Cardinael, R., Dupraz, C., Jourdan, C., Kim, J. H., Maeght, J. L., Mao, Z., Pierret, A., Portillo, N., et al.: Root
1065 functional parameters along a land-use gradient: evidence of a community-level economics spectrum, Journal of Ecology, 103, 361–373, 2015.

Pulungan, M. A., Suzuki, S., Gavina, M. K. A., Tubay, J. M., Ito, H., Nii, M., Ichinose, G., Okabe, T., Ishida, A., Shiyomi, M., Togashi, T., Yoshimura, J., and Morita, S.: Grazing enhances species diversity in grassland communities, Scientific Reports, 9, https://doi.org/10.1038/s41598-019-47635-1, 2019.

1070 Pärtel, M., Bruun, H., and Sammul, M.: Biodiversity in temperate European grasslands: origin and conservation, in: Integrating efficient grassland farming and biodiversity: Proceedings of the 13th international occasional symposium of the European grassland federation, vol. 10 of *Grassland Science in Europe*, pp. 1–14, 2005.

R Core Team: R: A Language and Environment for Statistical Computing, R Foundation for Statistical Computing, Vienna, Austria, https://www.R-project.org/, 2024.

1075 Reich, P. B.: The world-wide 'fast–slow' plant economics spectrum: a traits manifesto, Journal of ecology, 102, 275–301, 2014.

Reich, P. B., Walters, M. B., and Ellsworth, D. S.: Leaf Life-Span in Relation to Leaf, Plant, and Stand Characteristics among Diverse Ecosystems, Ecological Monographs, 62, 365–392, https://doi.org/10.2307/2937116, 1992.

Riedo, M., Grub, A., Rosset, M., and Fuhrer, J.: A pasture simulation model for dry matter production, and fluxes of carbon, nitrogen, water and energy, Ecological Modelling, 105, 141–183, https://doi.org/10.1016/S0304-3800(97)00110-5, 1998.

1080 Rolinski, S., Müller, C., Heinke, J., Weindl, I., Biewald, A., Bodirsky, B. L., Bondeau, A., Boons-Prins, E. R., Bouwman, A. F., Leffelaar, P. A., Te Roller, J. A., Schaphoff, S., and Thonicke, K.: Modeling vegetation and carbon dynamics of managed grasslands at the global scale with LPJmL 3.6, Geoscientific Model Development, 11, 429–451, https://doi.org/10.5194/gmd-11-429-2018, 2018.

Rubner, Y., Tomasi, C., and Guibas, L. J.: The Earth Mover's Distance as a Metric for Image Retrieval, International Journal of Computer Vision, 40, 99–121, https://doi.org/10.1023/a:1026543900054, 2000.

1085 Schapendonk, A. H. C. M., Stol, W., van Kraalingen, D. W. G., and Bouman, B. A. M.: LINGRA, a sink/source model to simulate grassland productivity in Europe, European Journal of Agronomy, 9, 87–100, https://doi.org/10.1016/S1161-0301(98)00027-6, 1998.

Schils, R. L. M., Newell Price, P., Klaus, V., Tonn, B., Hejduk, S., Stypinski, P., Hiron, M., Fernández, P., Ravetto Enri, S., Lellei-Kovács, E., Annett, N., Markovic, B., Lively, F., Ten Berge, H., Smith, K., Forster-Brown, C., Jones, M., Buchmann, N., Janicka, M., Fernandez, J., Rankin, J., McConnell, D., Aubry, A., and Korevaar, H.: European permanent grasslands mainly threatened by abandonment, heat

1090 and drought, and conversion to temporary grassland, https://doi.org/10.3929/ETHZ-B-000448642, 2020.

Schroeder-Georgi, T., Wirth, C., Nadrowski, K., Meyer, S. T., Mommer, L., and Weigelt, A.: From pots to plots: hierarchical trait-based prediction of plant performance in a mesic grassland, Journal of Ecology, 104, 206–218, https://doi.org/10.1111/1365-2745.12489, 2016.

Schöning, I.: Soil carbon and nitrogen concentrations - soil sampling campaign 2021, all experimental plots (EPs), 0-10 cm, https:

1095 //www.bexis.uni-jena.de/ddm/data/Showdata/31210?version=13, dataset ID: 31210, 2023.

Schöning, I., Klötzing, T., Apostolakis, A., Trumbore, S., and Schrumpf, M.: MinSoil 2017 - Soil Carbon and Nitrogen Concentrations, https://www.bexis.uni-jena.de/ddm/data/Showdata/23846?version=10, dataset ID: 23846, 2021a.

Schöning, I., Solly, E., Klötzing, T., Trumbore, S., and Schrumpf, M.: MinSoil 2011 - Soil Carbon and Nitrogen Concentrations, https://www.bexis.uni-jena.de/ddm/data/Showdata/14446?version=19, dataset ID: 14446, 2021b.

1100 Schöning, I., Solly, E., Klötzing, T., Trumbore, S., and Schrumpf, M.: MinSoil 2011 - Soil Texture, https://www.bexis.uni-jena.de/ddm/data/Showdata/14686?version=10, dataset ID: 14686, 2021c.

Schöning, I., Solly, E., Klötzing, T., Trumbore, S., and Schrumpf, M.: MinSoil 2011 - Soil Bulk Density and Carbon and Nitrogen stocks, https://www.bexis.uni-jena.de/ddm/data/Showdata/17086?version=4, dataset ID: 17086, 2021d.

Schöning, I., Trumbore, S., Schrumpf, M., Klötzing, T., and Gan, H. Y.: MinSoil 2014 - Soil Carbon and Nitrogen Concentrations,

1105 https://www.bexis.uni-jena.de/ddm/data/Showdata/18787?version=6, dataset ID: 18787, 2021e.

Siefert, A., Violle, C., Chalmandrier, L., Albert, C. H., Taudiere, A., Fajardo, A., Aarssen, L. W., Baraloto, C., Carlucci, M. B., Cianciaruso, M. V., et al.: A global meta-analysis of the relative extent of intraspecific trait variation in plant communities, Ecology letters, 18, 1406–1419, https://doi.org/10.1111/ele.12508, 2015.

Siehoff, S., Lennartz, G., Heilburg, I. C., Roß-Nickoll, M., Ratte, H. T., and Preuss, T. G.: Process-based modeling of grassland dynamics built on ecological indicator values for land use, Ecological Modelling, 222, 3854–3868, https://doi.org/10.1016/j.ecolmodel.2011.10.003, 2011.

Silva, G. P., Fialho, C. A., Carvalho, L. R., Fonseca, L., Carvalho, P. C. F., Bremm, C., and Da Silva, S. C.: Sward structure and short-term herbage intake in Arachis pintoi cv. Belmonte subjected to varying intensities of grazing, The Journal of Agricultural Science, 156, 92–99, https://doi.org/10.1017/S0021859617000855, 2018.

Taubert, F., Frank, K., and Huth, A.: A review of grassland models in the biofuel context, Ecological Modelling, 245, 84–93, https://doi.org/10.1016/j.ecolmodel.2012.04.007, 2012.

Taubert, F., Hetzer, J., Schmid, J. S., and Huth, A.: Confronting an individual-based simulation model with empirical community patterns of grasslands, PLOS ONE, 15, e0236 546, https://doi.org/10.1371/journal.pone.0236546, 2020.

Tälle, M., Deák, B., Poschlod, P., Valkó, O., Westerberg, L., and Milberg, P.: Grazing vs. mowing: A meta-analysis of biodiversity benefits for grassland management, Agriculture, Ecosystems & Environment, 222, 200–212, https://doi.org/10.1016/j.agee.2016.02.008, 2016.

Van Der Heijden, M. G. A., Martin, F. M., Selosse, M., and Sanders, I. R.: Mycorrhizal ecology and evolution: the past, the present, and the future, New Phytologist, 205, 1406–1423, https://doi.org/10.1111/nph.13288, 2015.

Van Oijen, M., Bellocchi, G., and Höglind, M.: Effects of Climate Change on Grassland Biodiversity and Productivity: The Need for a Diversity of Models, Agronomy, 8, 14, https://doi.org/10.3390/agronomy8020014, 2018.

Van Oijen, M., Barcza, Z., Confalonieri, R., Korhonen, P., Kröel-Dulay, G., Lellei-Kovács, E., Louarn, G., Louault, F., Martin, R., Moulin, T., Movedi, E., Picon-Cochard, C., Rolinski, S., Viovy, N., Wirth, S. B., and Bellocchi, G.: Incorporating Biodiversity into Biogeochemistry Models to Improve Prediction of Ecosystem Services in Temperate Grasslands: Review and Roadmap, Agronomy, 10, 259, https://doi.org/10.3390/agronomy10020259, 2020.

Vehtari, A., Gelman, A., Simpson, D., Carpenter, B., and Bürkner, P.-C.: Rank-normalization, folding, and localization: An improved $\hat{R}$ for assessing convergence of MCMC (with discussion), Bayesian analysis, 16, 667–718, https://doi.org/10.1214/20-BA1221, 2021.

Villani, C.: Optimal Transport - Old and New, Springer Berlin Heidelberg, ISBN 9783540710509, https://doi.org/10.1007/978-3-540-71050-9, 2009.

Violle, C., Enquist, B. J., McGill, B. J., Jiang, L., Albert, C. H., Hulshof, C., Jung, V., and Messier, J.: The return of the variance: intraspecific variability in community ecology, Trends in ecology & evolution, 27, 244–252, https://doi.org/10.1016/j.tree.2011.11.014, 2012.

Virtanen, P., Gommers, R., Oliphant, T. E., Haberland, M., Reddy, T., Cournapeau, D., Burovski, E., Peterson, P., Weckesser, W., Bright, J., van der Walt, S. J., Brett, M., Wilson, J., Millman, K. J., Mayorov, N., Nelson, A. R. J., Jones, E., Kern, R., Larson, E., Carey, C. J., Polat, İ., Feng, Y., Moore, E. W., VanderPlas, J., Laxalde, D., Perktold, J., Cimrman, R., Henriksen, I., Quintero, E. A., Harris, C. R., Archibald, A. M., Ribeiro, A. H., Pedregosa, F., van Mulbregt, P., and SciPy 1.0 Contributors: SciPy 1.0: Fundamental Algorithms for Scientific Computing in Python, Nature Methods, 17, 261–272, https://doi.org/10.1038/s41592-019-0686-2, 2020.

Vogt, J., Weisser, W., Ayasse, M., Fischer, M., Schumacher, U., Schreiber, C., Lauterbach, R., Franke, A., Ostrowski, A., Teuscher, M., and Pompe, S.: Grassland management parameter as input data for a computer model based on interview data of the Biodiversity Exploratories project, https://www.bexis.uni-jena.de/ddm/data/Showdata/31715?version=9, dataset ID: 31715, 2024.

1145 Wang, D.: MODIS/Terra+Aqua Photosynthetically Active Radiation Daily/3-Hour L3 Global 0.05Deg CMG V061, https://doi.org/10.5067/MODIS/MCD18C2.061, nASA EOSDIS Land Processes Distributed Active Archive Center. Accessed on 09.03.2023, 2021.

Watson, D. J.: Comparative Physiological Studies on the Growth of Field Crops: I. Variation in Net Assimilation Rate and Leaf Area between Species and Varieties, and within and between Years, Annals of Botany, 11, 41–76,
1150 https://doi.org/10.1093/oxfordjournals.aob.a083148, 1947.

Went, F.: The effect of temperature on plant growth, Annual Review of Plant Physiology, 4, 347–362, https://doi.org/10.1146/annurev.pp.04.060153.002023, 1953.

Westoby, M., Falster, D. S., Moles, A. T., Vesk, P. A., and Wright, I. J.: Plant ecological strategies: some leading dimensions of variation between species, Annual review of ecology and systematics, 33, 125–159,
1155 https://doi.org/10.1146/annurev.ecolsys.33.010802.150452, 2002.

Wilson, J. B., Peet, R. K., Dengler, J., and Pärtel, M.: Plant species richness: the world records, Journal of Vegetation Science, 23, 796–802, https://doi.org/10.1111/j.1654-1103.2012.01400.x, 2012.

Wirth, S. B., Taubert, F., Tietjen, B., Müller, C., and Rolinski, S.: Do details matter? Disentangling the processes re- lated to plant species interactions in two grassland models of different complexity, Ecological Modelling, 460, 109 737,
1160 https://doi.org/j.ecolmodel.2021.109737, 2021.

Wirth, S. B., Poyda, A., Taube, F., Tietjen, B., Müller, C., Thonicke, K., Linstädter, A., Behn, K., Schaphoff, S., von Bloh, W., and Rolinski, S.: Connecting competitor, stress-tolerator and ruderal (CSR) theory and Lund Potsdam Jena managed Land 5 (LPJmL 5) to assess the role of environmental conditions, management and functional diversity for grassland ecosystem functions, Biogeosciences, 21, 381–410, https://doi.org/10.5194/bg-21-381-2024, 2024.

1165 Wright, G. C., Hubick, K. T., Farquhar, G. D., and Rao, R. N.: Genetic and environmental variation in transpiration efficiency and its correlation with carbon isotope discrimination and specific leaf area in peanut, in: Stable isotopes and plant carbon-water relations, pp. 247–267, Elsevier, 1993.

Wright, I. J., Reich, P. B., Westoby, M., Ackerly, D. D., Baruch, Z., Bongers, F., Cavender-Bares, J., Chapin, T., Cornelissen, J. H. C., Diemer, M., Flexas, J., Garnier, E., Groom, P. K., Gulias, J., Hikosaka, K., Lamont, B. B., Lee, T., Lee, W., Lusk, C.,
1170 Midgley, J. J., Navas, M.-L., Niinemets, Ü., Oleksyn, J., Osada, N., Poorter, H., Poot, P., Prior, L., Pyankov, V. I., Roumet, C., Thomas, S. C., Tjoelker, M. G., Veneklaas, E. J., and Villar, R.: The worldwide leaf economics spectrum, Nature, 428, 821–827, https://doi.org/10.1038/nature02403, 2004.

Wöllauer, S., Hänsel, F., Nauss, T., and Forteva, S.: Climate data - Time Series Web Interface, https://www.bexis.uni-jena.de/tcd/ PublicClimateData/, dataset ID: 19007, 2023.